The New Era of X-Ray Computed Tomography

Marc Kachelrieß

German Cancer Research Center (DKFZ)
Heidelberg, Germany
www.dkfz.de/ct

DEUTSCHES
KREBSFORSCHUNGSZENTRUM
IN DER HELMHOLTZ-GEMEINSCHAFT

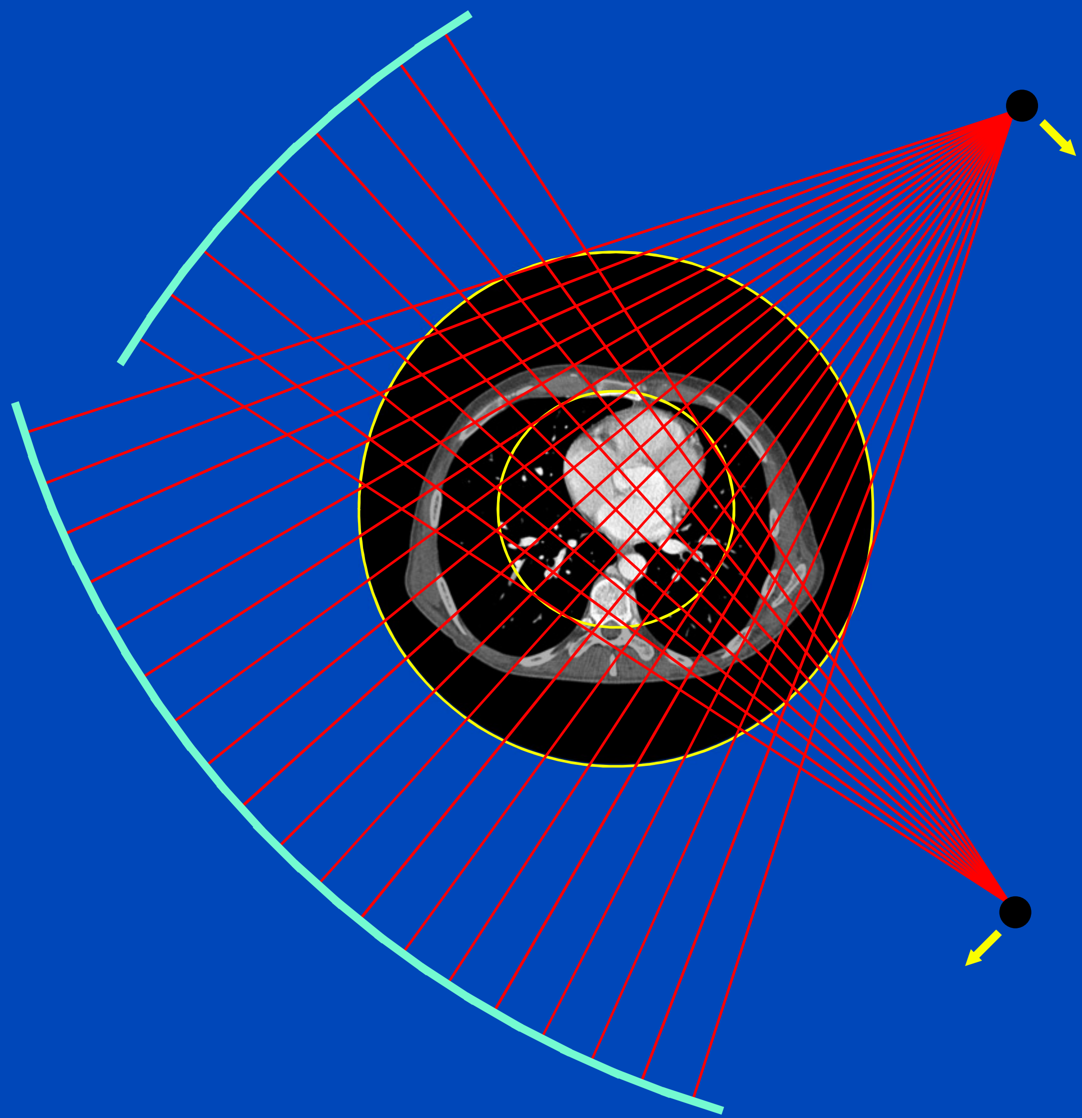

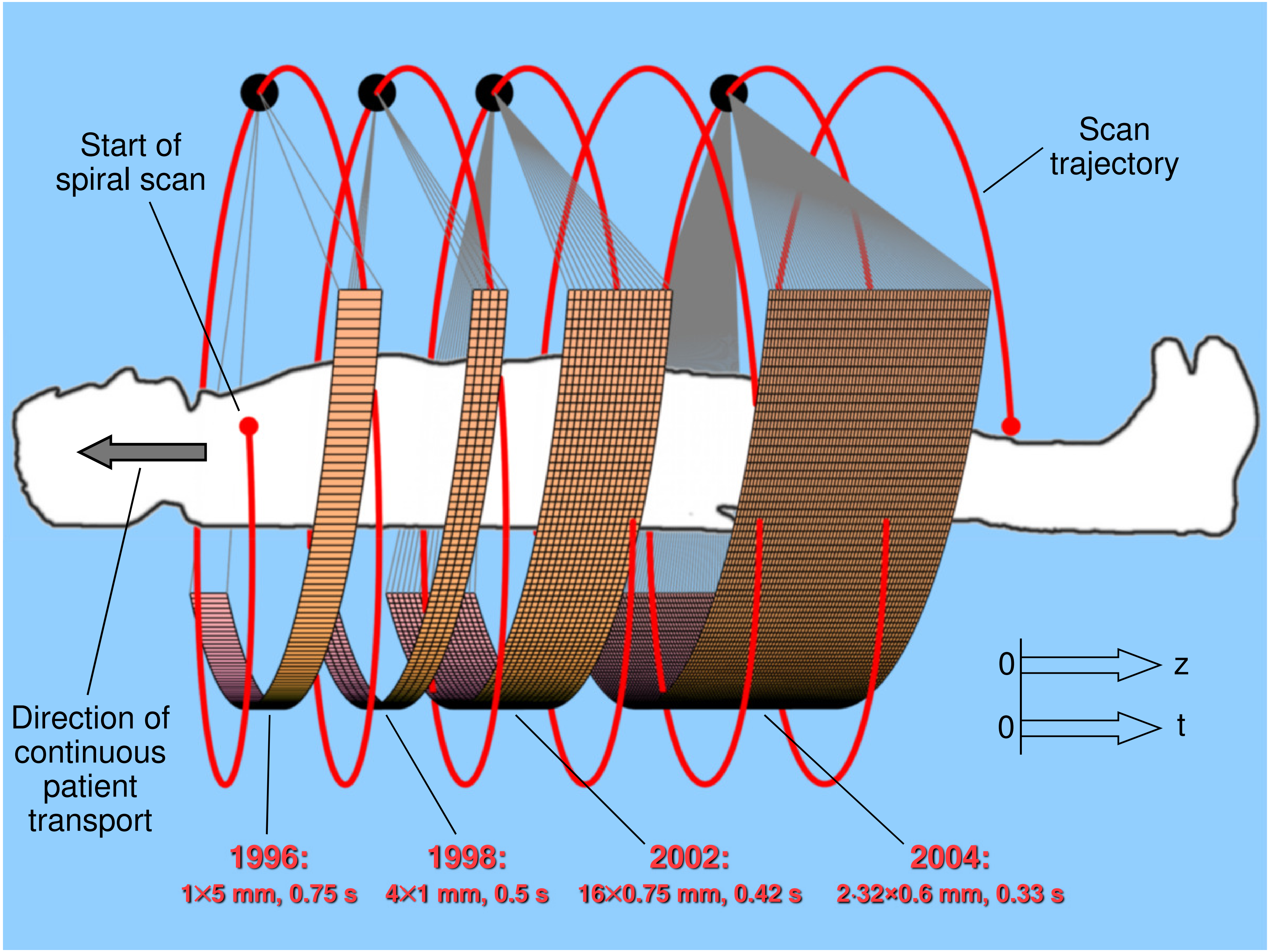

Start of
spiral scan
Scan
trajectory
Direction of
continuous
patient
transport
0
z
0
t
1996:
1×5 mm, 0.75 s
1998:
4×1 mm, 0.5 s
2002:
16×0.75 mm, 0.42 s
2004:
2·32×0.6 mm, 0.33 s

Canon Aquilion ONE Vision

GE Revolution CT

Philips IQon Spectral CT

Siemens Somatom Force

In-plane resolution: 0.4 … 0.7 mm

Nominal slice thickness: S = 0.5 … 1.5 mm

Tube (max. values): 120 kW, 150 kV, 1300 mA

Effective tube current: $\mathrm{mAs}_{\mathrm{eff}}$ = 10 mAs … 1000 mAs

Rotation time: T_{rot} = 0.25 … 0.5 s

Simultaneously acquired slices: M = 16 … 320

Table increment per rotation: d = 1 … 183 mm

Scan speed: up to 73 cm/s

Temporal resolution: 50 … 250 ms

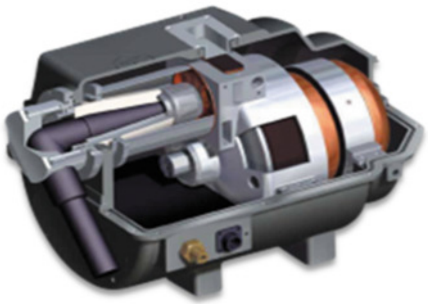

Canon Megacool Vi

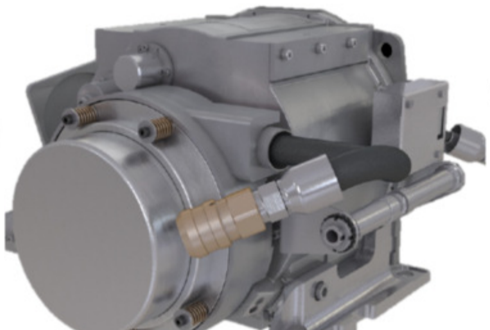

GE Performix HDw

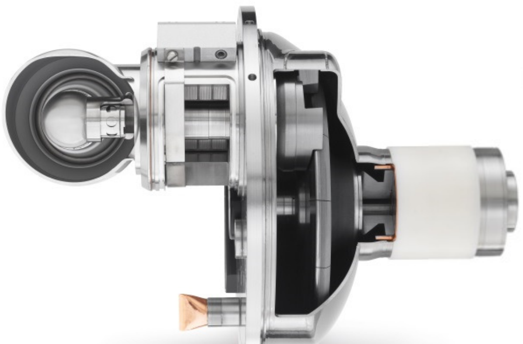

Philips iMRC

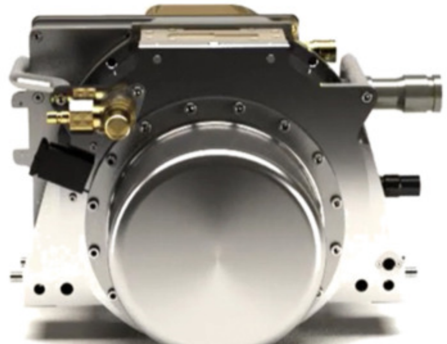

Siemens Vectron

Very Fast Scanning (Somatom Force)

Procedure:
Transcatheter aortic valve implantation (TAVI)

Patient age: 80 years

Tube voltage: 80 kV
Current: 340 ref mAs/rot

Rotation time: 0.25 s
Pitch: 3.2
Slice thickness: 0.75 mm
Scan length: 557 mm
Scan time: 0.76 s
Scan speed: 737 mm/s

Kernel : B40
Recon: ADMIRE 3

CTDIvol: 2.7 mGy
DLP: 162 mGy·cm
Effective dose: 2.3 mSv

Case information

Axial slices, C = 0 HU, W = 1500 HU

Volume rendering

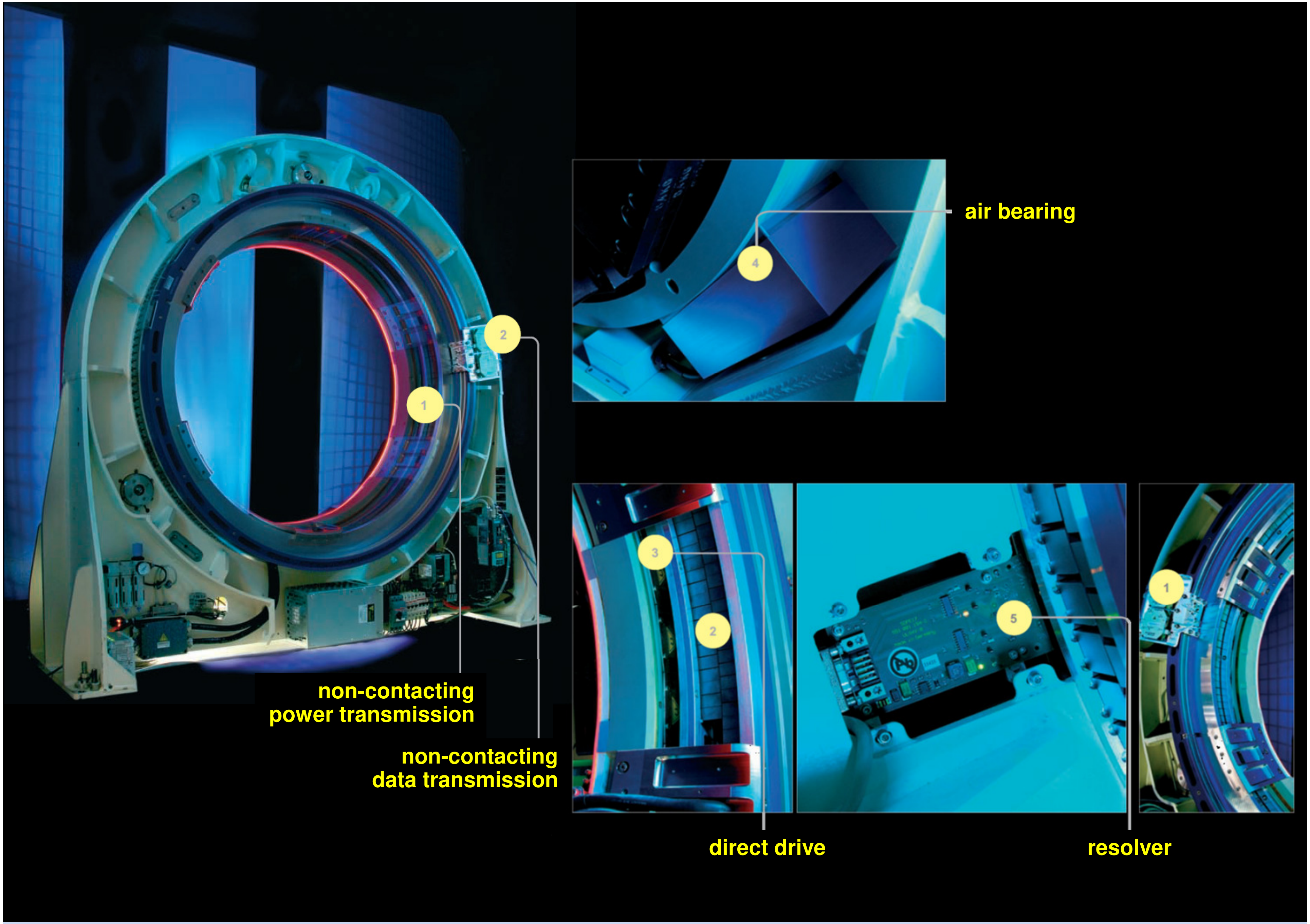

Data courtesy of Schleifring GmbH, Fürstenfeldbruck, Germany
and of rsna2011.rsna.org/exbData/1678/docs/Gantry_Subsystem.pdf

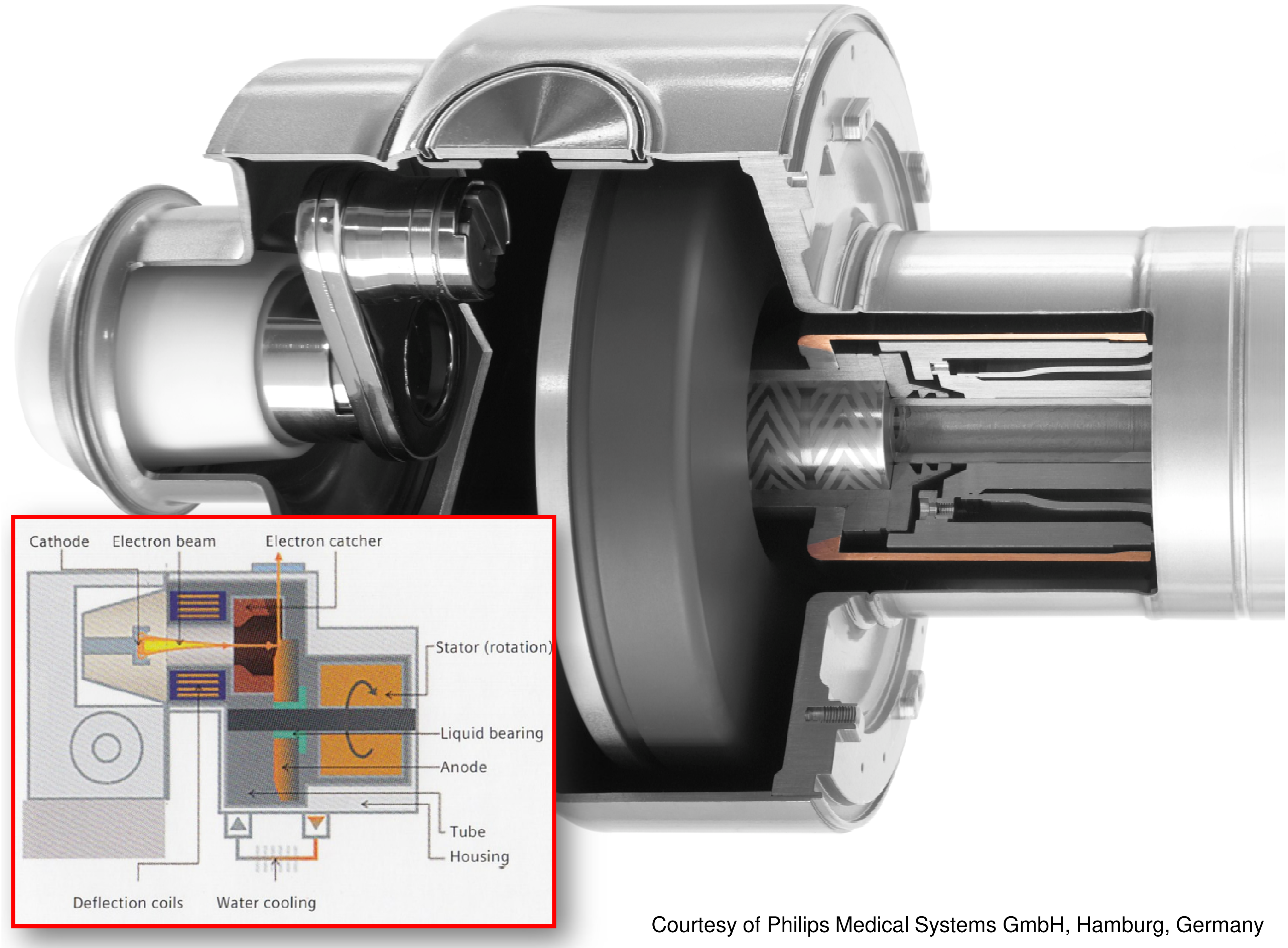

Courtesy of Philips Medical Systems GmbH, Hamburg, Germany

Detector Technology

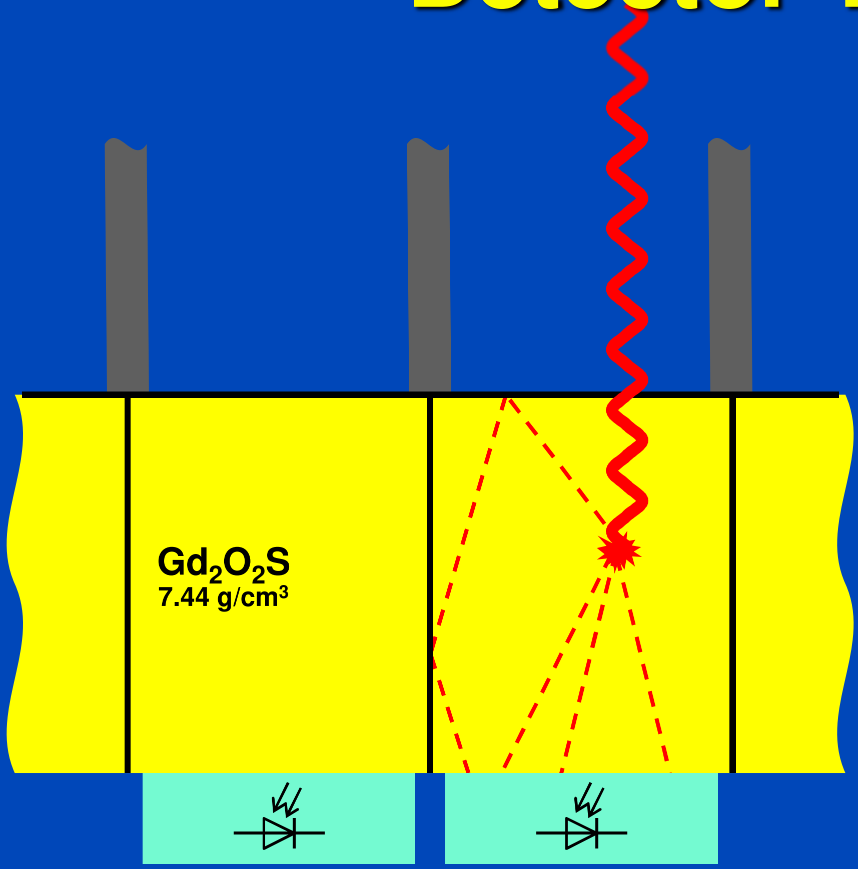

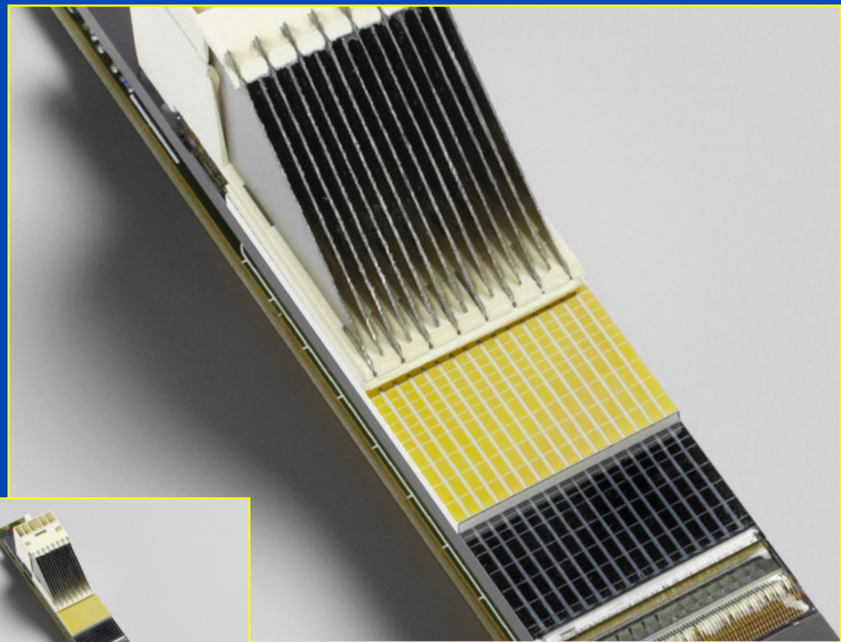

Photo courtesy of Siemens Healthcare, Forchheim, Germany

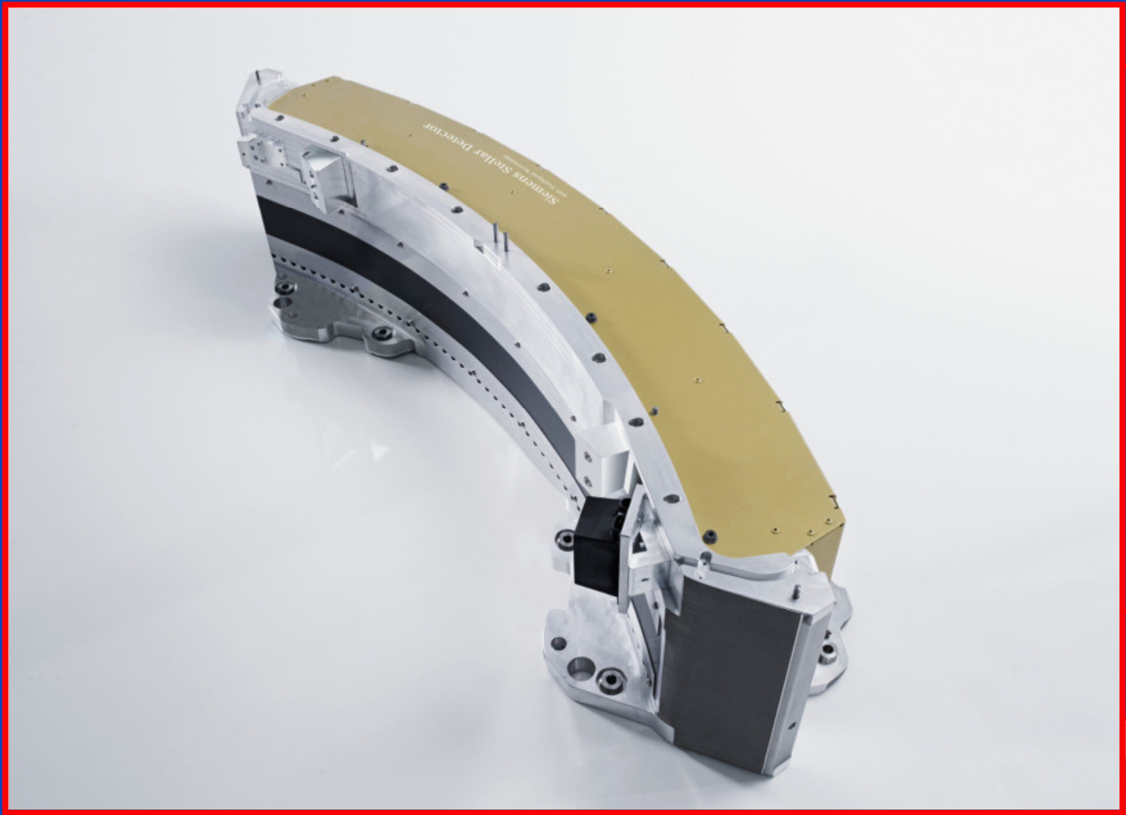

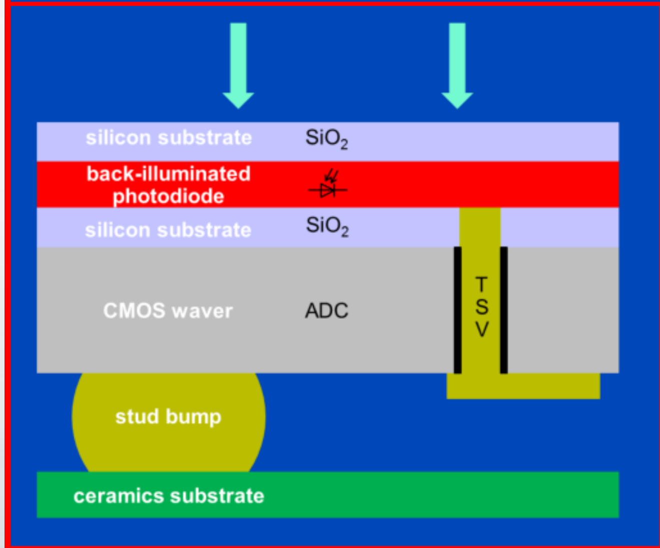

"Stellar detector", modular and 2D tilable, focussed 2D anti scatter grid (Photo courtesy by Siemens)

Somatom Force:
Ultra Low Dose Lung Imaging

- Atypical pneumonia in inspiration and expiration
- Turbo Flash mode, 737 mm/s, 100 kV Sn
- DLP = 7 mGy·cm ≈ 0.1 mSv per scan

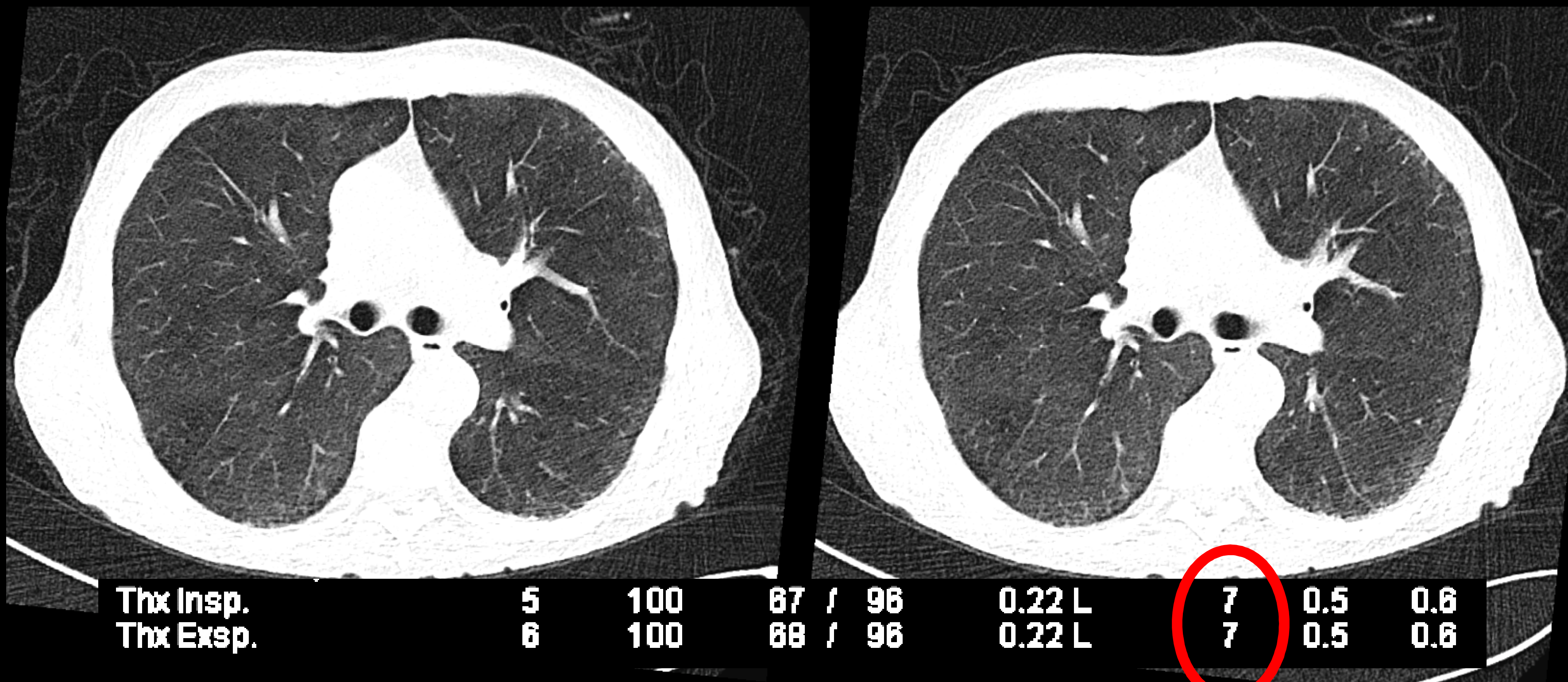

Courtesy of University Hospital Mannheim

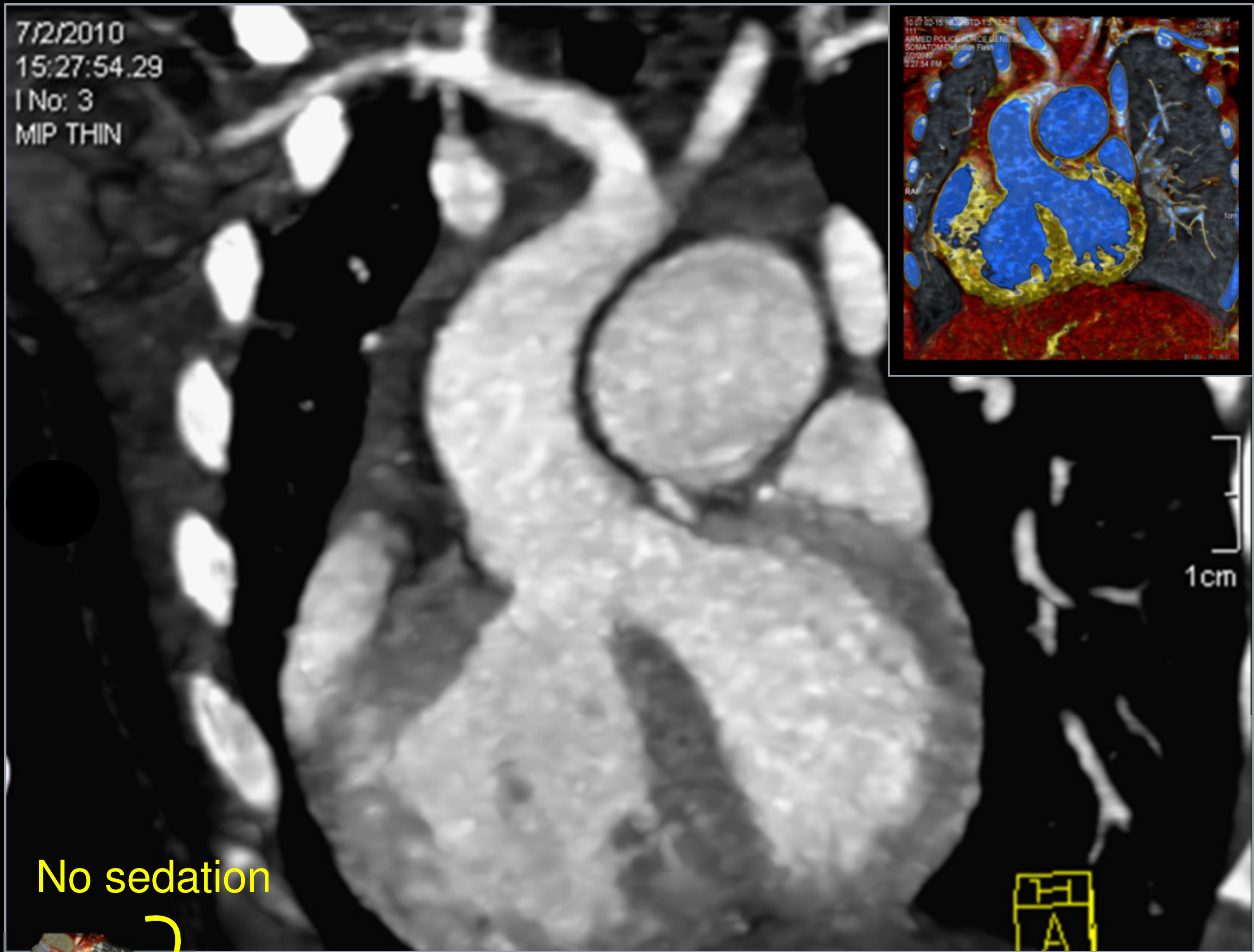

Courtesy of Armed Police Forces Center/ Beijing, China

Child, 12 months

Temporal resolution: 75 ms
Collimation: 2·64×0.6 mm
Spatial resolution: 0.6 mm
Scan time: 0.23 s
Scan length: 78 mm
Rotation time: 0.28 s
80 kV, 36 mAs / rotation

Flash Spiral

Eff. dose: 0.05 mSv

Photon Counting
is the
New Detector Era!

dkfz.

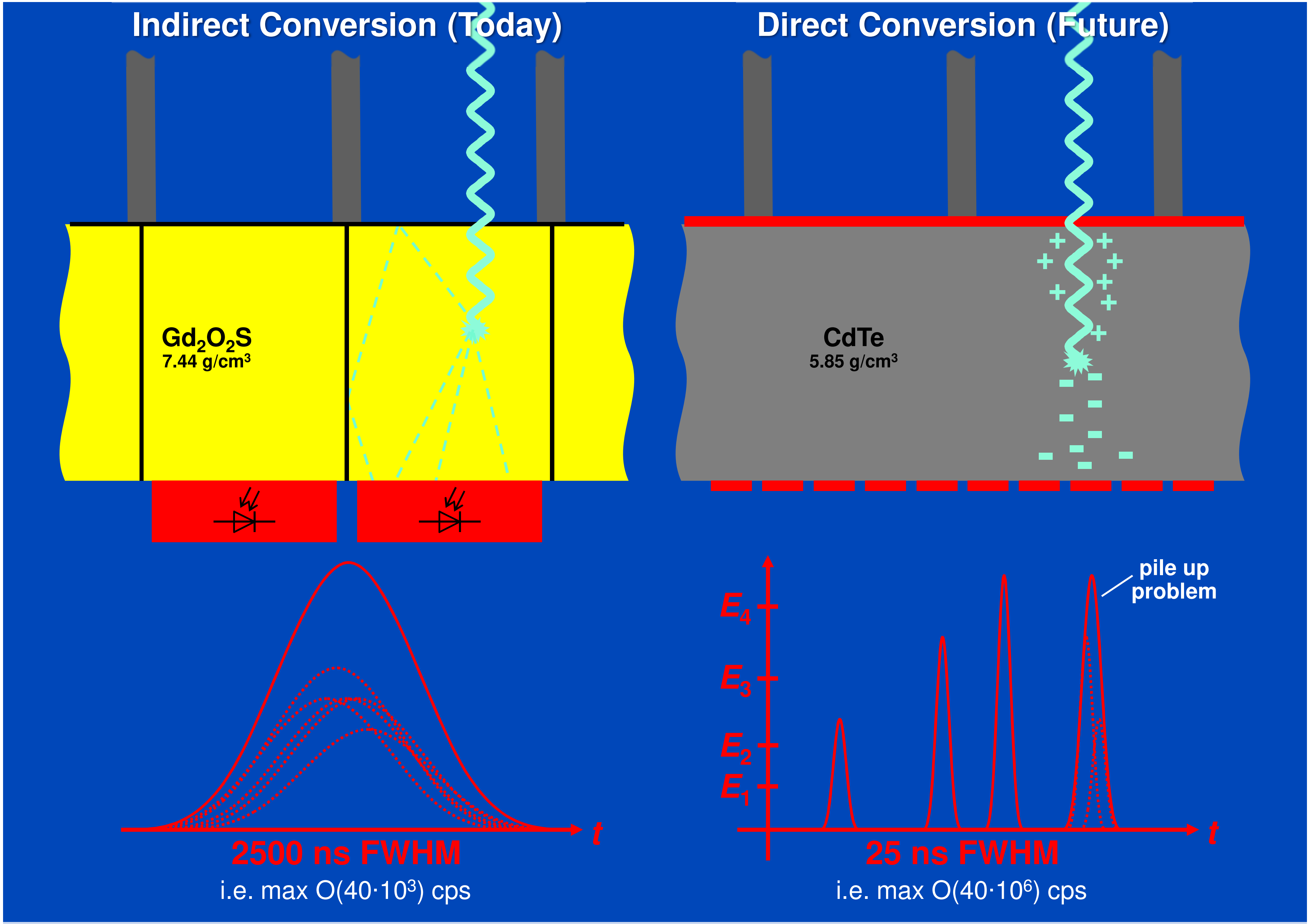

Requirements for CT: up to 10^9 x-ray photon counts per second per mm^2.
Hence, photon counting only achievable for direct converters.

Diagnostic CT (Conventional Detector) of a Low Contrast Phantom

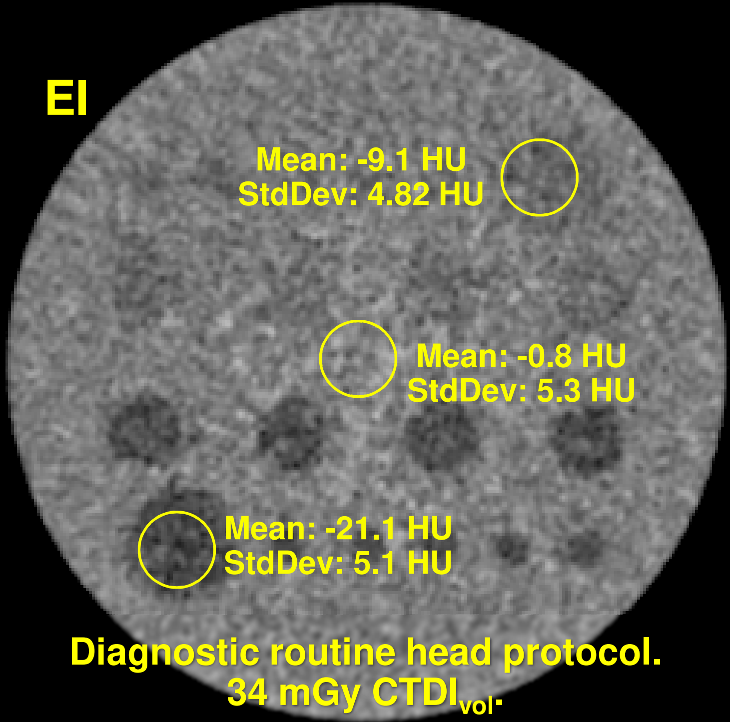

Diagnostic routine head protocol. 34 mGy $CTDI_{vol}$.

Photon Counting Detector CT of a Low Contrast Phantom

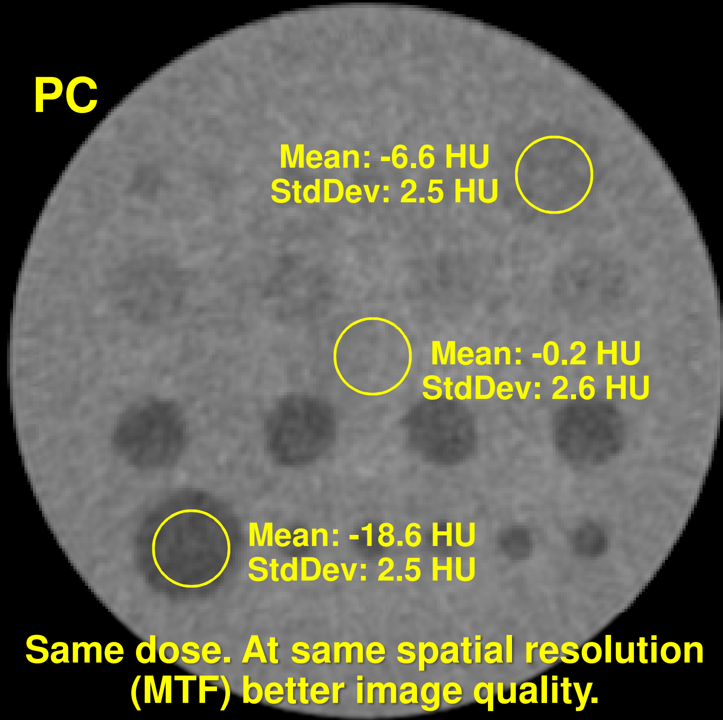

Same dose. At same spatial resolution (MTF) better image quality.

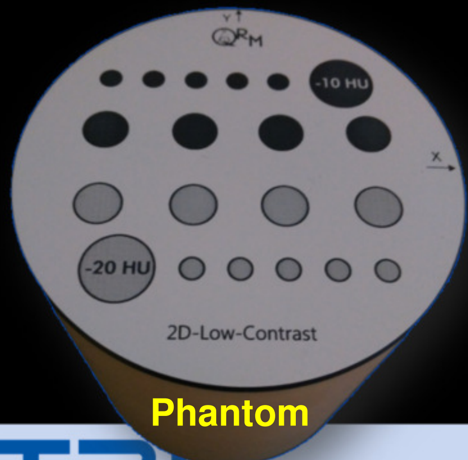

Phantom

Photon Counting Detector

C = 0 HU, W = 80 HU

Dark Image of Photon Counter Shows Background Radiation

18 frames, 5 min integration time per frame

	Energy Integrating (Dexela)	Photon Counting (Dectris Santis)
Events per Frame	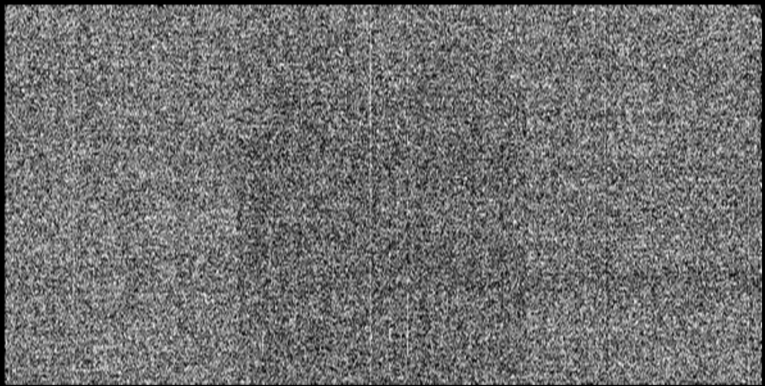 C/W = 0 a.u./70 a.u.	 C/W = 1 cnts/2 cnts
Accumulated Signal	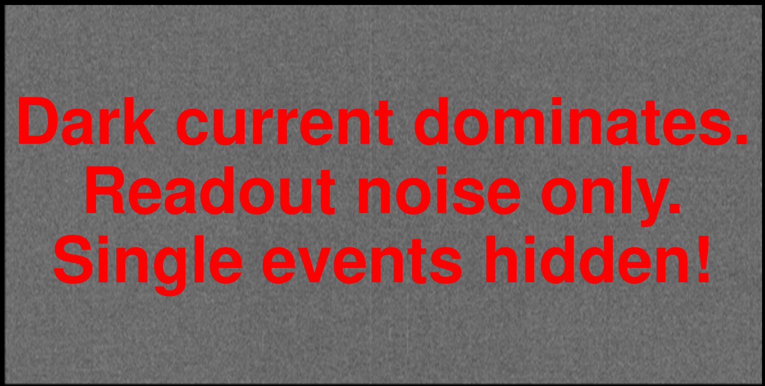 C/W = 30 a.u./450 a.u.	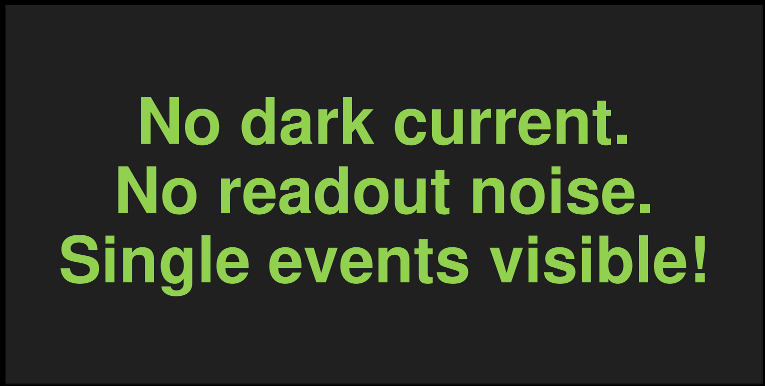 C/W = 3 cnts/8 cnts

Santis: 1 mm CdTe, 150 µm pixel size, 4 thresholds.

No Electronic Noise!

- Photon counting detectors have no electronic noise.
- Extreme low dose situations will benefit
  - Pediadric scans at even lower dose
  - Obese patients with less noise
  - …

Energy Integrating
(Detected Spectra at 100 kV and 140 kV)

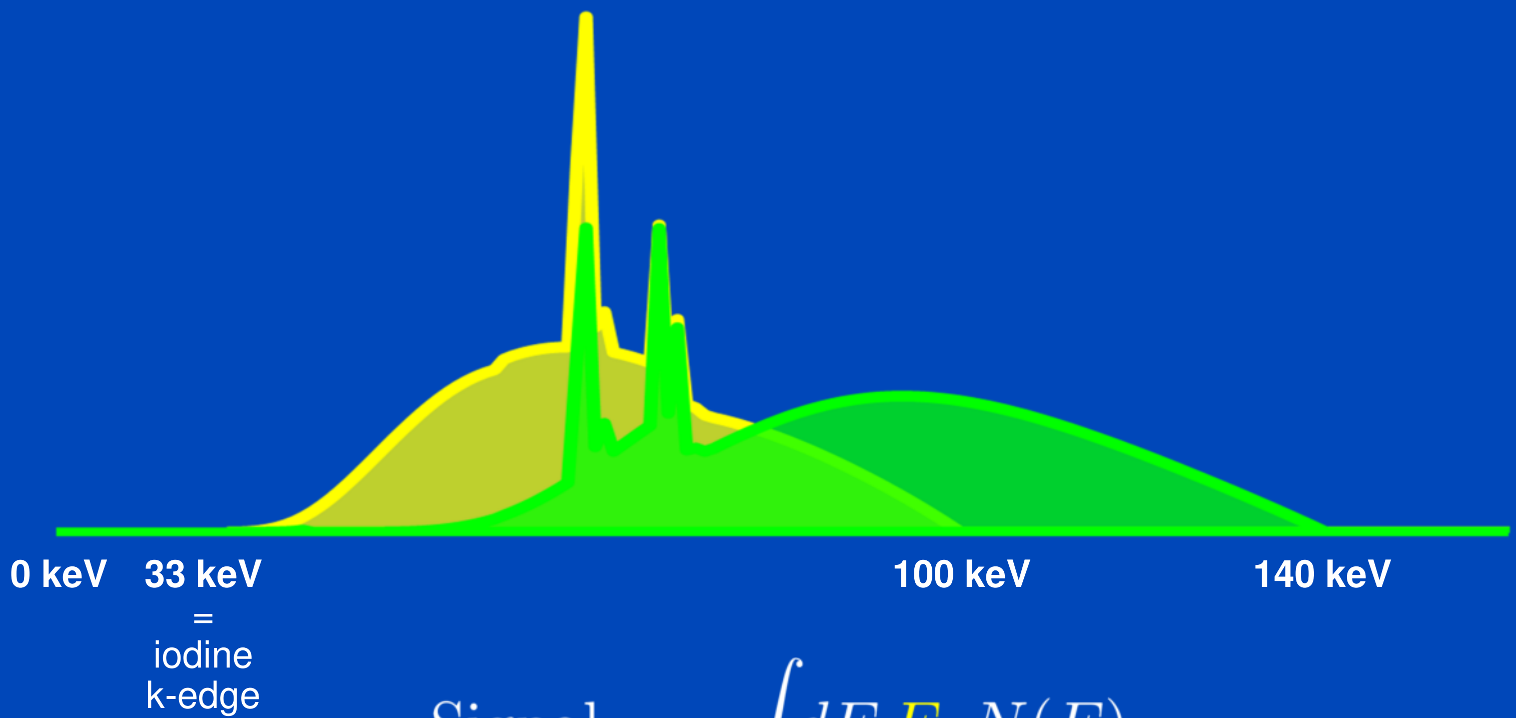

$$\mathrm{Signal}_{\mathrm{EI}} = \int dE\, E\ \ N(E)$$

Spectra as seen after having passed a 32 cm water layer.

Photon Counting
(Detected Spectra at 100 kV and 140 kV)

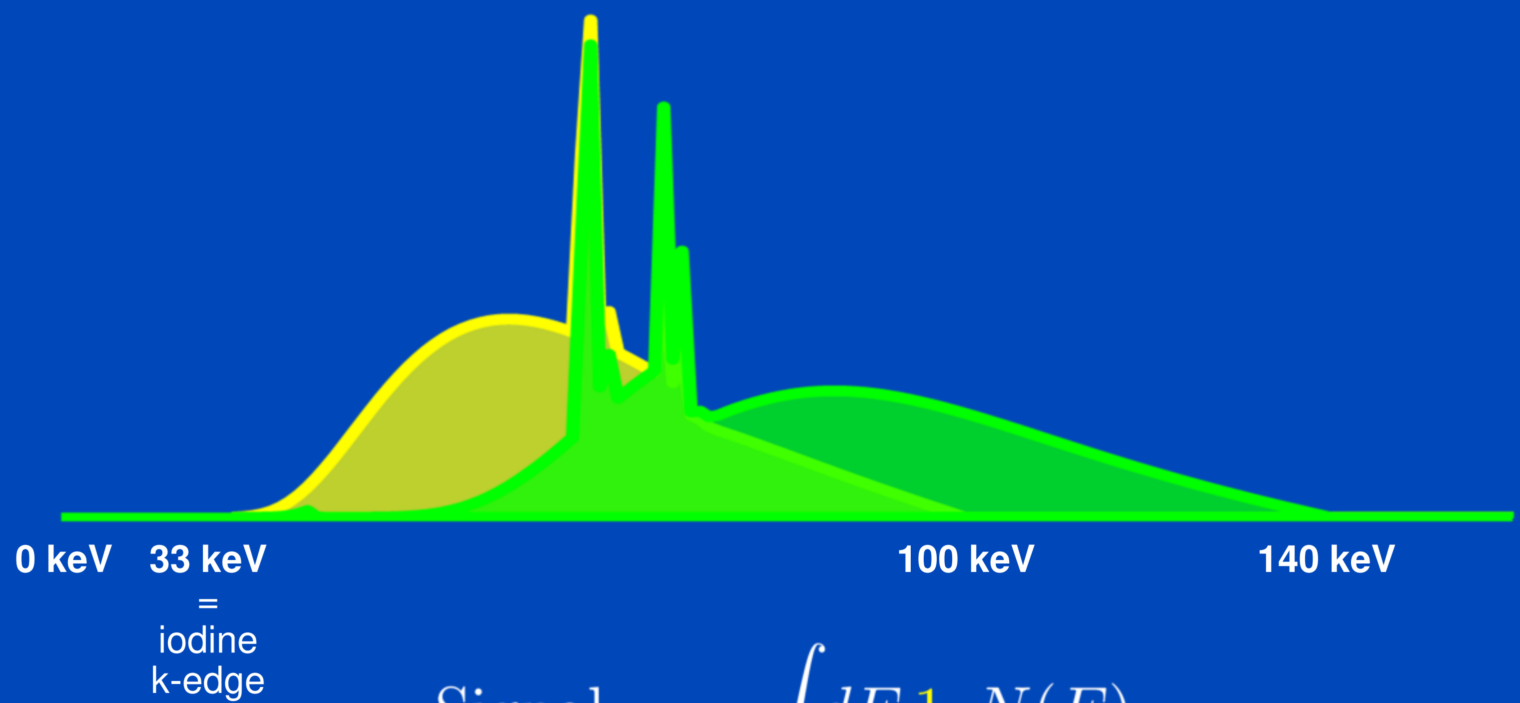

$$\mathrm{Signal}_{\mathrm{PC}} = \int dE\, 1\ N(E)$$

Spectra as seen after having passed a 32 cm water layer.

Expected Value and Variance

- **Transmitted number of photons *N*:**

$$N(E) = N_0(E)e^{-p\psi(E)}$$

- **Poisson distribution:** $\mathrm{E}N(E) = \mathrm{Var}N(E)$
- **Detected signal *S* with sensitivity *s*(*E*):**

$$S = \int dE\, s(E)N(E)$$

- **Expected value and variance of the signal *S*:**

$$\mathrm{E}S = \int dE\, s(E)\mathrm{E}N(E) \text{ and } \mathrm{Var}S = \int dE\, s^2(E)\mathrm{E}N(E)$$

- **Detector sensitivity: PC** $s(E) = 1$**, but EI** $s(E) \propto E$ **!**

Swank Factor

- The Swank factor measures the relative SNR^2, and thus the relative dose efficiency between photon counting (PC) and energy integrating (EI).
- PC always has the highest SNR.

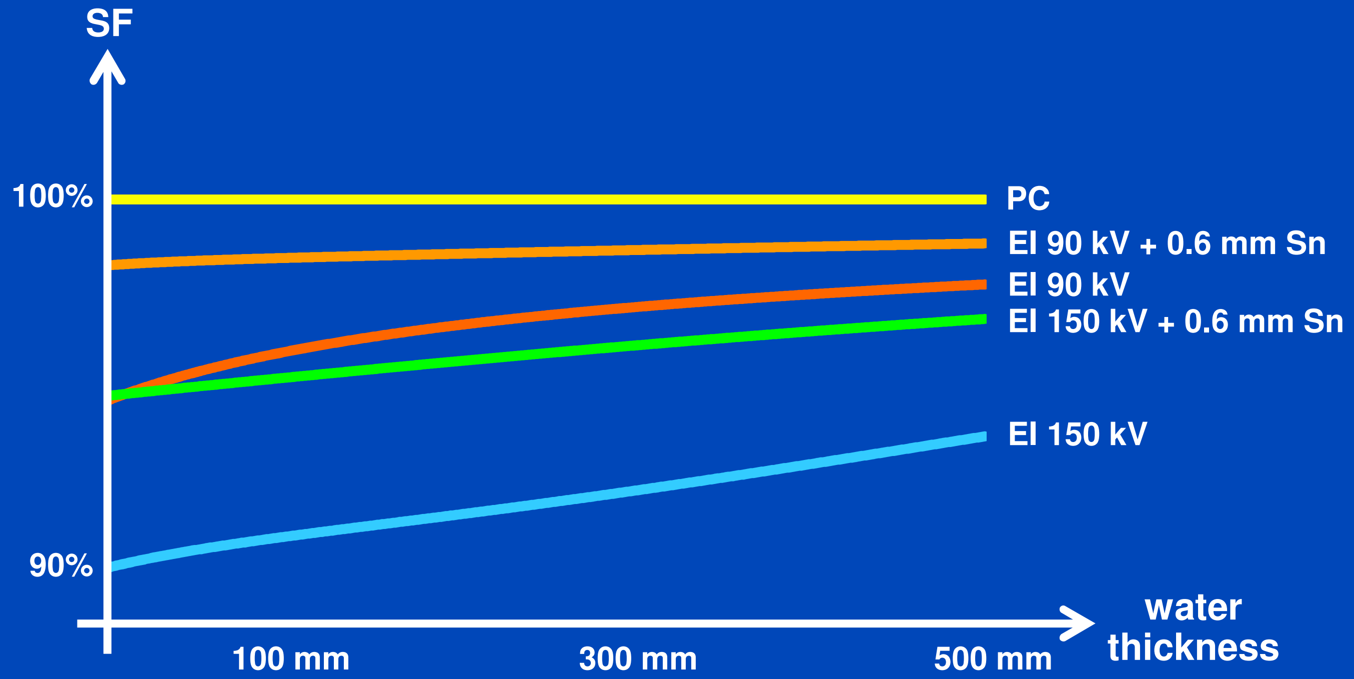

$$\mathrm{SF} = \frac{\mathrm{SNR}_{\mathrm{EI}}^2}{\mathrm{SNR}_{\mathrm{PC}}^2} = \frac{\left(\int dE\, E N(E)\right)^2}{\left(\int dE\, N(E)\right)\left(\int dE\, E^2 N(E)\right)} \leq 1$$

due to Schwarz' inequality

dkfz.

Photon Counting used to Maximize CNR

- With PC energy bins can be weighted individually.
- To optimize the CNR the optimal bin weighting factor is given by (weighting after log):

$$w_b \propto \frac{C_b}{V_b}$$

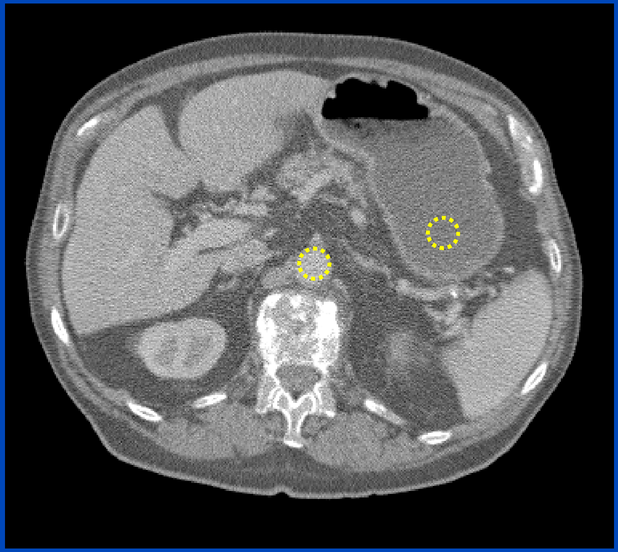

- The resulting CNR is

$$\mathrm{CNR}^2 = \frac{\left(\sum_b w_b C_b\right)^2}{\sum_b w_b^2 V_b}$$

- At the optimum this evaluates to

$$\mathrm{CNR}^2 = \sum_{b=1}^{B} \mathrm{CNR}_b^2$$

Energy Integrating vs. Photon Counting
with 1 bin from 20 to 140 keV

Energy Integrating

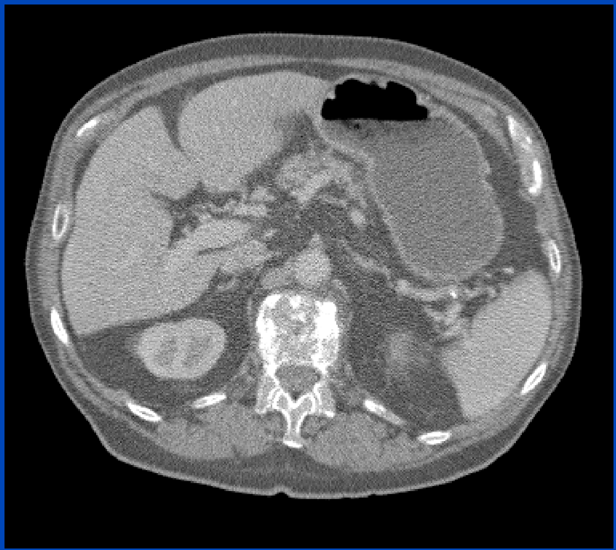

PC minus EI

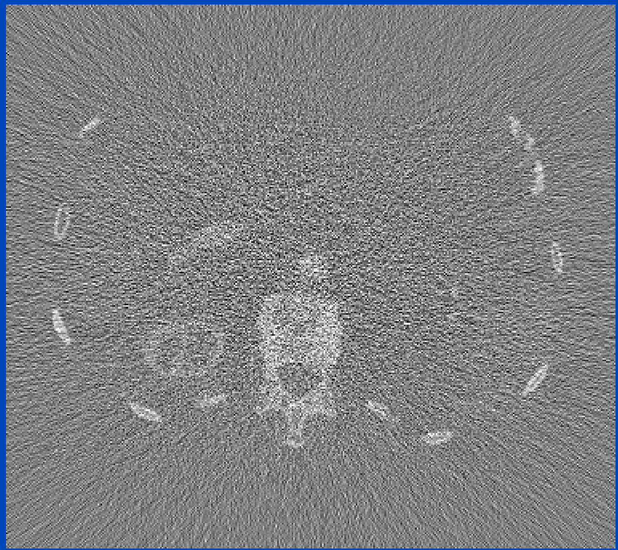

Photon Counting

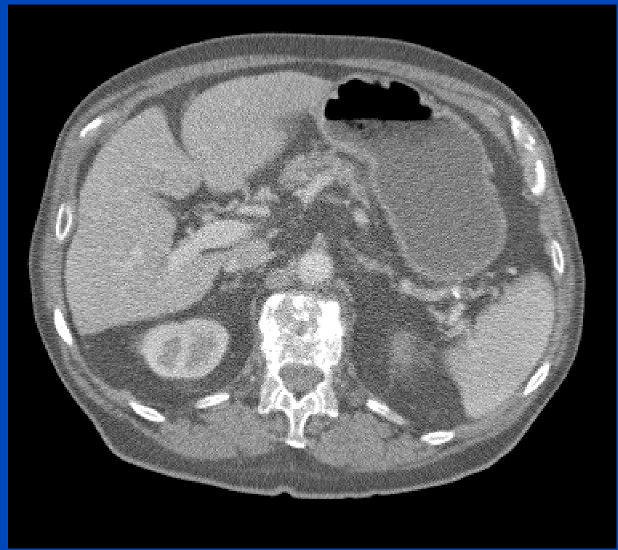

CNR = 2.11

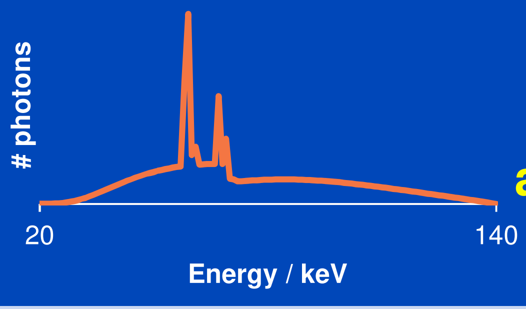

CNR = 2.95

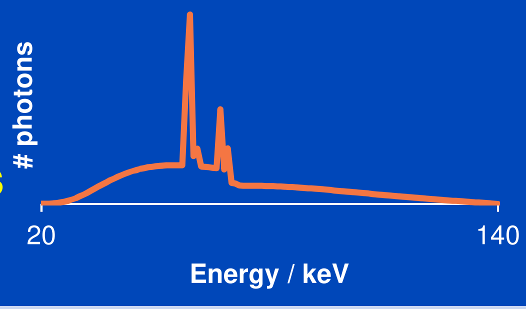

40% CNR improvement or 49% dose reduction achievable due to improved Swank factor and more weight on low energies (iodine contrast benefits).

Images: *C* = 0 HU, *W* = 700 HU, difference image: *C* = 0 HU, *W* = 350 HU, bins start at 20 keV

dkfz.

Energy Integrating vs. Photon Counting
with 4 bins from 20 to 140 keV

Energy Integrating

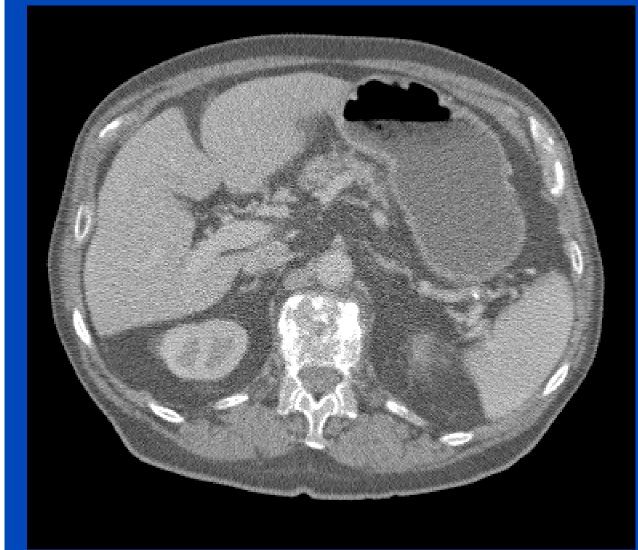

CNR = 2.11

PC minus EI

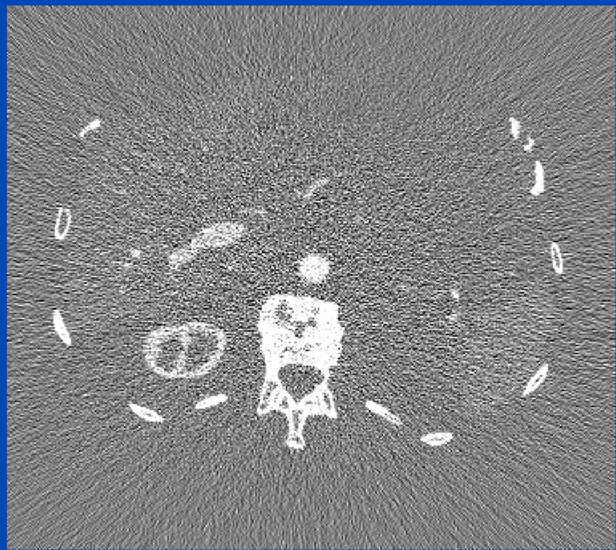

Photon Counting

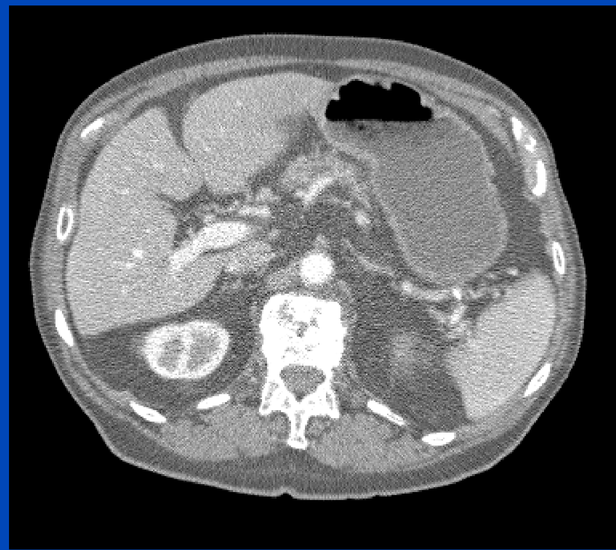

CNR = 4.19

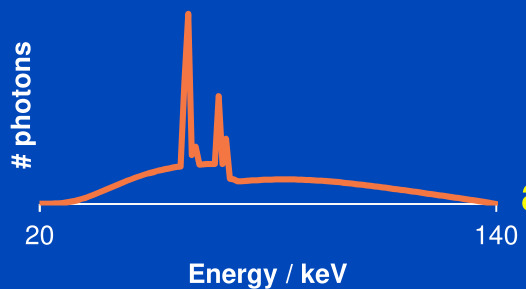

99% CNR improvement or 75% dose reduction achievable due to improved Swank factor and optimized energy weighting.

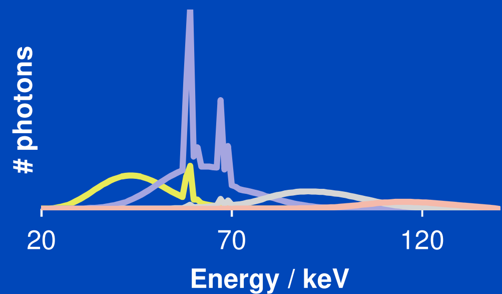

Images: *C* = 0 HU, *W* = 700 HU, difference image: *C* = 0 HU, *W* = 350 HU, bins start at 20 keV

dkfz.

Spatial Resolution

- Small electrodes are necessary to avoid pile-up.
- High bias voltages (around 300 V) limit charge diffusion and thus blurring in the non-structured semiconductor layer.
- Thus, higher spatial resolution is achievable.

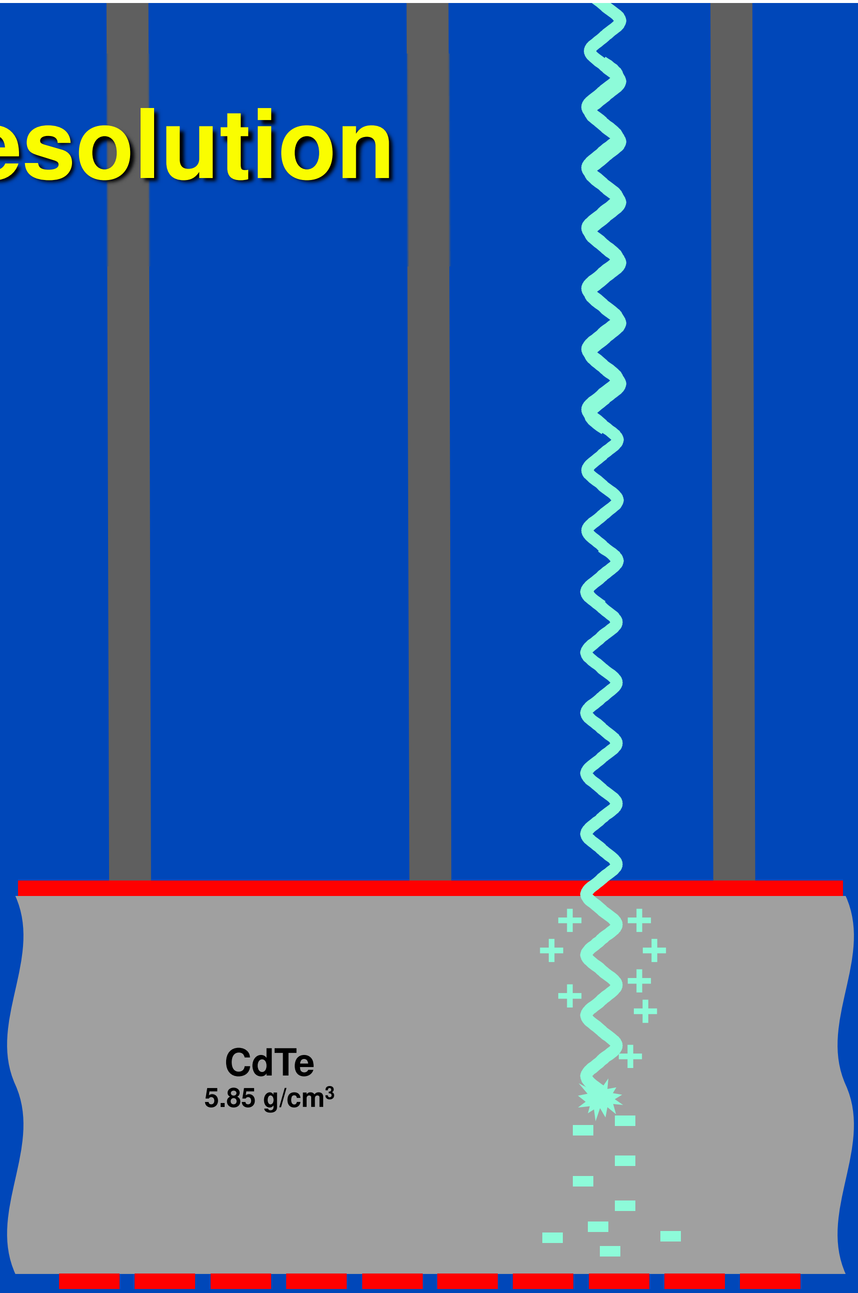

To Bin or not to Bin?

(the continuous view)

- We have $\mathrm{PSF}(x) = s(x) * a(x)$ and $\mathrm{MTF}(u) = S(u)A(u)$.
- From Rayleigh‘s theorem we find noise is

$$N^2 = \int dx\, a^2(x) = \int du\, A^2(u) = \int du\, \frac{\mathrm{MTF}^2(u)}{S^2(u)}$$

Avoid binning, if possible!

- Compare s… arge (B) detector pixels:

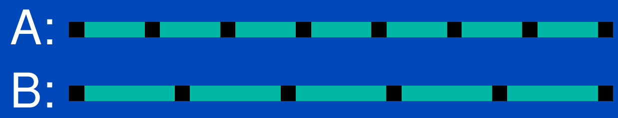

- We have $S_\mathrm{A}(u) > S_\mathrm{B}(u)$ and thus $N_\mathrm{A}^2 < N_\mathrm{B}^2$.
- This means that a desired PSF/MTF is often best achieved with smaller detectors.

To Bin or not to Bin?

(the discrete view)

- Let detector B be the 2-binned version of detector A:

$$B_{2n} = \tfrac{1}{2}(A_{2n} + A_{2n+1}) \qquad \operatorname{Var} B = \tfrac{1}{2}\operatorname{Var} A$$

- Assume LI to be used to find in-between pixel values. Wlog we may then consider B to be upsampled with mid-point interpolatio… …ector A:

$$\hat{B} = (\ldots \ldots B_6,\ \ldots)$$

- To obtai… …ed detector we need…

$$a = \tfrac{1}{2}(1,\ 1) * \tfrac{1}{4}(1,\ 2,\ 1) = \tfrac{1}{8}(1,\ 3,\ 3,\ 1)$$

20% more noise may be compensated by 20% more x-ray dose. Any alternative? Yes:

Avoid binning, if possible!

In 2D binning implies 44% more noise or dose. Again, the answer is: „not to bin“.

- Noise propagation yields 20% more noise (variance) for the binned detector:

$$\operatorname{Var}\hat{A} = \tfrac{20}{64}\operatorname{Var}A = \tfrac{5}{16}\operatorname{Var}A$$

$$\operatorname{Var}\hat{B} = \tfrac{3}{8}\operatorname{Var}A = \tfrac{6}{5}\operatorname{Var}\hat{A} = 1.2\operatorname{Var}\hat{A}$$

To Bin or not to Bin

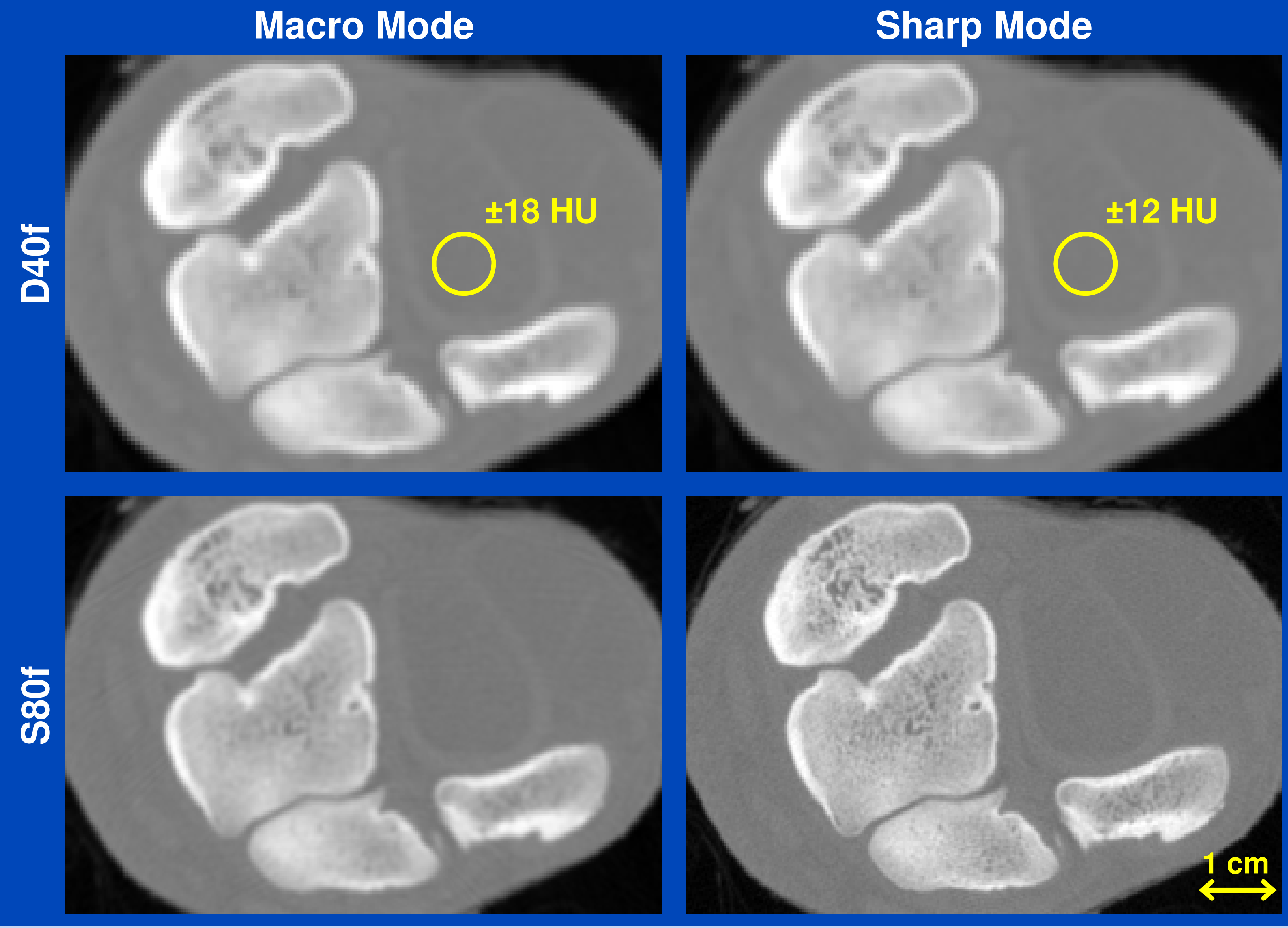

Images taken at Somatom CounT at the DKFZ by Sawall, Kachelrieß et al. *C* = - 50 HU, *W* = 1900 HU

dkfz.

CounT Std | CounT HighRes

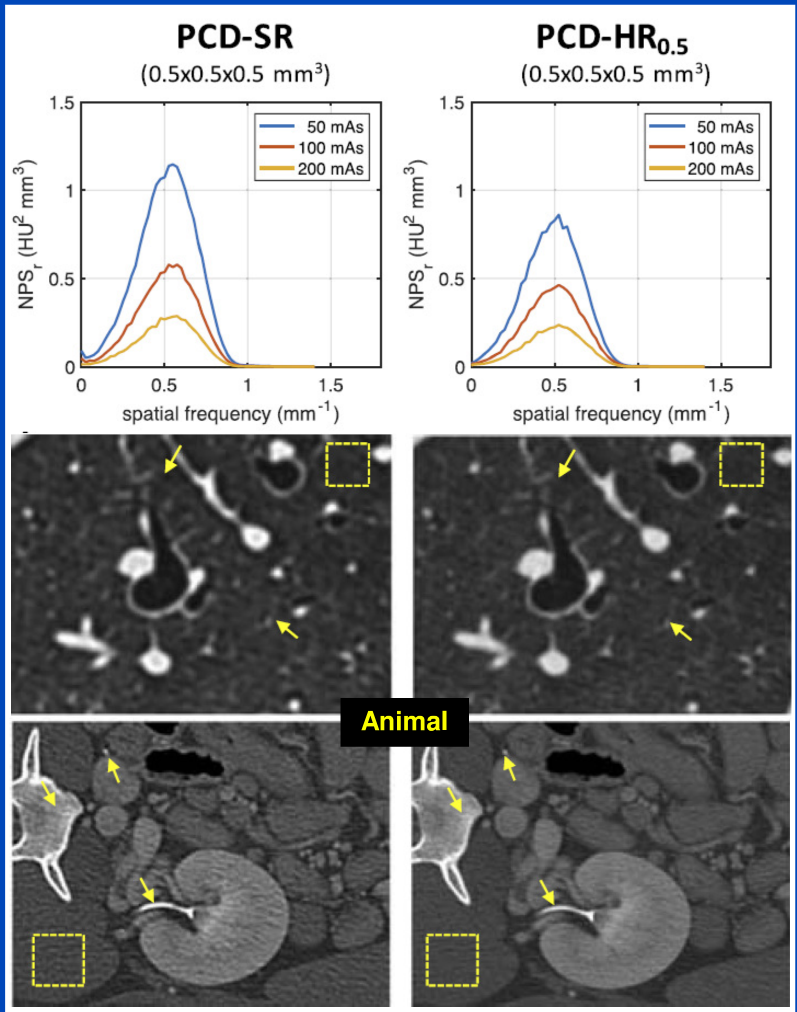

“However, when comparing with standard resolution data at same in-plane resolution and slice thickness, the PCD 0.25 mm detector mode showed **19% less image noise** in phantom, animal, and human scans.”

CounT Std | CounT HighRes

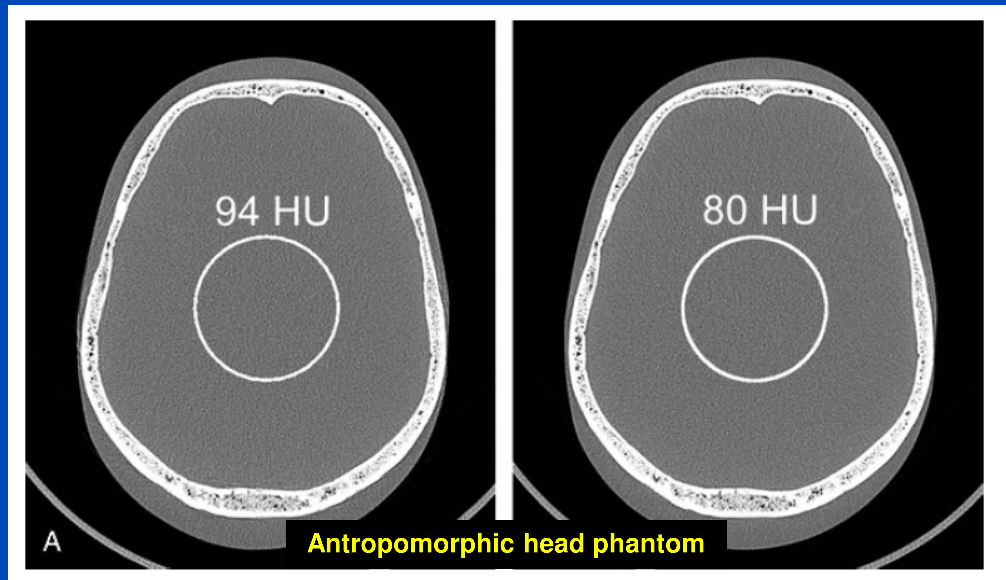

Pourmorteza et al. Dose Efficiency of Quarter-Millimeter Photon-Counting Computed Tomography: First-in-Human Results. Invest. Radiol. 53(6), 2018.

Leng et al. 150 µm Spatial Resolution Using Photon-Counting Detector Computed Tomography Technology. Invest. Radiol. 53(11), 2018

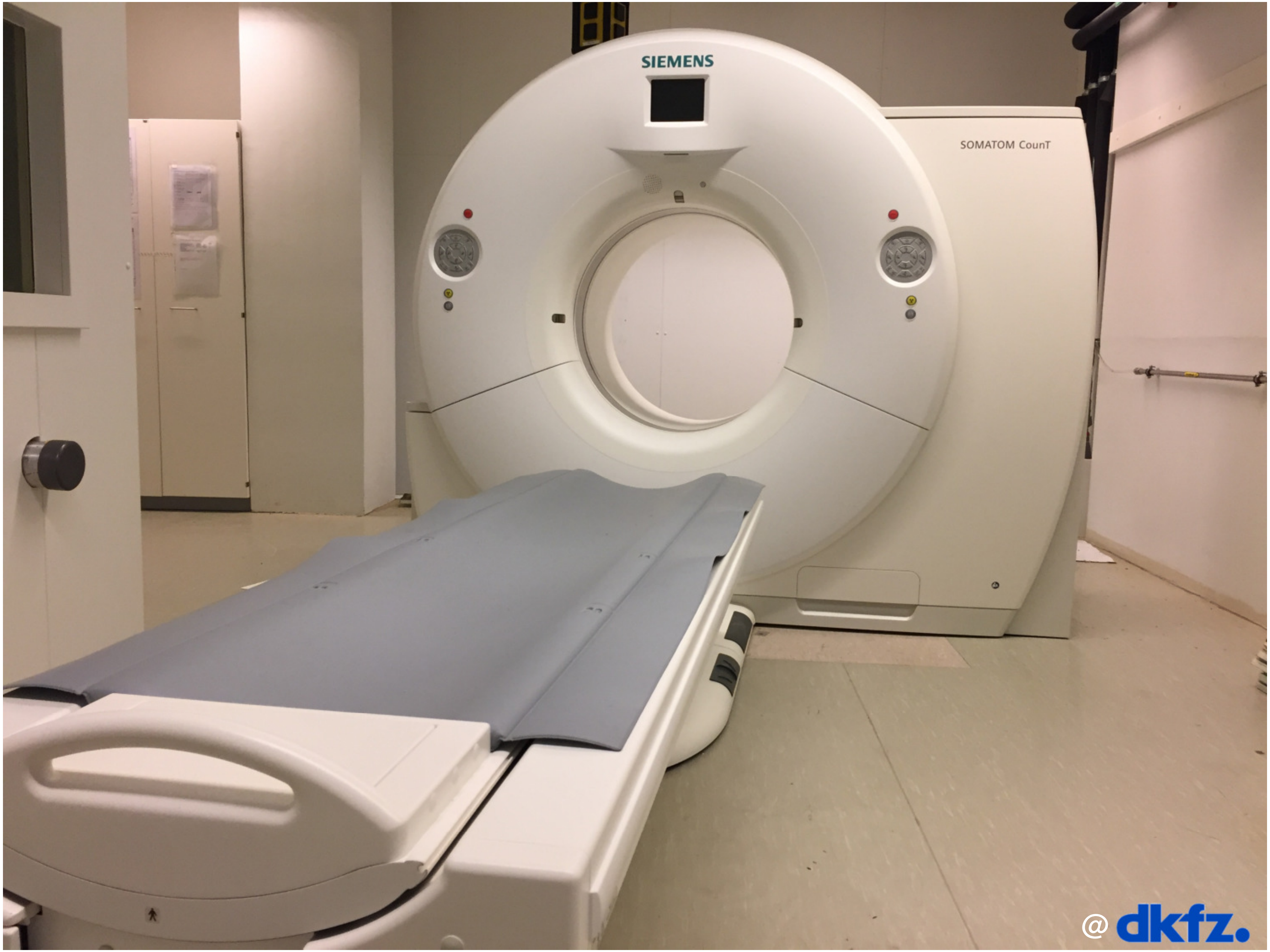
SIEMENS
SOMATOM CounT
@ dkfz.

Readout Modes of the Siemens CounT

Macro Mode
1×2 readouts
16 mm z-coverage

12	12	12	12
12	12	12	12
12	12	12	12
12	12	12	12

Chess Mode
2×2 readouts
16 mm z-coverage

12	34	12	34
34	12	34	12
12	34	12	34
34	12	34	12

Sharp Mode
5×1 readouts
12 mm z-coverage

1	1	1	1
1	1	1	1
1	1	1	1
1	1	1	1

2	2	2	2
2	2	2	2
2	2	2	2
2	2	2	2

UHR Mode
4×2 readouts
8 mm z-coverage

12	12	12	12
12	12	12	12
12	12	12	12
12	12	12	12

No FFS on thread B (photon counting detector).
4×4 subpixels of 225 µm size = 0.9 mm pixels (0.5 mm at isocenter).
The whole detector consists of 128×1920 subpixels = 32×480 macro pixels.

Ultra-High Resolution on Demand

Energy Integrating CT
(Somatom Flash)

Photon Counting CT
(Somatom CounT. UHR-Mode)

MAYO CLINIC

Courtesy of Cynthia McCollough, Mayo Clinic, Rochester, USA.

MECT

Ca-Gd-I Decomposition

Chess pattern mode
140 kV, 20/35/50/65 keV
***C* = 0 HU, *W* = 1200 HU**

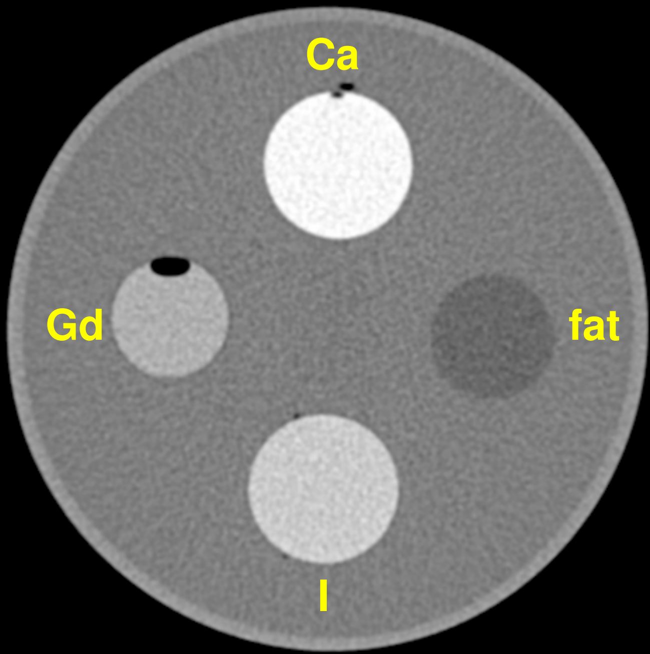

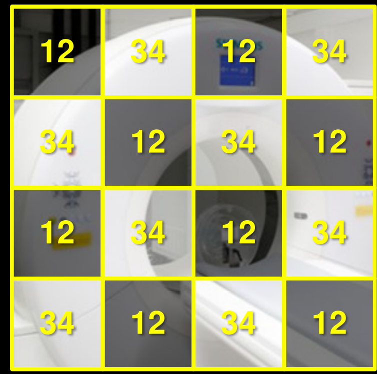

Calcium image

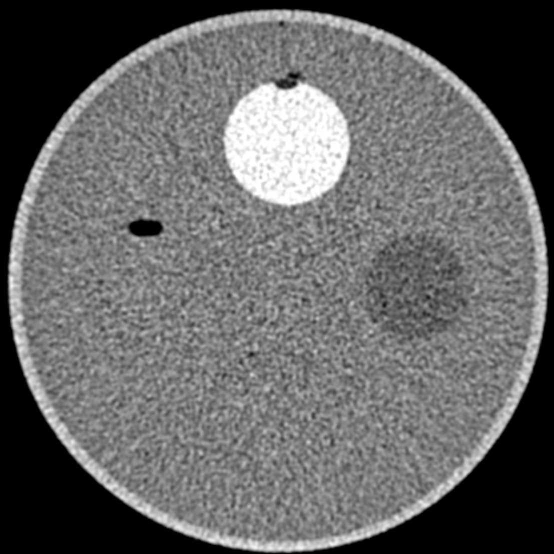

Gadolinium image

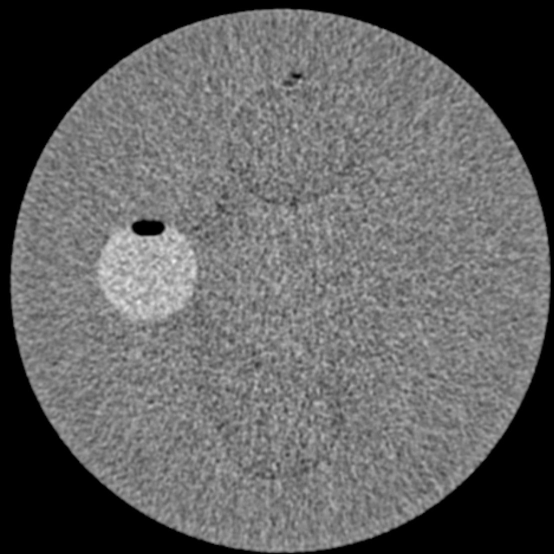

Iodine image

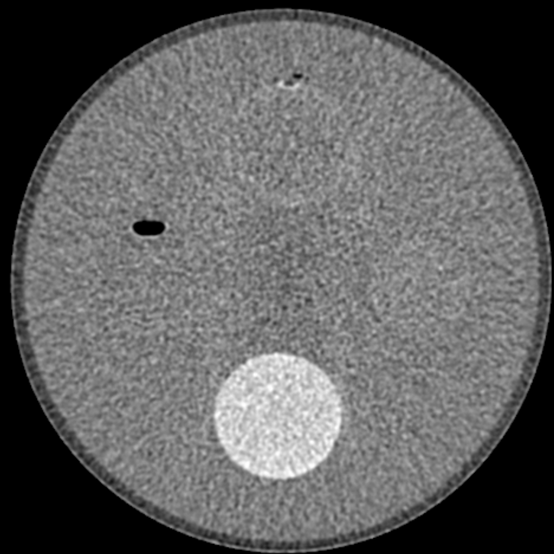

Courtesy of Siemens Healthcare

DECT Examples

(Slide Courtesy of Siemens Healthcare)

DE bone removal

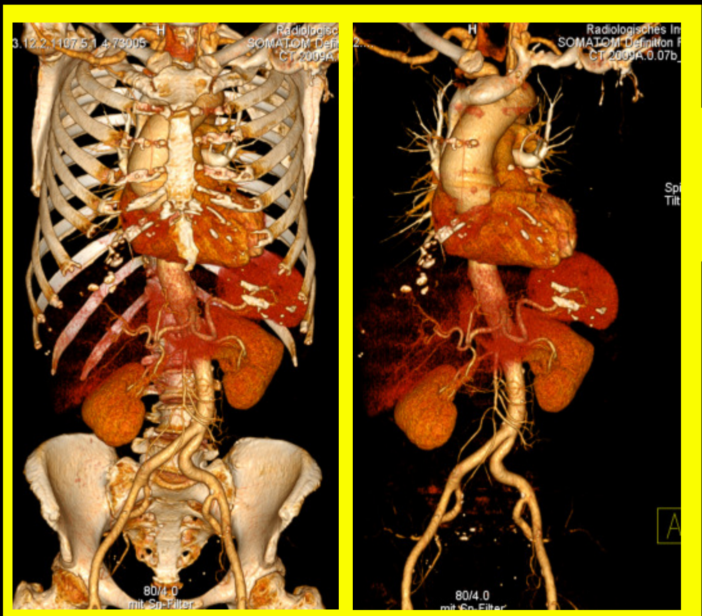

Single DECT scan

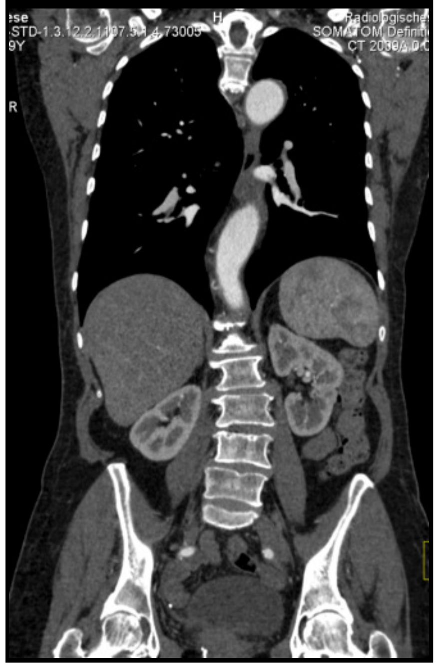

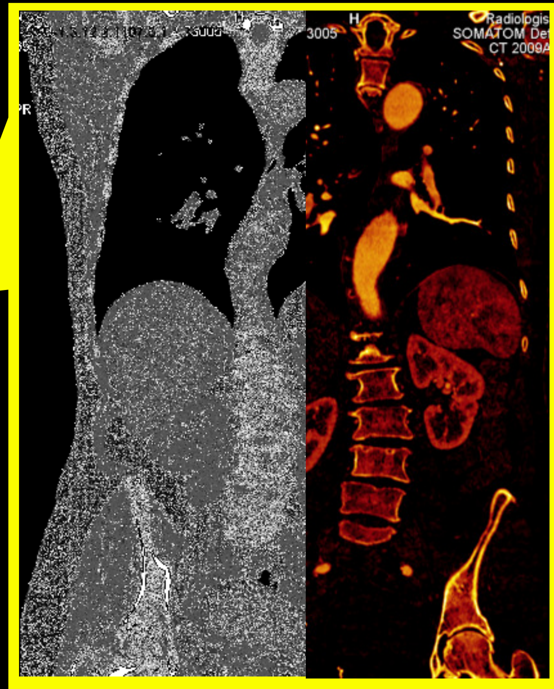

Virtual non-contrast and iodine image

Dual Energy whole body CTA: 100/140 Sn kV @ 0.6 mm

Courtesy of Friedrich-Alexander University Erlangen-Nürnberg

DECT Examples

(Slide Courtesy of Siemens Healthcare)

- **“Spectroscopy“: more specific tissue characterization**
  → Detection and visualization of calcium, iron, uric acid, …..

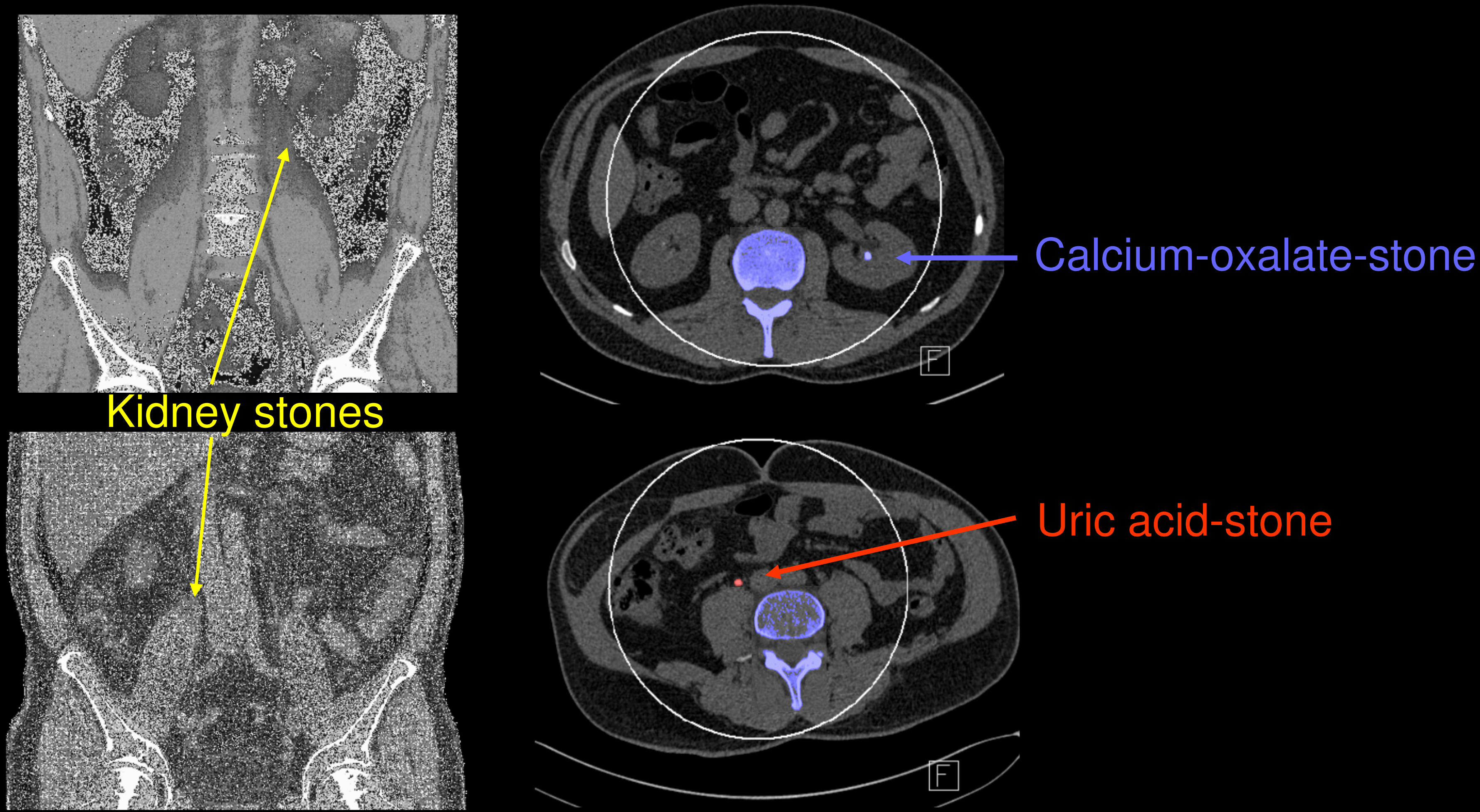

Courtesy of Klinikum Großhadern, LMU München

First Peer Reviewed Publication on CounT from NIH February 2016

EI (Definition Flash)

PC (CounT)

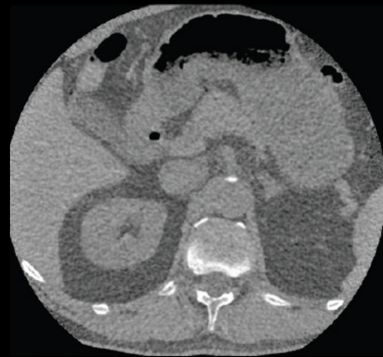

PC Virtual Non-Contrast

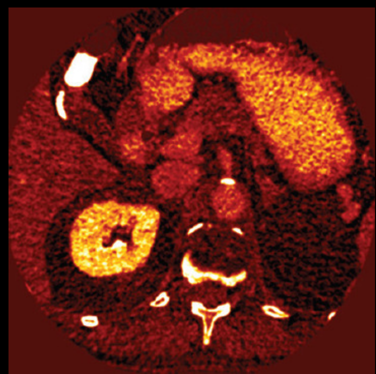

PC Iodine Map

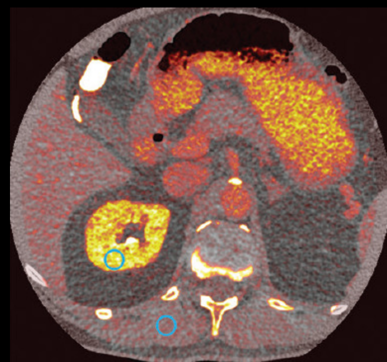

PC Merged

Courtesy of National Institutes of Health, Berthesda, USA

Pourmorteza A et al., Abdominal Imaging with Contrast-enhanced Photon-counting CT: First Human Experience. Radiology. 2016 Apr;279(1):239-45

Potential Advantages of Photon Counting Detectors in CT

- Higher spatial resolution due to
  - smaller pixels
  - lower cross-talk between pixels
- Lower dose/noise due to
  - energy bin weighting
  - no electronic noise
  - Swank factor = 1
  - smaller pixels
- Spectral information on demand
  - single energy
  - dual energy
  - multiple energy
  - virtual monochromatic
  - K-edge imaging
  - …

Motion Modelling is the new Reconstruction Era!

CT is much faster than one motion cycle!

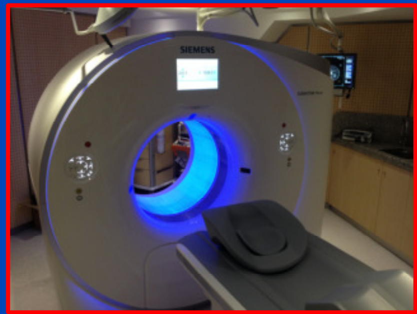

Siemens Somatom Force DSCT

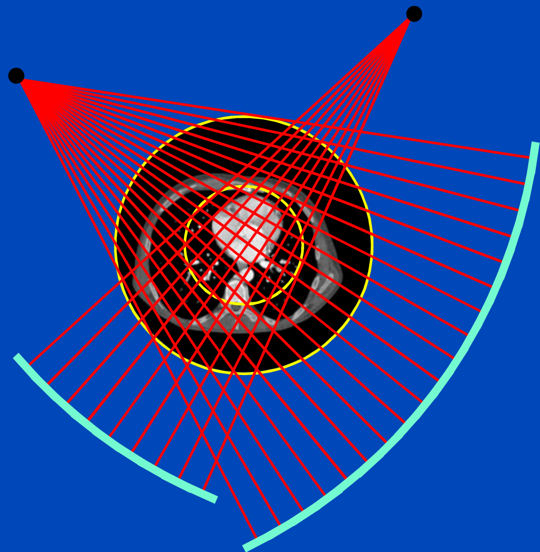

CBCT is much slower than one motion cycle!

Varian True Beam CBCT

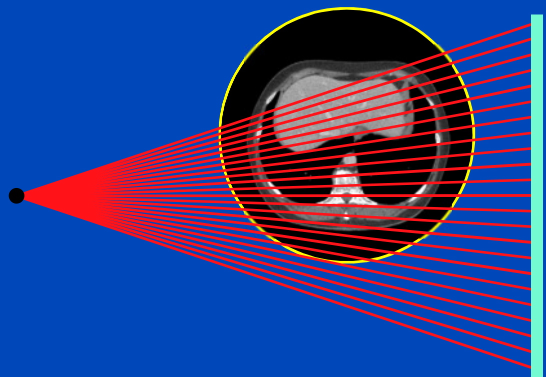

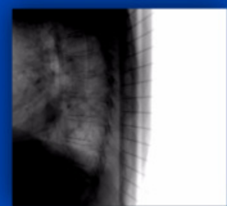

Motion in Cardiac CT

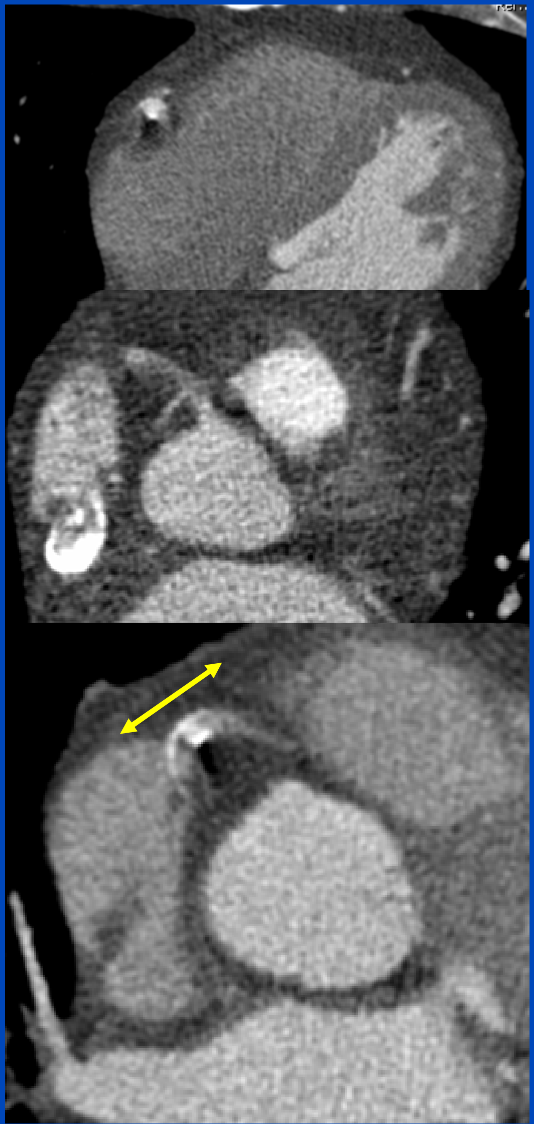

- In cardiac CT, the imaging of small and fast moving vessels places high demands on the spatial and temporal resolution of the reconstruction.
- Mean displacements of $d \approx \frac{t_{rot}}{2}\,\bar{v} \approx \frac{250}{2}\,\mathrm{ms}\; 50\,\frac{\mathrm{mm}}{\mathrm{s}} = 6.25\,\mathrm{mm}$ are possible (RCA mean velocity measurements[1,2,3,4]).
- Standard FDK-based cardiac reconstruction might have an insufficient temporal resolution introducing strong motion artifacts.

[1] Husmann et al. Coronary Artery Motion and Cardiac Phases: Dependency on Heart Rate - Implications for CT Image Reconstruction. Radiology, Vol. 245, Nov 2007.
[2] Shechter et al. Displacement and Velocity of the Coronary Arteries: Cardiac and Respiratory Motion. IEEE Trans Med Imaging, 25(3): 369-375, Mar 2006
[3] Vembar et al. A dynamic approach to identifying desired physiological phases for cardiac imaging using multislice spiral CT. Med. Phys. 30, Jul 2003.
[4] Achenbach et al. In-plane coronary arterial motion velocity: measurement with electron-beam CT. Radiology, Vol. 216, Aug 2000.

PAMoCo

Generate 2K+1 Partial Angle Reconstructions

Initial segmented stack volume

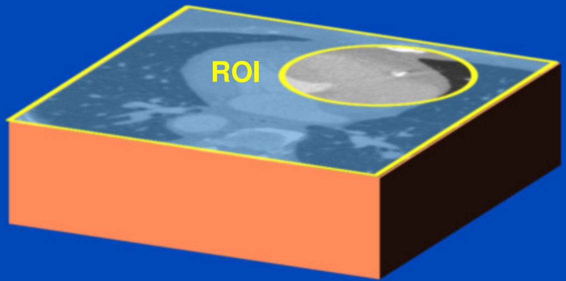

Subdivide the projection data $p'(\vartheta, \xi)$ **into 2K + 1 overlapping sectors**

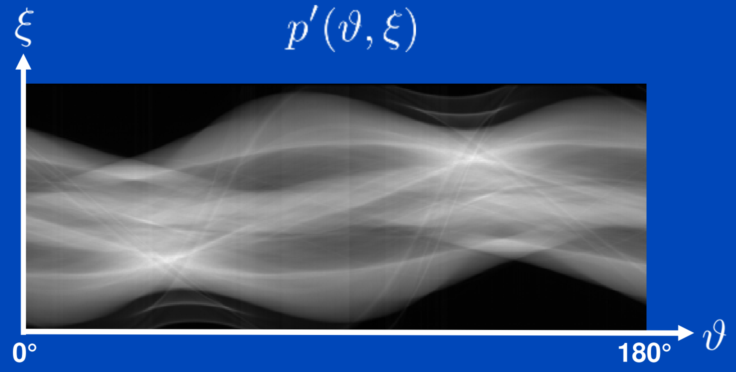

PAMoCo

Generate 2K+1 Partial Angle Reconstructions

Initial segmented stack volume

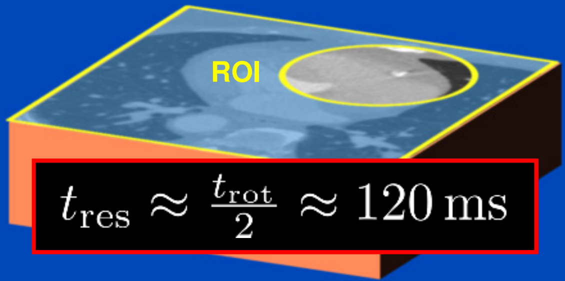

$$t_{\mathrm{res}} \approx \frac{t_{\mathrm{rot}}}{2} \approx 120\,\mathrm{ms}$$

Subdivide the projection data $p'(\vartheta, \xi)$ into 2K + 1 overlapping sectors

ξ $p'(\vartheta,\xi)$

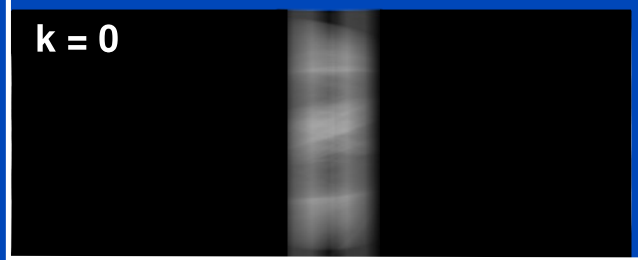

0° 180° ϑ

$\underbrace{\qquad}_{2\Delta\vartheta}$

$$p_k(\vartheta,\xi) = w_k(\vartheta)p'(\vartheta,\xi)$$

$$w_k(\vartheta) = \Lambda((\vartheta - \vartheta_k)/2\Delta\vartheta)$$

Partial angle reconstructions $f_k(\boldsymbol{r})$

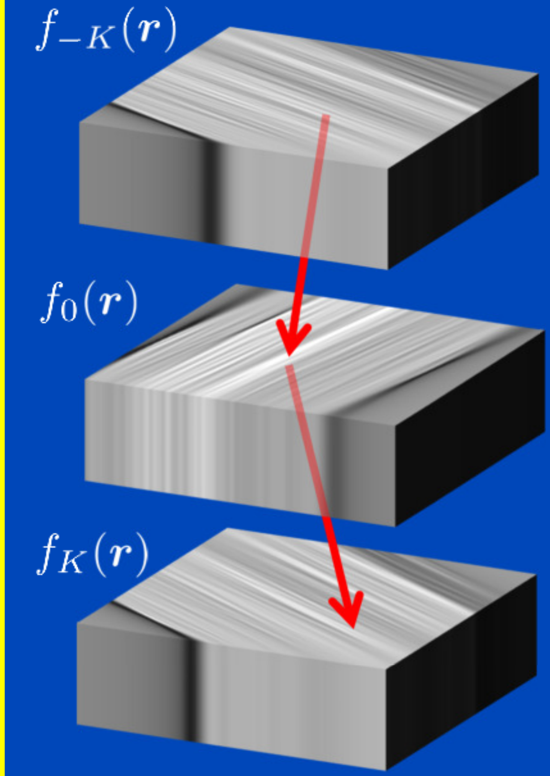

$$t_{\mathrm{res}} \approx \frac{t_{\mathrm{rot}}/2}{(2K+1)/2} \approx 10\,\mathrm{ms}$$

FWHM = $\Delta\vartheta$ **K = 12**

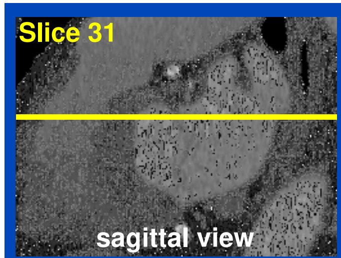

Patient 1

FBP **PAMoCo**

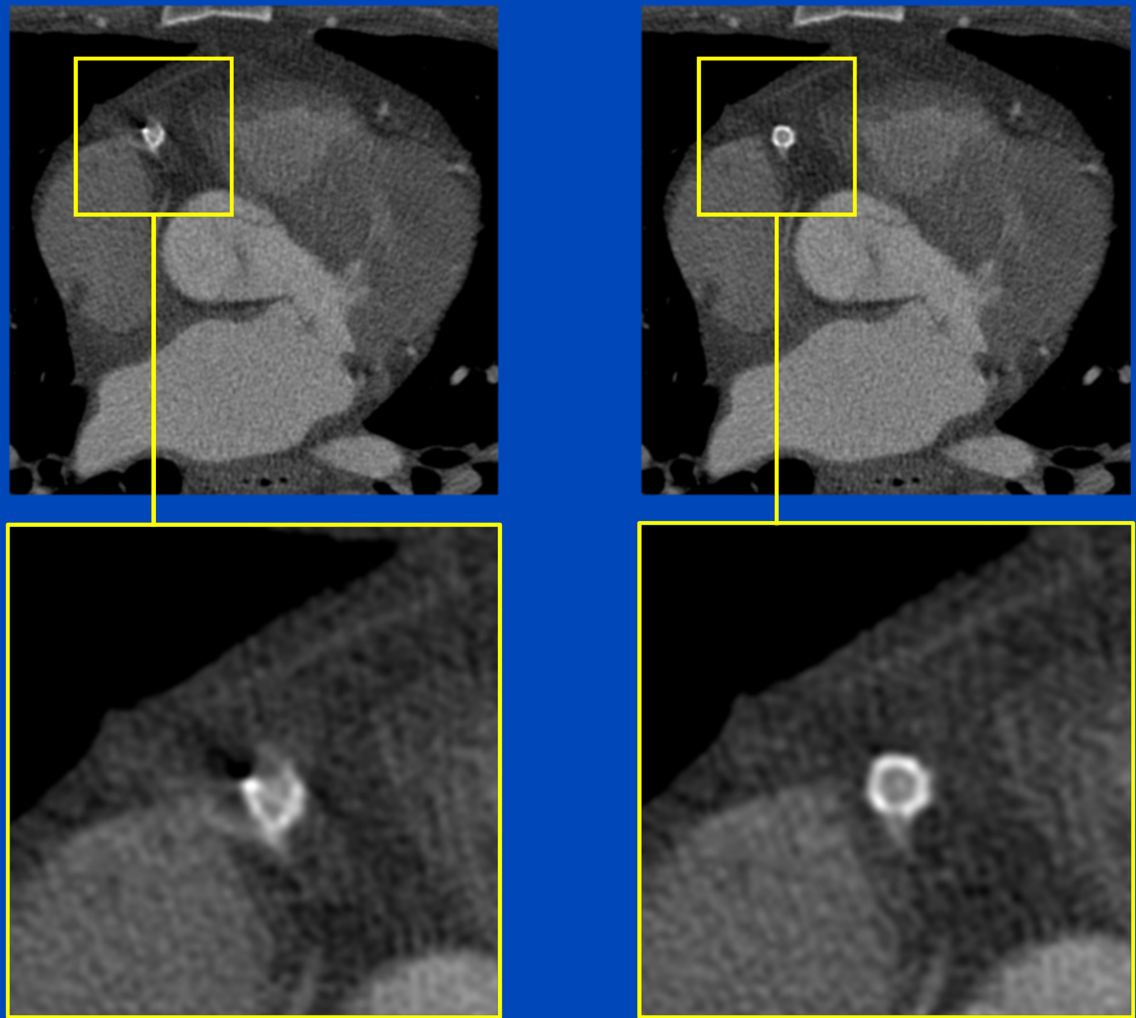

SIEMENS

$\overline{\mathrm{HR}}$ = 74 bpm, c = 30%,
C = 400 HU, W = 1500 HU

PAMoCo with $N_t \times N_\lambda \times 3 = 3 \times 3 \times 3 = 27$
parameter each stack

dkfz.

Patient 1

FBP

PAMoCo

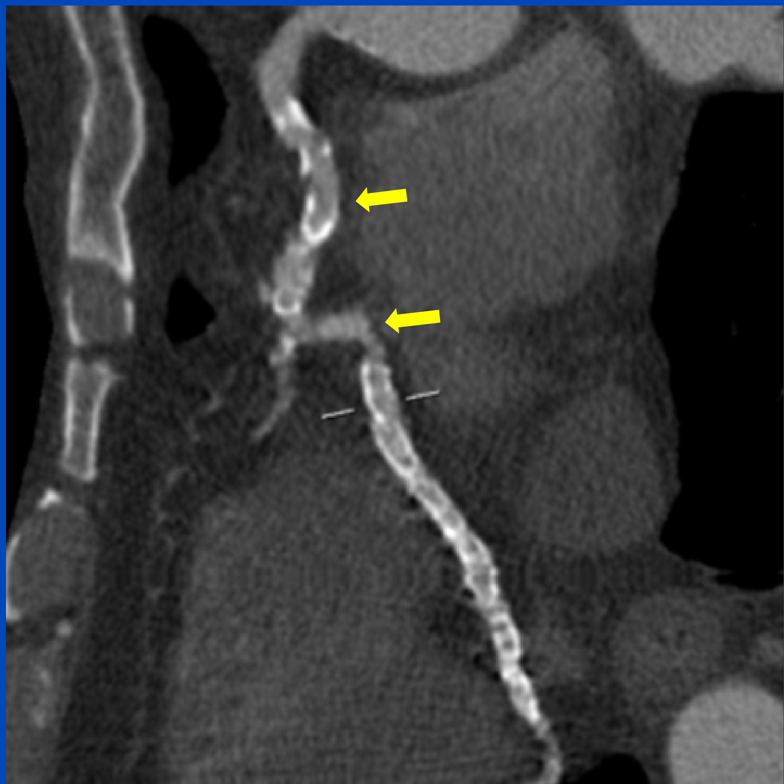

curved MPRs of the RCA

Stack 1

Patient 2

Slice 27 | Slice 34 | Slice 154

FBP

PAMoCo

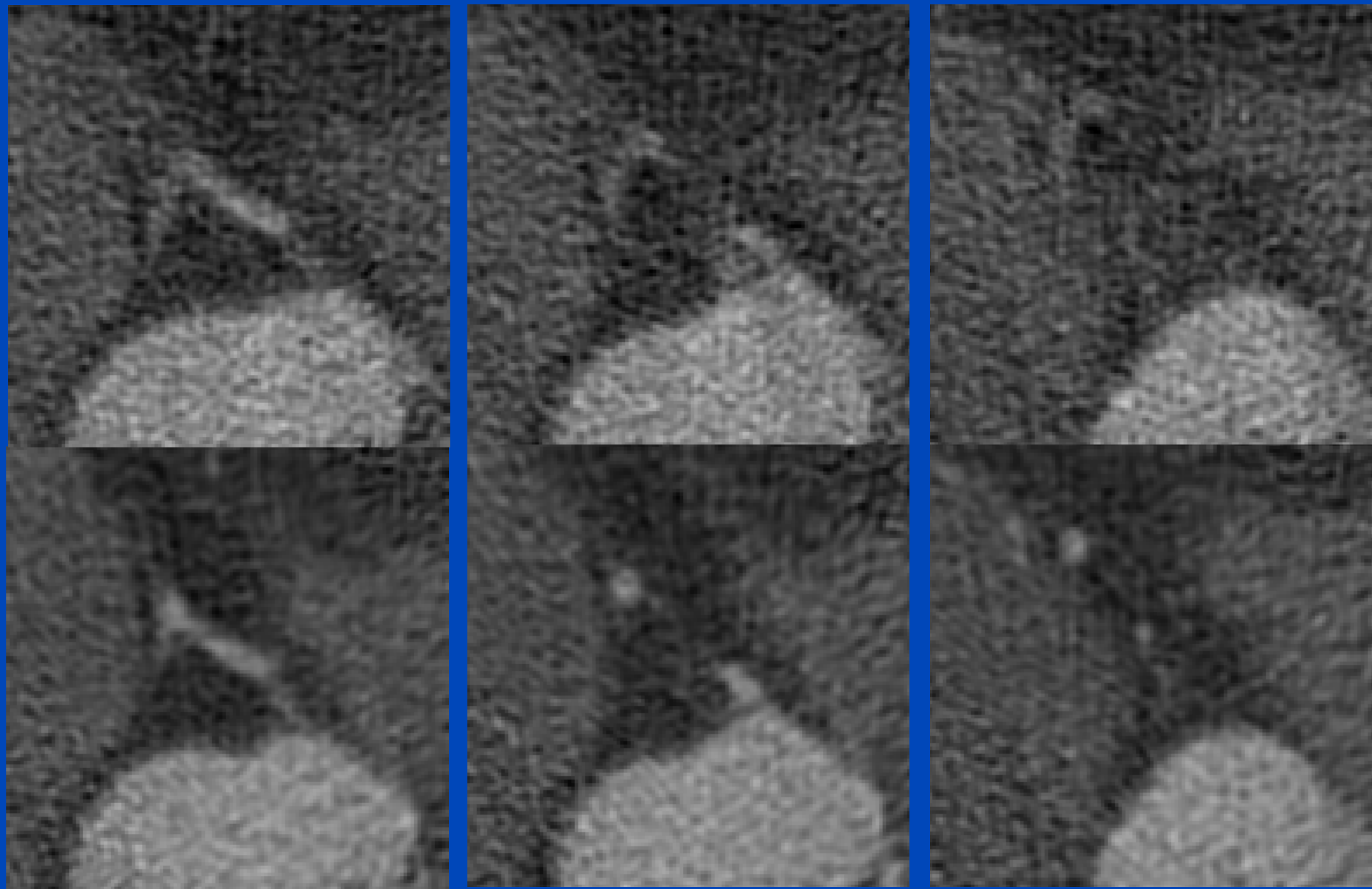

$\overline{HR}$ = 70 bpm, c = 50%,
C = 400 HU, W = 1500 HU

Patient 2

FBP

PAMoCo

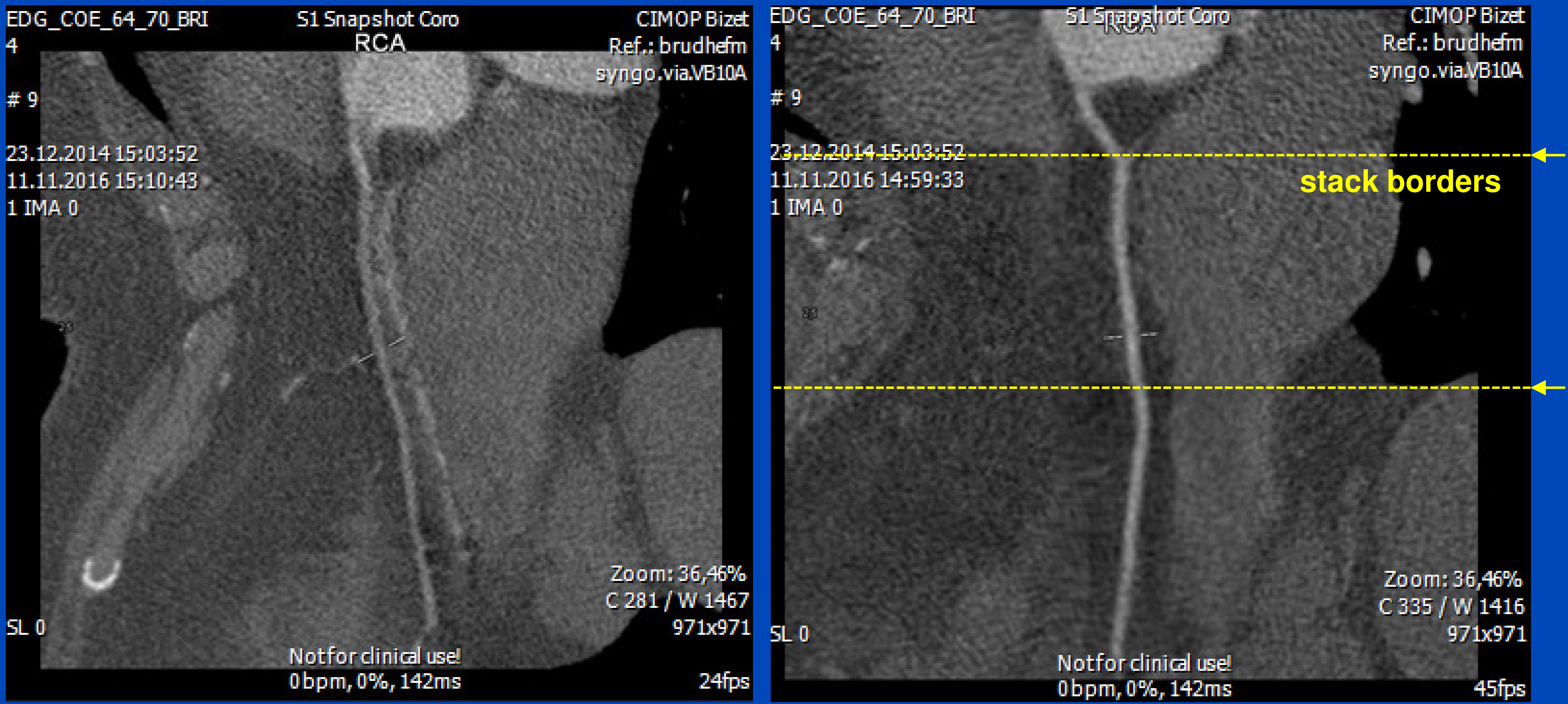

curved MPRs created with syngo.via

SIEMENS

$\overline{HR}$ = 70 bpm, c = 50%,
C = 400 HU, W = 1500 HU

dkfz.

Stack 1

Patient 3

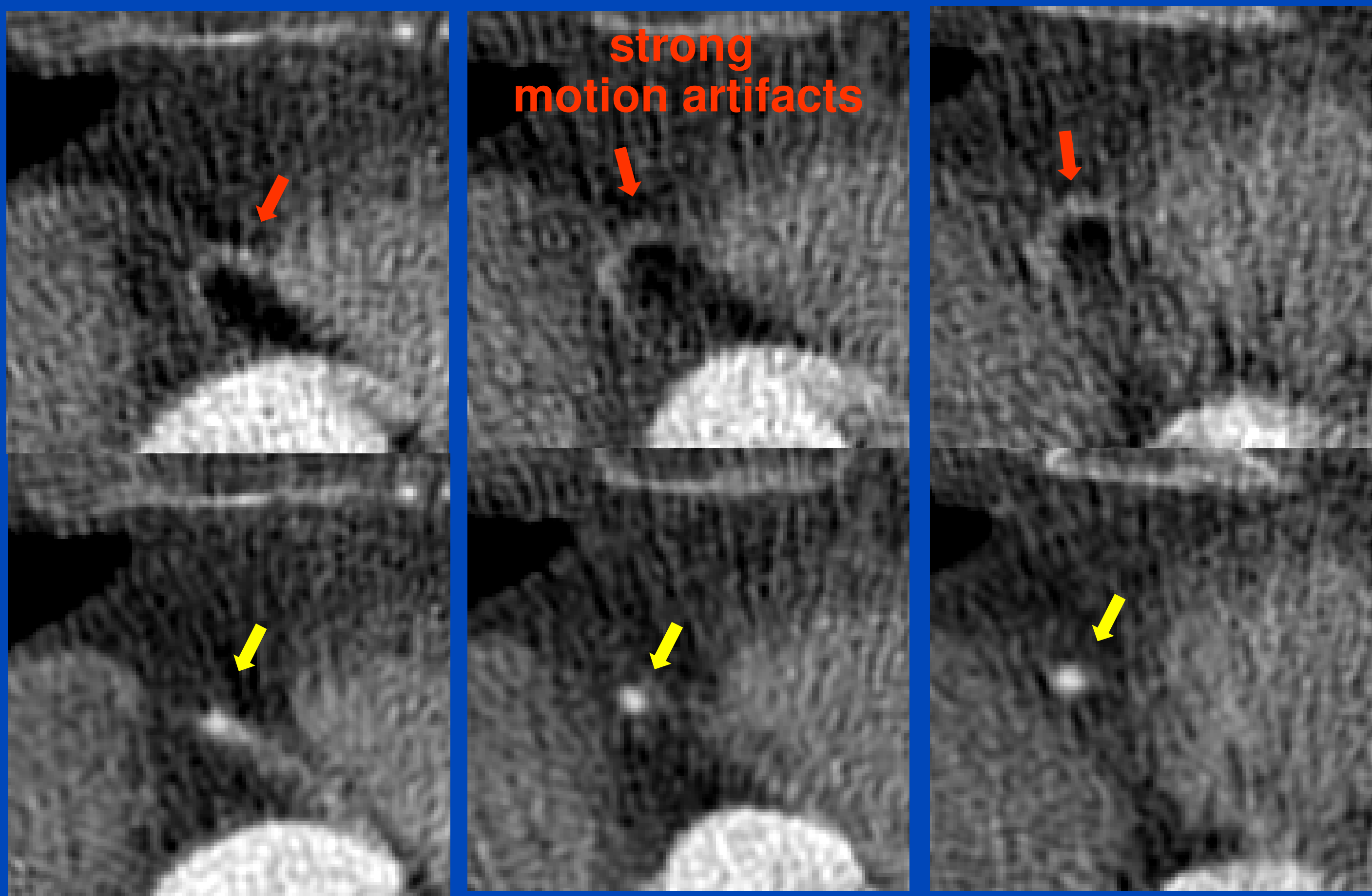

$\overline{HR}$ = 69 bpm, c = 50%,
C = 400 HU, W = 1500 HU

Motion in CBCT

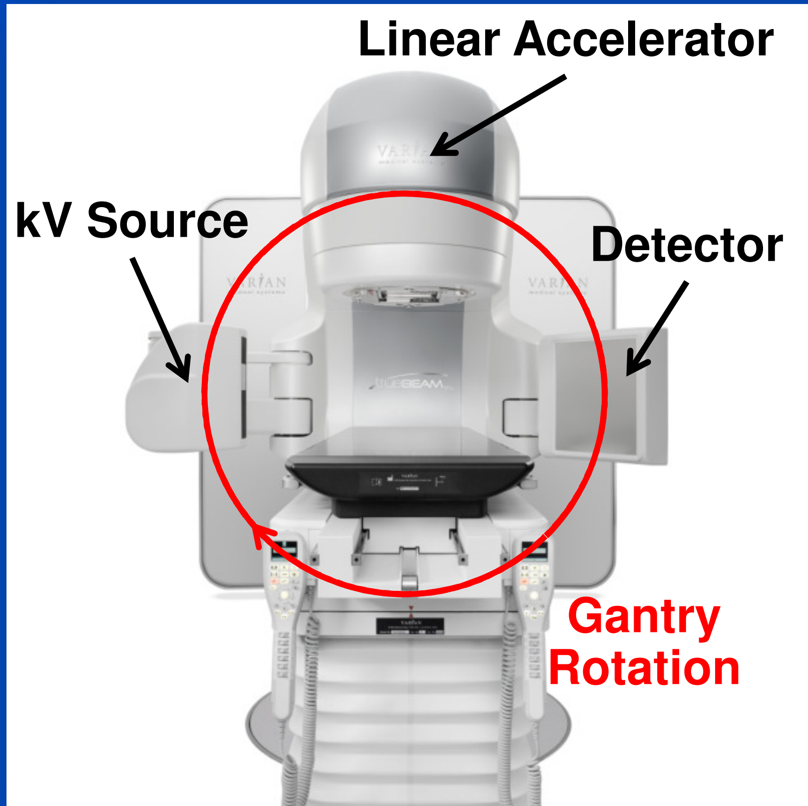

4D CBCT Scan with Retrospective Gating

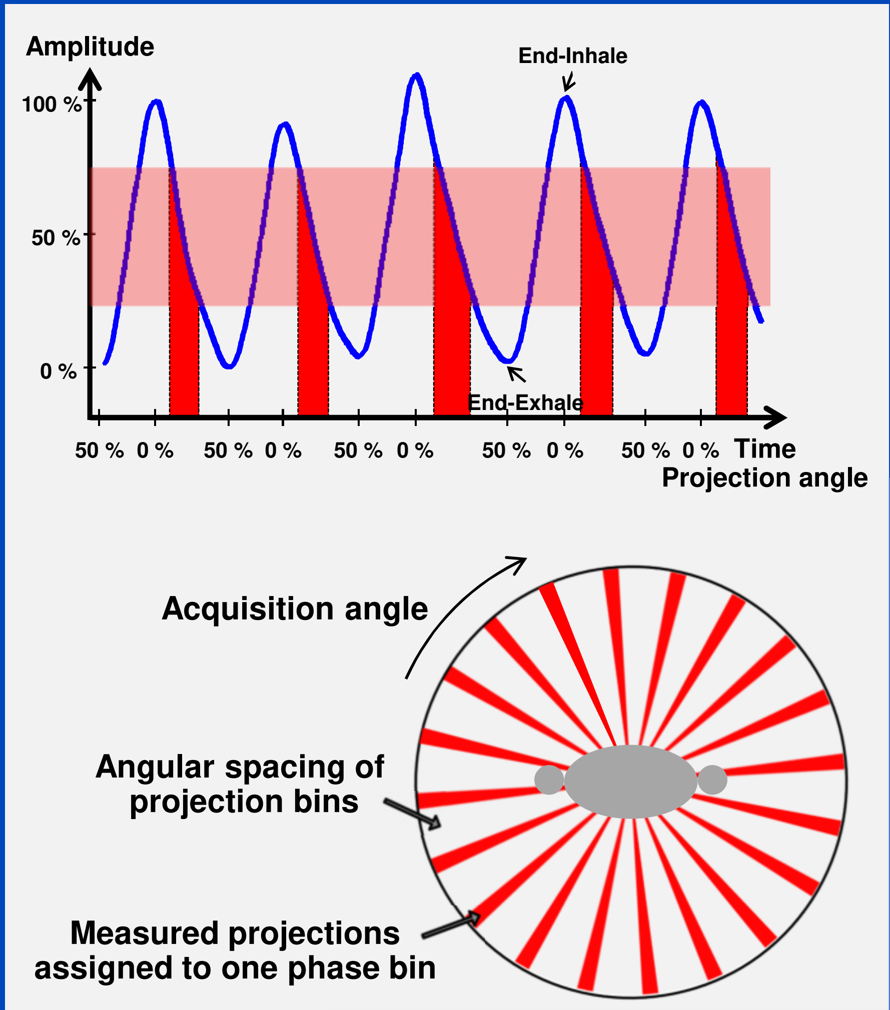

Without gating (3D):
Motion artifacts

With gating (4D):
Sparse-view artifacts

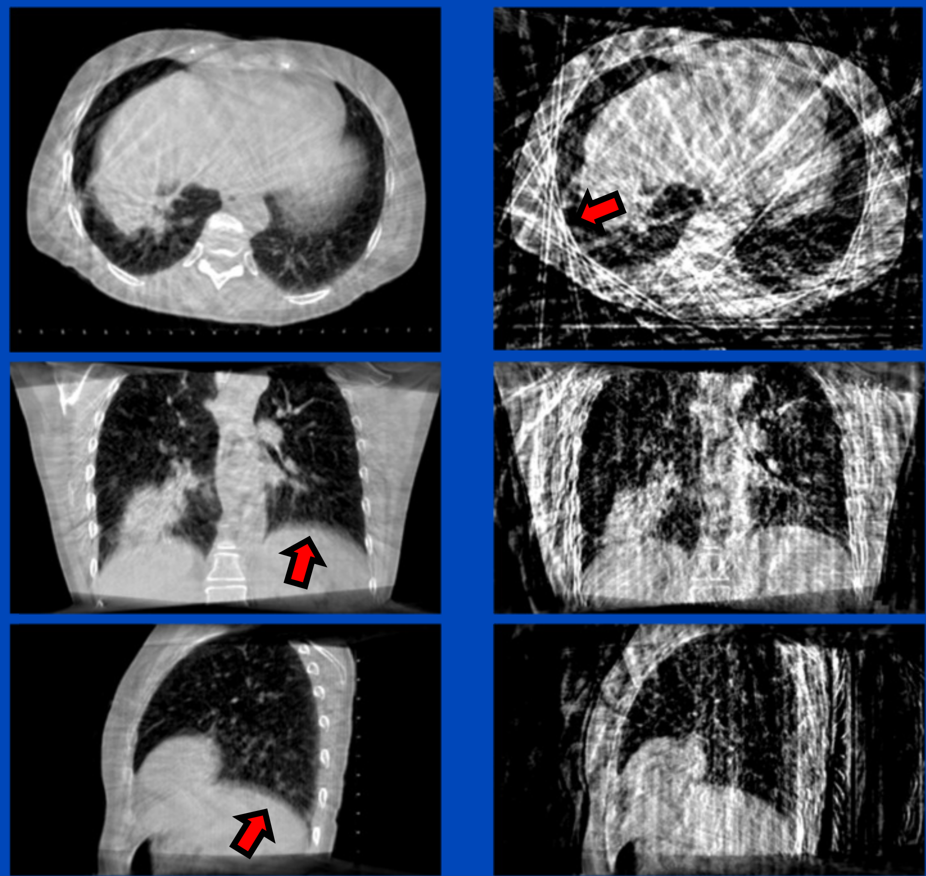

varian dkfz.

A Standard Motion Estimation and Compensation Approach (sMoCo)

- Motion estimation via standard 3D-3D registration

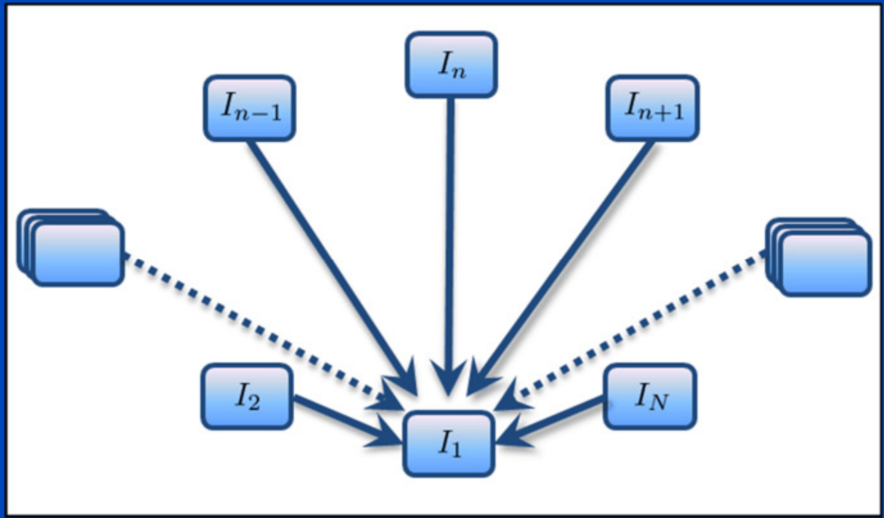

- Has to be repeated for each reconstructed phase

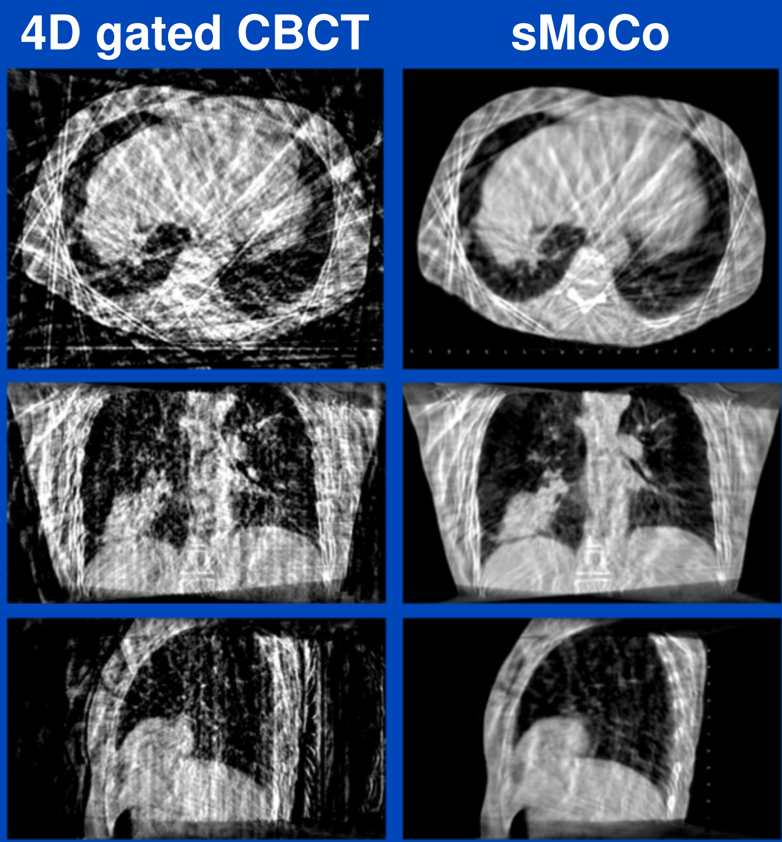

- Streak artifacts from gated reconstructions propagate into sMoCo results

Li, Koong, and Xing, "Enhanced 4D cone–beam CT with inter–phase motion model," Med. Phys. 51(9), 3688–3695 (2007).

The Cyclic Motion Estimation and Compensation Approach (cMoCo)

- Motion estimation only between adjacent phases
- Incorporate additional knowledge
  - A priori knowledge of quasi periodic breathing pattern
  - Non-cyclic motion is penalized
  - Error propagation due to concatenation is reduced

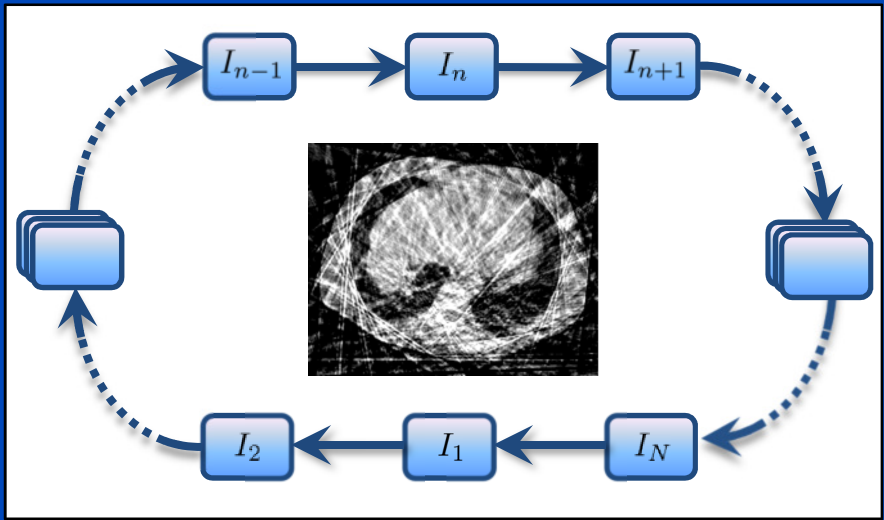

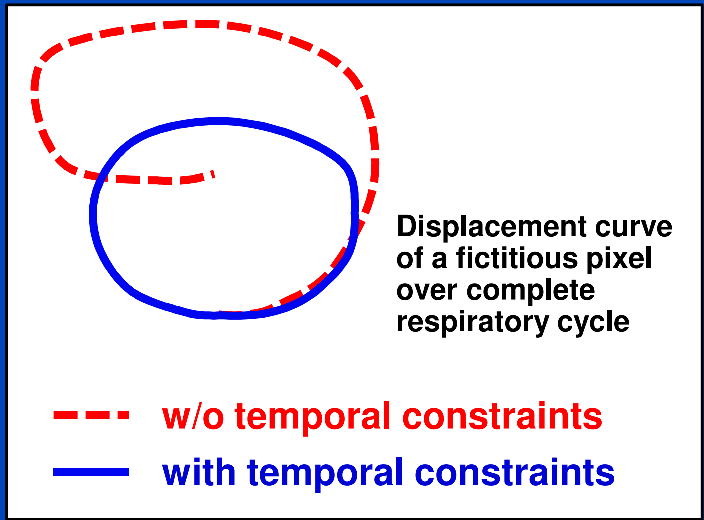

Brehm, Paysan, Oelhafen, Kunz, and Kachelrieß, "Self-adapting cyclic registration for motion-compensated cone-beam CT in image-guided radiation therapy," Med. Phys. 39(12):7603-7618, 2012.

Artifact Model-Based MoCo (aMoCo)

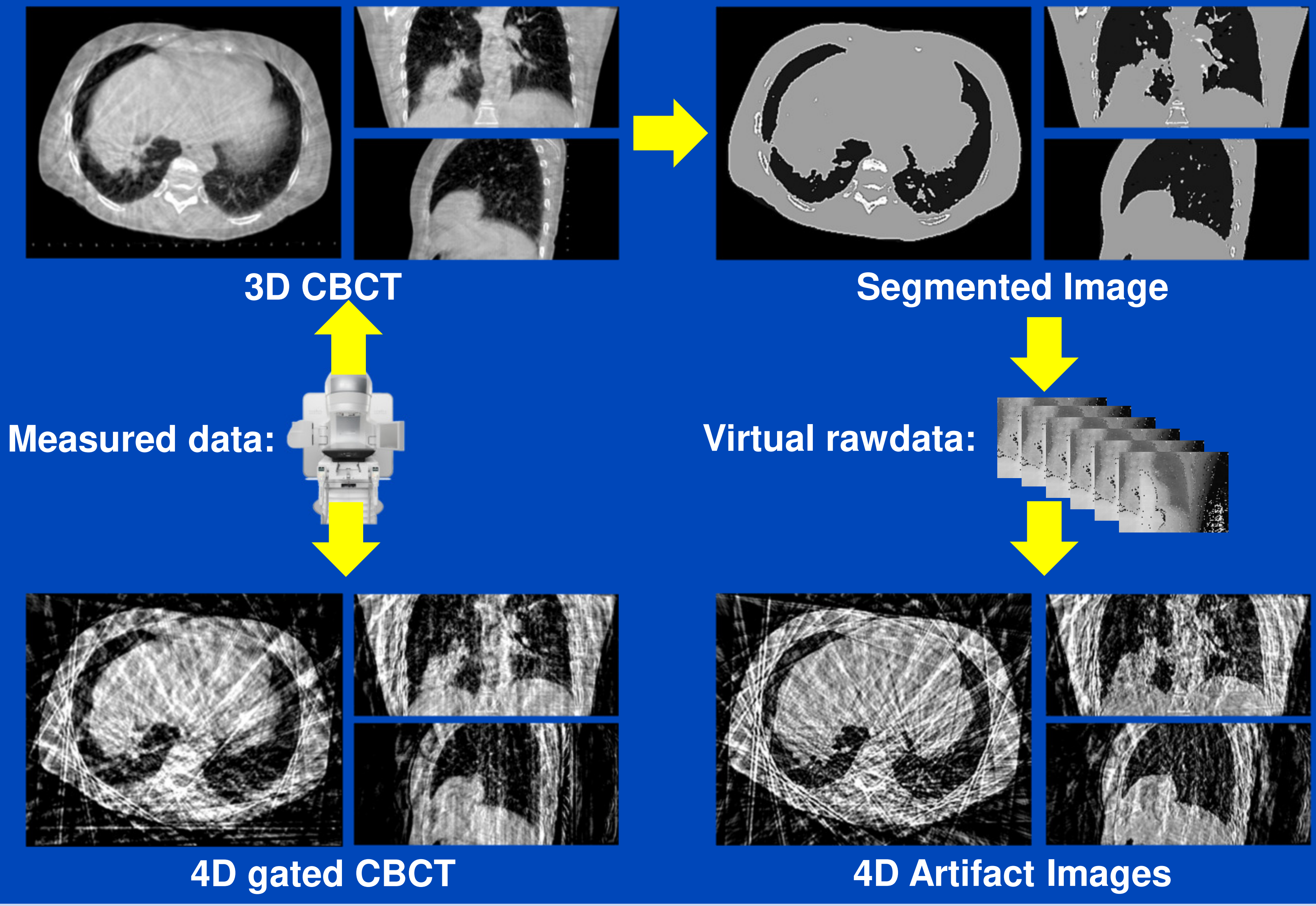

Brehm, Paysan, Oelhafen, and Kachelrieß, "Artifact-resistant motion estimation with a patient-specific artifact model for motion-compensated cone-beam CT" Med. Phys. 40(10):101913, 2013.

Patient Data – Results

3D CBCT	4D gated CBCT	sMoCo	acMoCo
Standard	Conventional Phase-Correlated	Standard Motion Compensation	Artifact Model-Based Motion Compensation

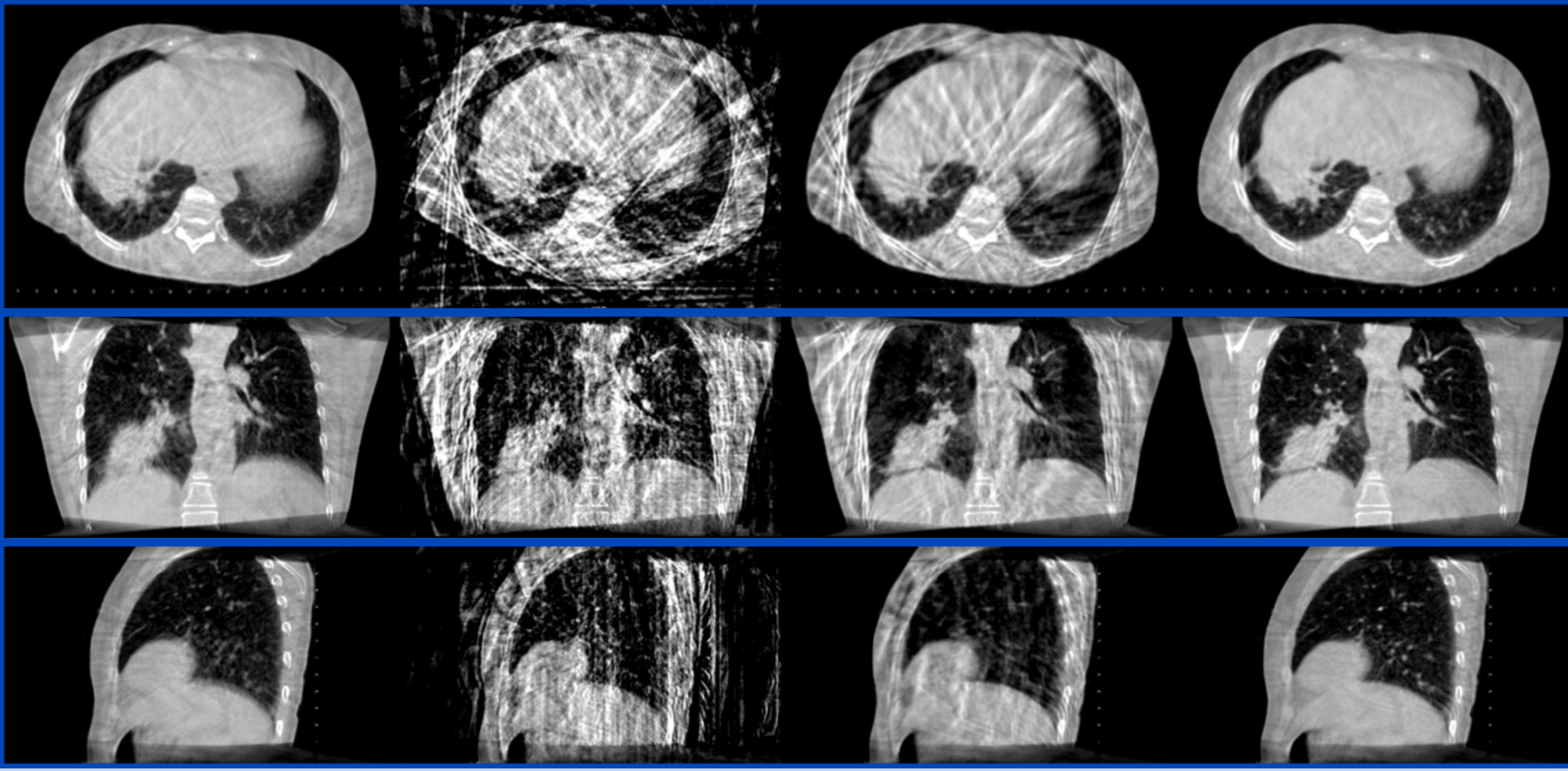

C = -200 HU, *W* = 1400 HU, displayed with 30 rpm.
Patient data provided by Memorial Sloan–Kettering Cancer Center, New York, NY.

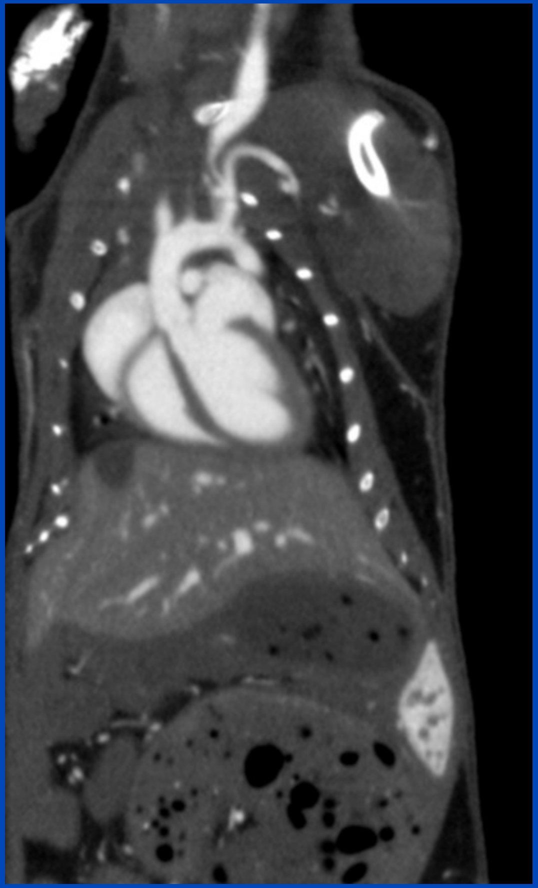

Data displayed as:

Heart: 280 bpm

Lung: 150 rpm

Mouse with 150 rpm and 280 bpm.

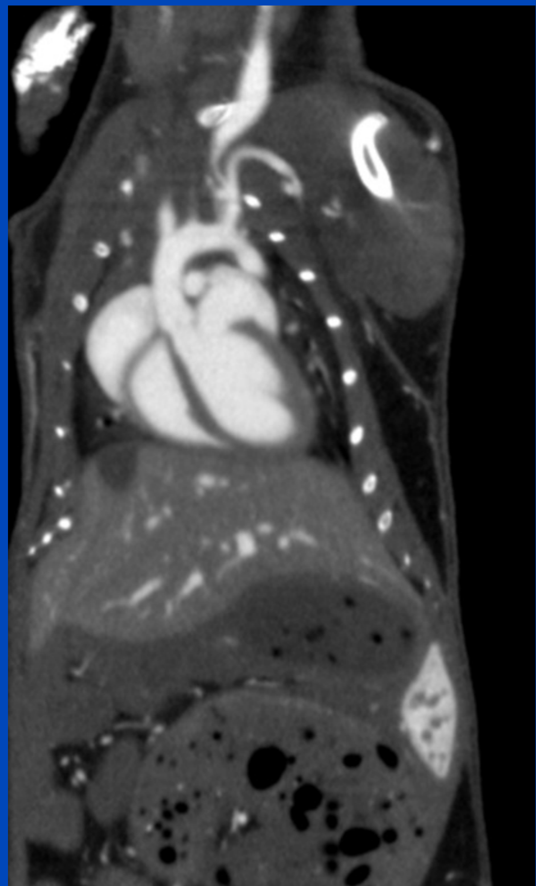

Data displayed as:

Heart: 180 bpm

Lung: 90 rpm

Mouse with 180 rpm and 240 bpm.

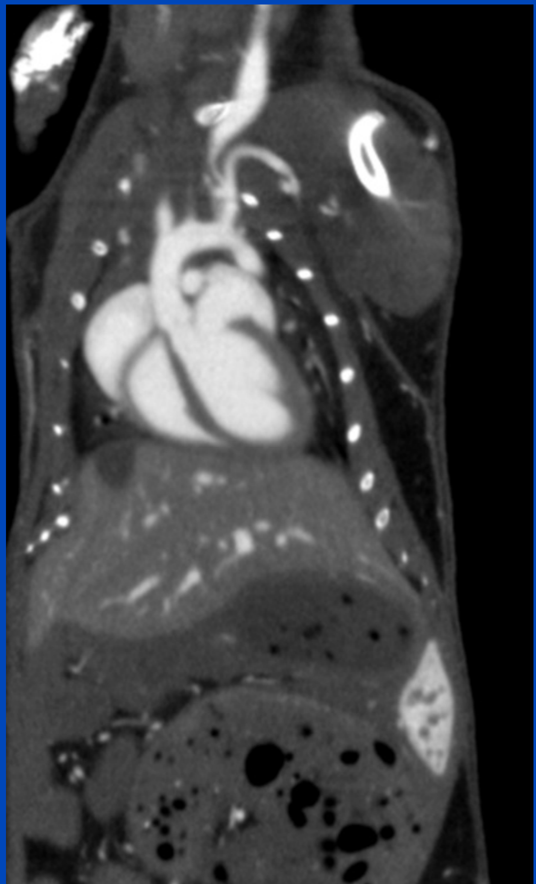

Data displayed as:

Heart: 90 bpm

Lung: 90 rpm

Mouse with 180 rpm and 240 bpm.

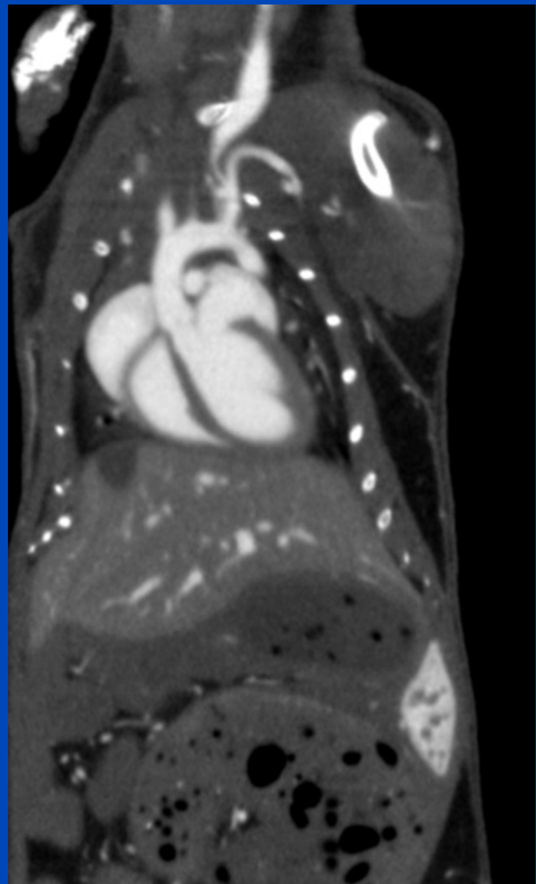

Data displayed as:

Heart: 0 bpm

Lung: 90 rpm

Mouse with 180 rpm and 240 bpm.

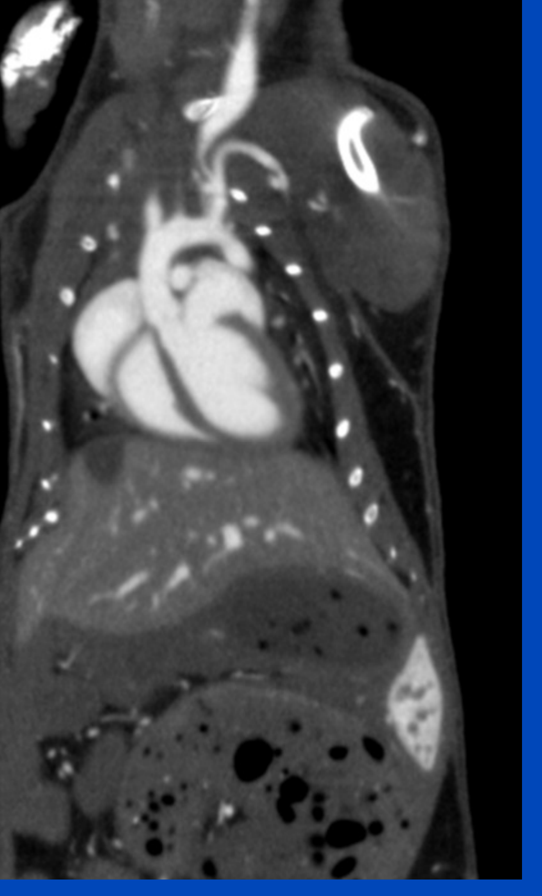

Data displayed as:

Heart: 90 bpm

Lung: 0 rpm

Mouse with 180 rpm and 240 bpm.

5D Motion Compensation

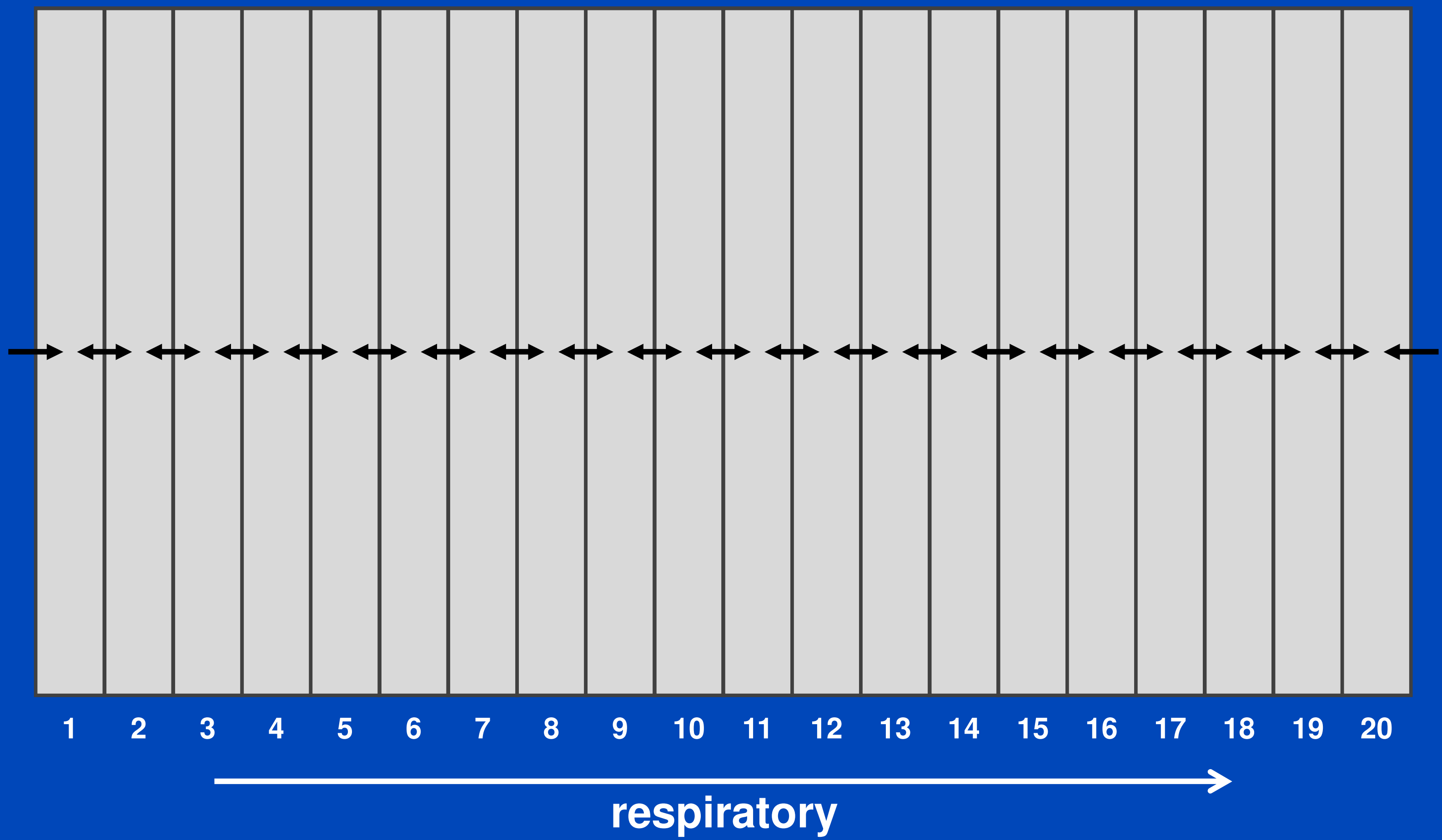

Brehm, Sawall, Maier, and Kachelrieß, “Cardio-respiratory motion-compensated micro-CT image reconstruction using an artifact model-based motion estimation” Med. Phys. 42(4):1948-1958, 2015.

dkfz.

5D Motion Compensation

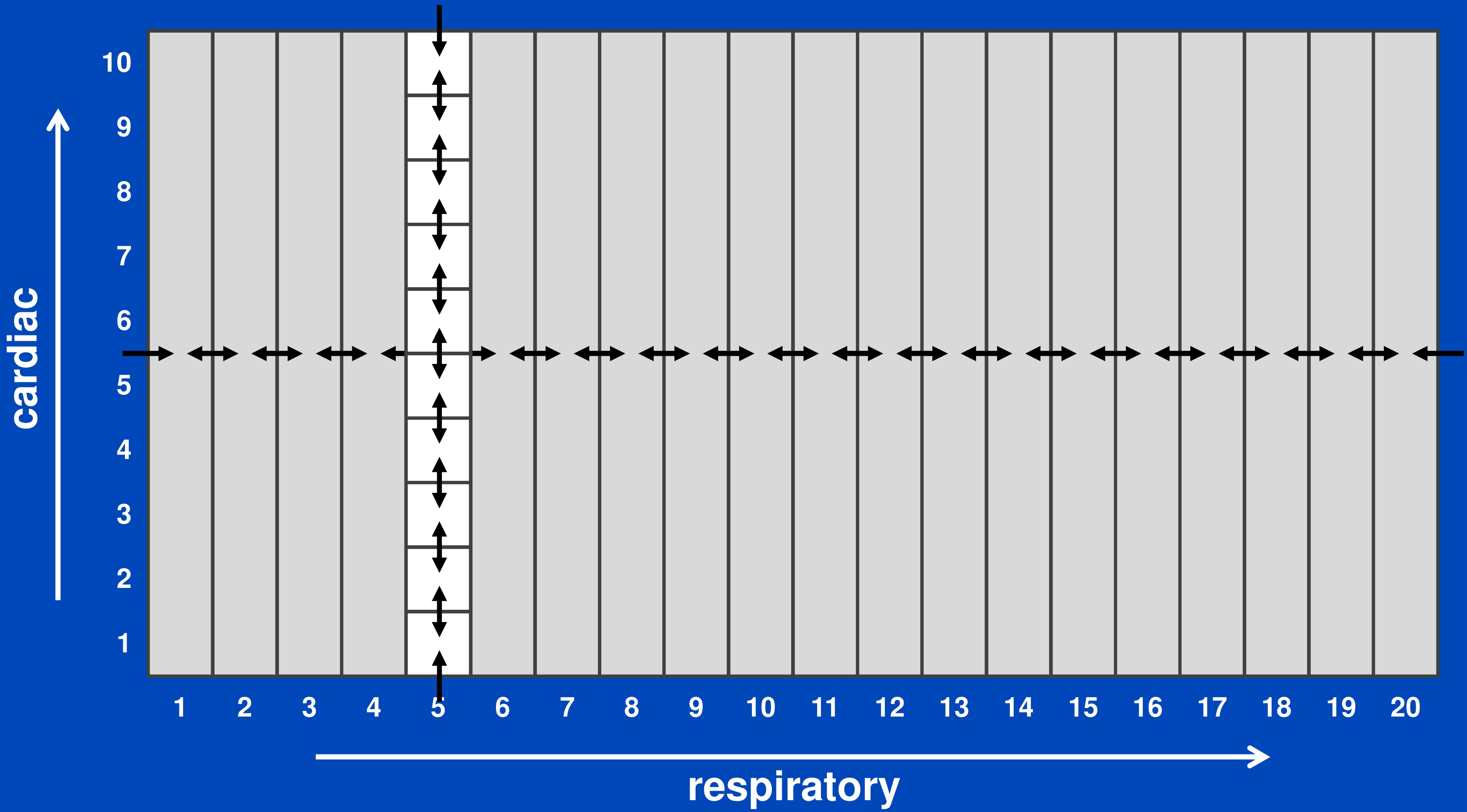

Brehm, Sawall, Maier, and Kachelrieß, “Cardio-respiratory motion-compensated micro-CT image reconstruction using an artifact model-based motion estimation” Med. Phys. 42(4):1948-1958, 2015.

dkfz.

5D Motion Compensation

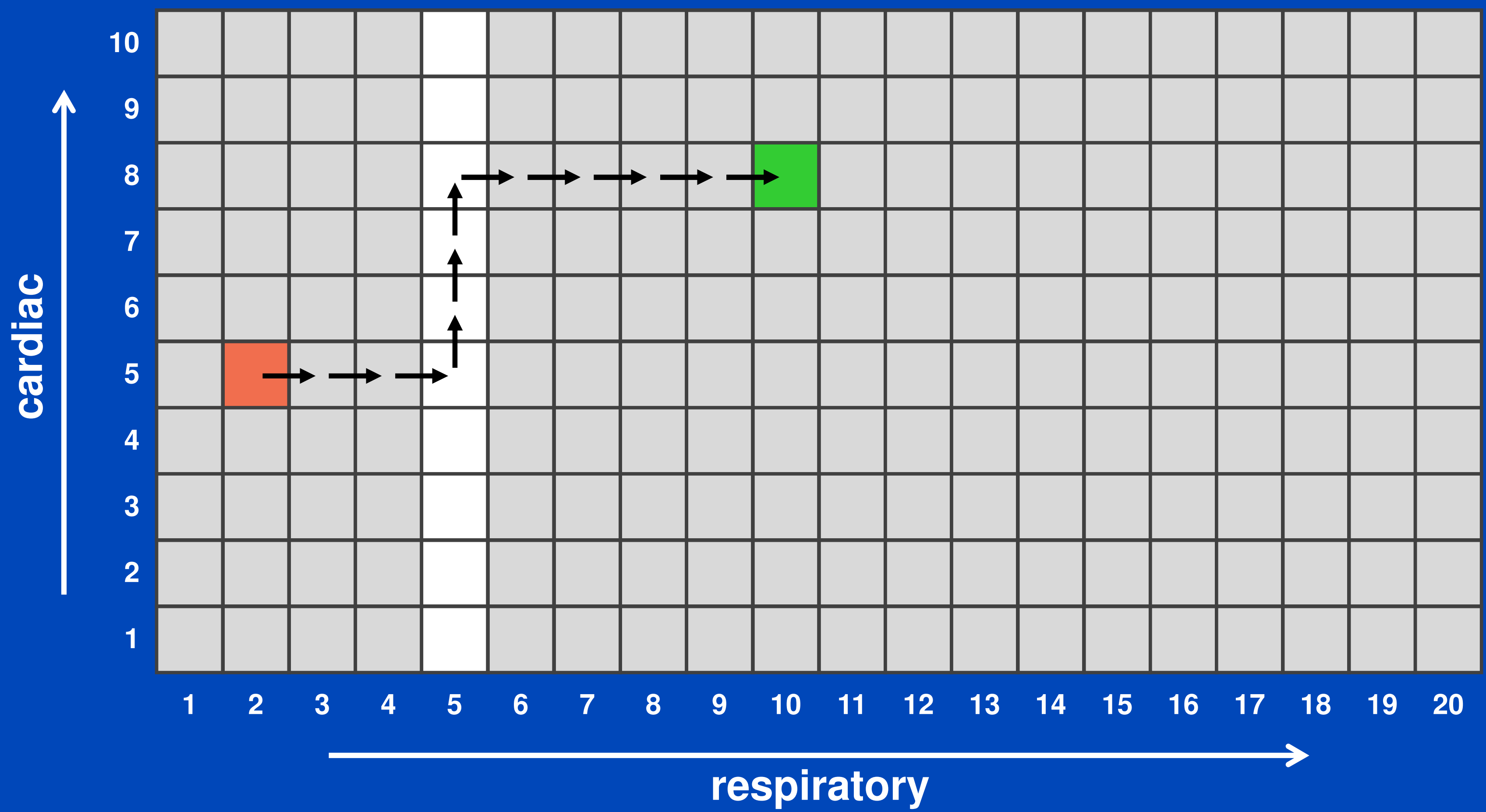

Brehm, Sawall, Maier, and Kachelrieß, “Cardio-respiratory motion-compensated micro-CT image reconstruction using an artifact model-based motion estimation” Med. Phys. 42(4):1948-1958, 2015.

5D Motion Compensation

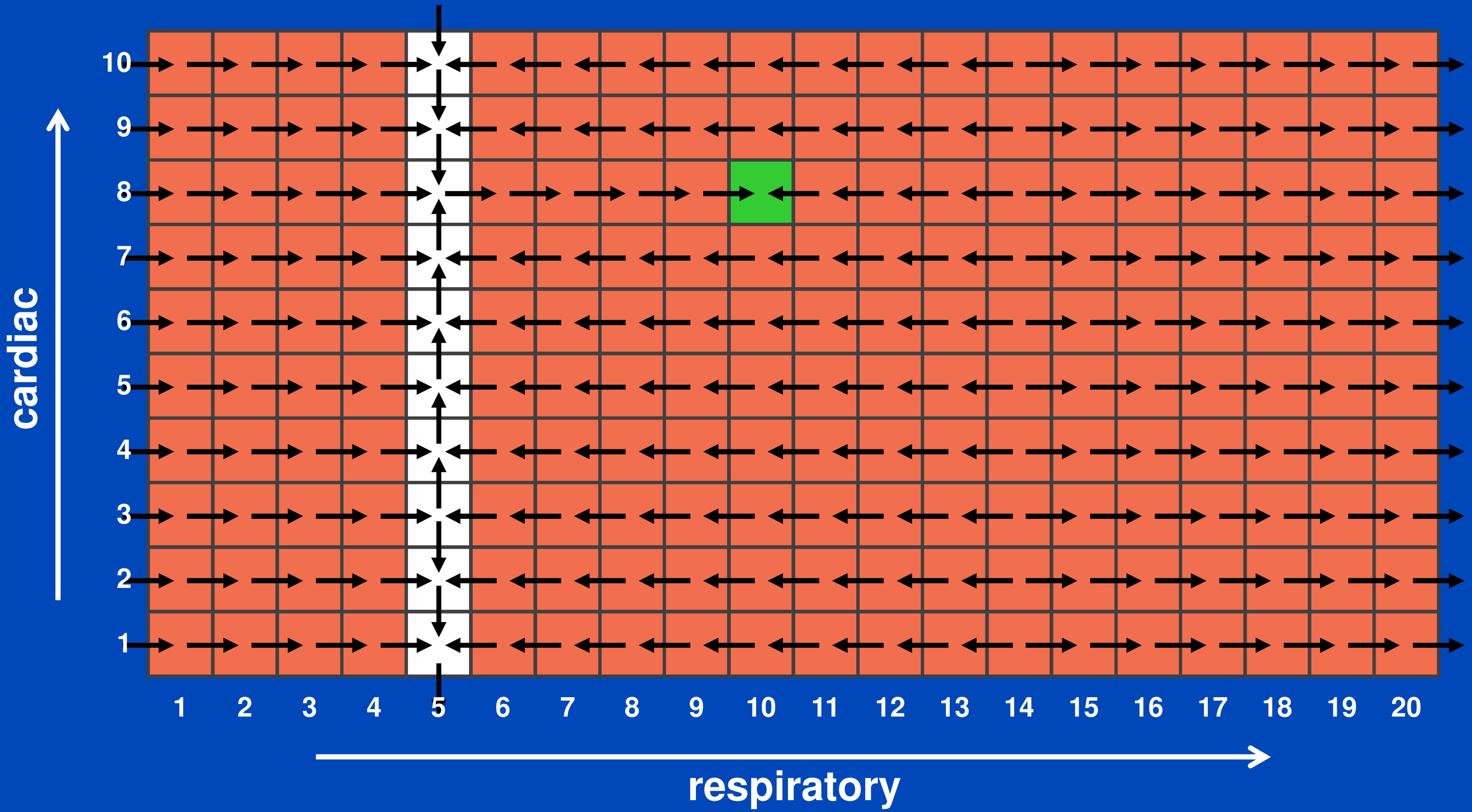

Brehm, Sawall, Maier, and Kachelrieß, "Cardio-respiratory motion-compensated micro-CT image reconstruction using an artifact model-based motion estimation" Med. Phys. 42(4):1948-1958, 2015.

Motion Compensation …

- will significantly improve cardiac CT
- may lead to new CBCT applications, in particular in
  - interventional imaging
  - imaging for radiation therapy

- MoCo also works for 4D and 5D PET, MR and PET/MR:

3D PET
motion average

5D double-gated PET
r = 1, *c*-loop

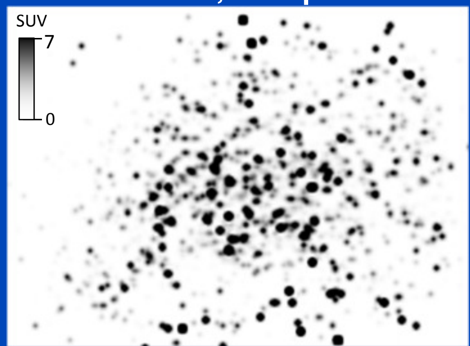

5D MoCo PET
r = 1, *c*-loop

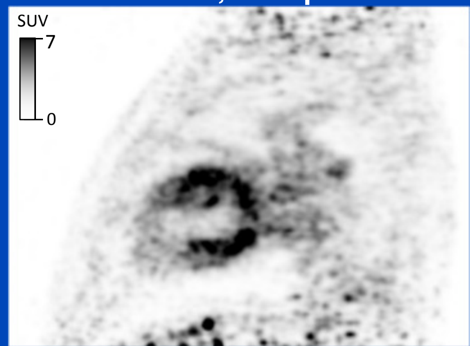

5D MoCo MR
r = 1, *c*-loop

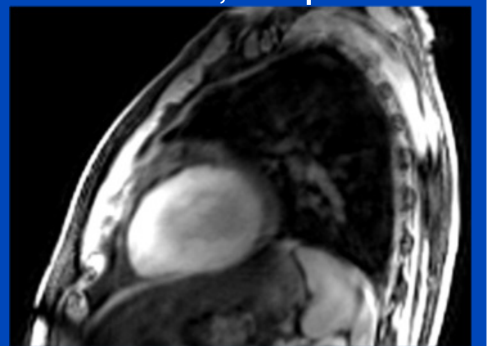

total PET/MR acquisition time: 5 min

Machine Learning is the New Era a.e.*

*Examples were shown at this BASP workshop.
A nice CT example was shown Monday afternoon by Ricardo Otazo.

Limited Angle Example

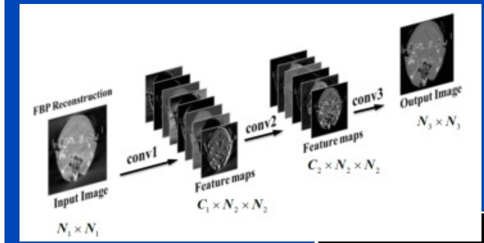

GT | FBP (150°) | CNN

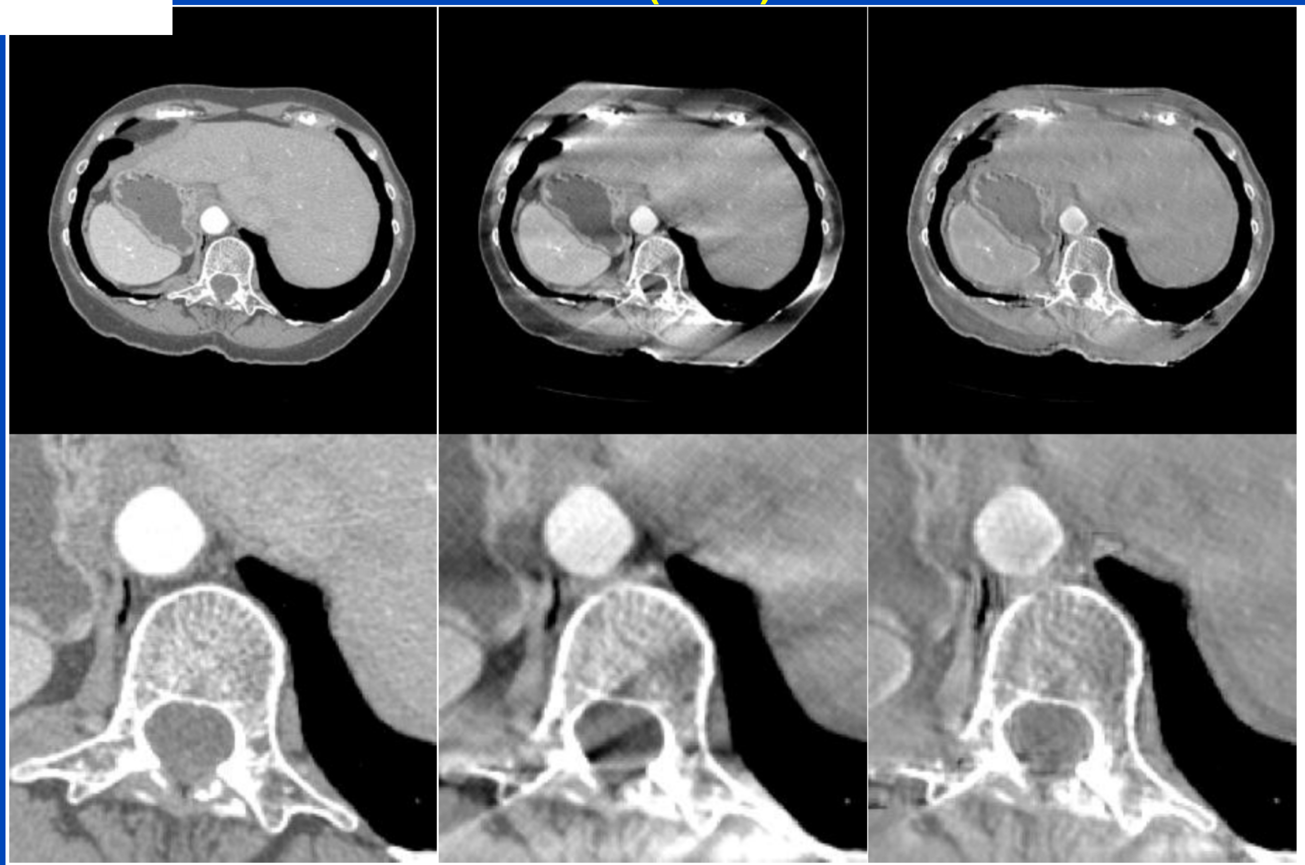

Image Prediction for Limited-Angle Tomography via Deep Learning with Convolutional Neural Network.
Hanming Zhang, Liang Li, Kai Qiao, Linyuan Wang, Bin Yan, Lei Li, Guoen Hu. arXiv 2016.

MAR Example

- Deep CNN-driven patch-based combination of the advantages of several MAR methods trained on simulated artifacts

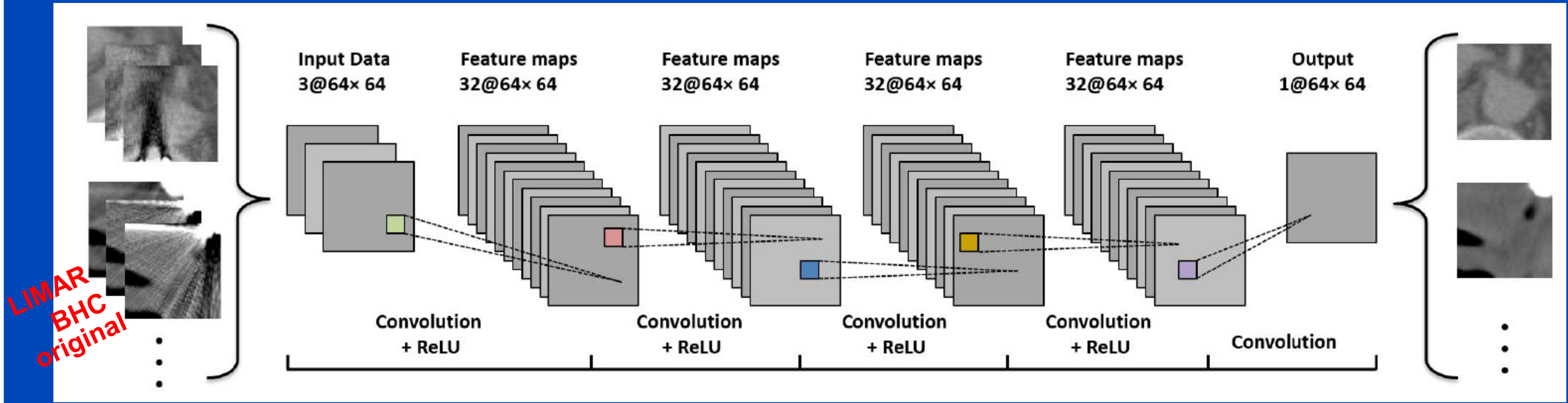

- followed by segmentation into tissue classes
- followed by forward projection of the CNN prior and replacement of metal areas of the original sinogram
- followed by reconstruction

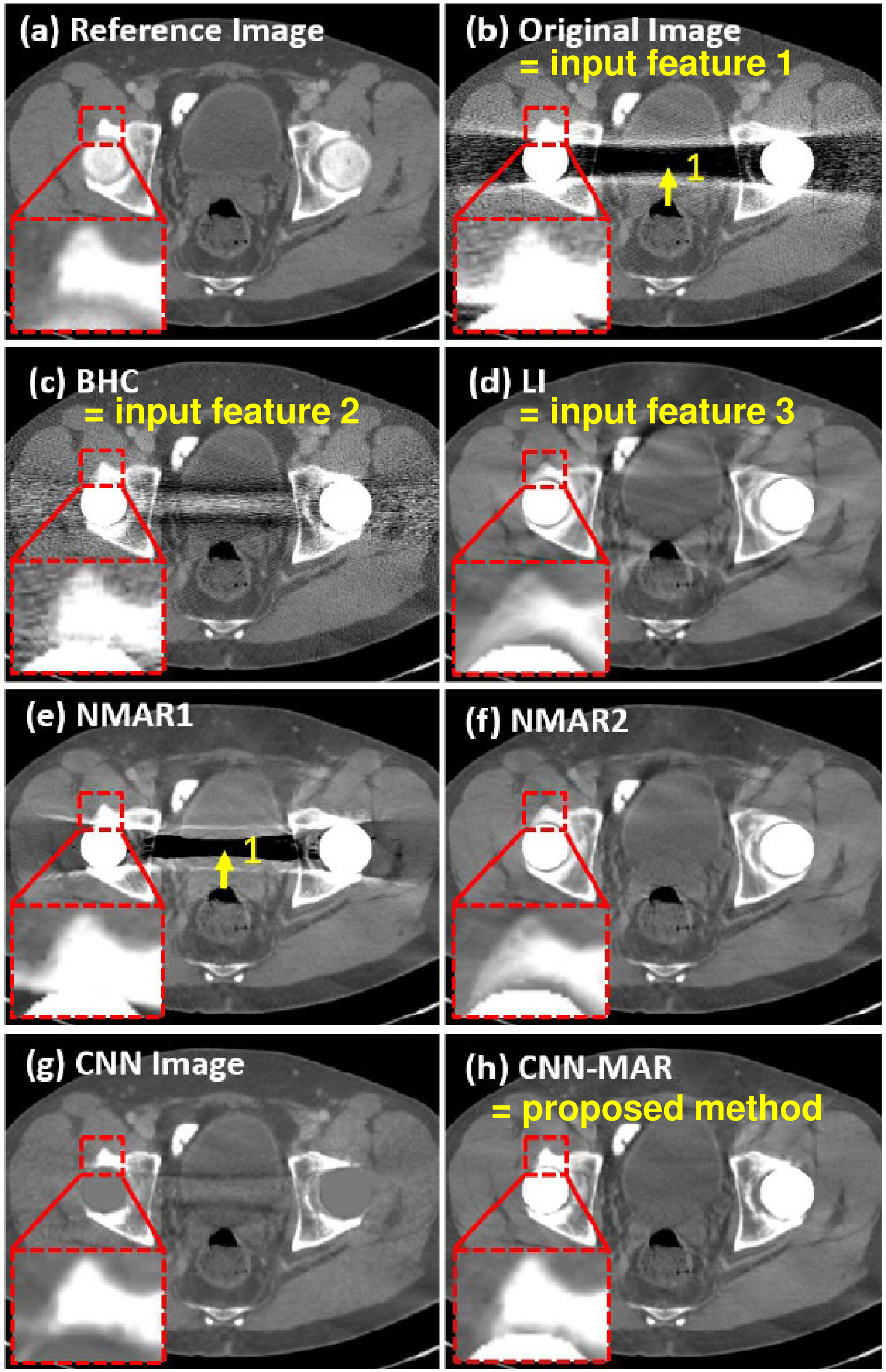

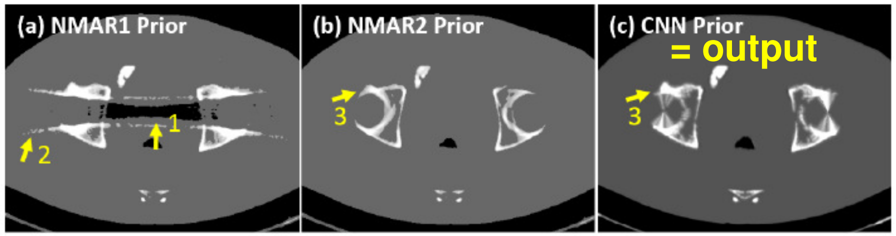

<u>NMAR and FSNMAR:</u>

E. Meyer, M. Kachelrieß. Normalized metal artifact reduction (NMAR) in computed tomography. Med. Phys. 37(10):5482-5493, Oct. 2010.

E. Meyer, M. Kachelrieß. Frequency split metal artifact reduction (FSMAR) in CT. Med. Phys. 39(4):1904-1916, April 2012.

Sparse View Reconstruction Example

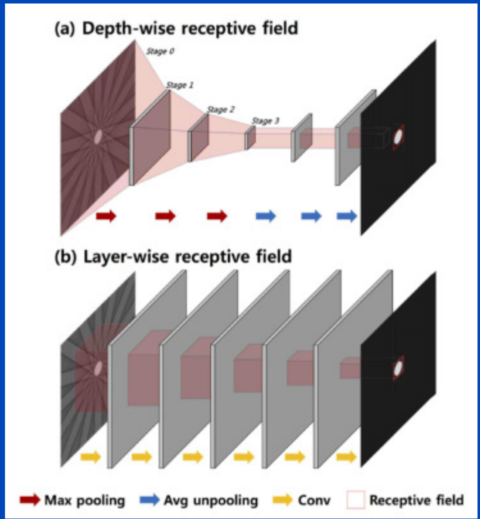

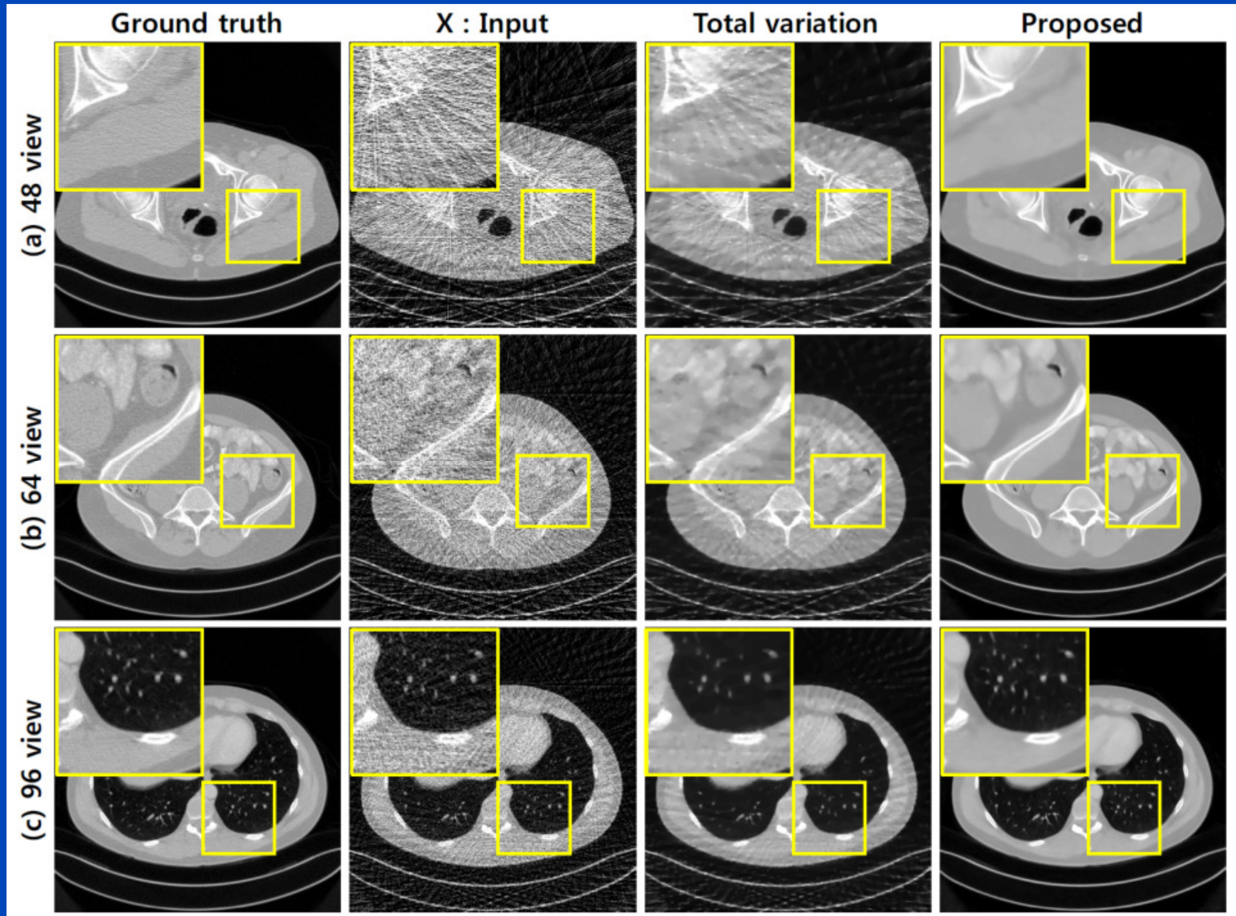

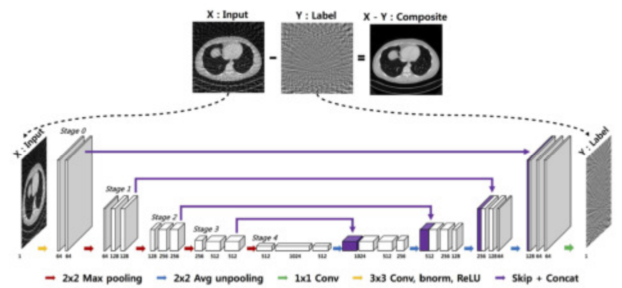

Figure 1. The proposed deep residual learning architecture for sparse view CT reconstruction.

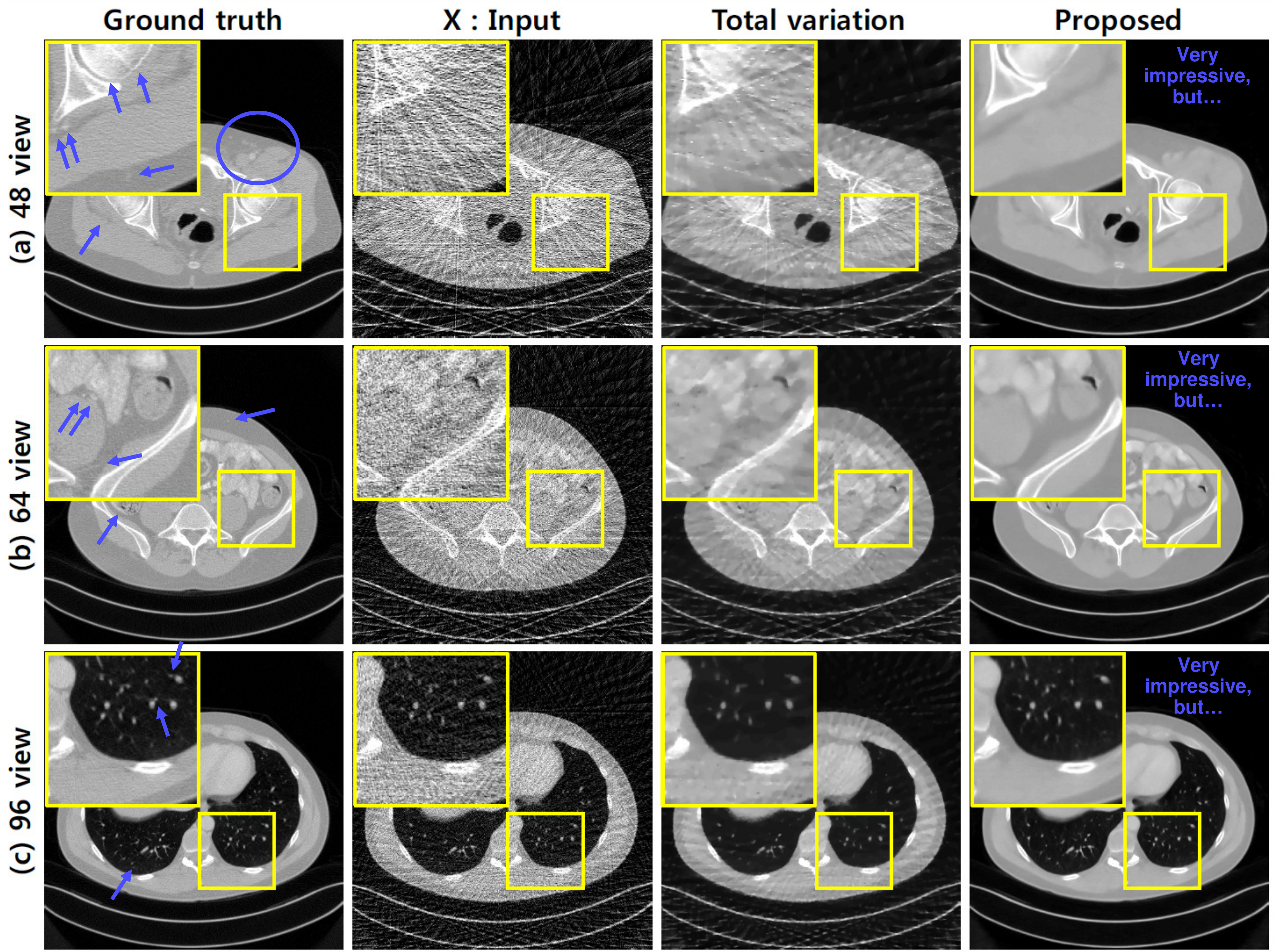

Ground truth
X : Input
Total variation
Proposed
(a) 48 view
(b) 64 view
(c) 96 view
Very impressive, but…
Very impressive, but…
Very impressive, but…

Sparse CT Recon with Data Consistency Layers (DCLs)

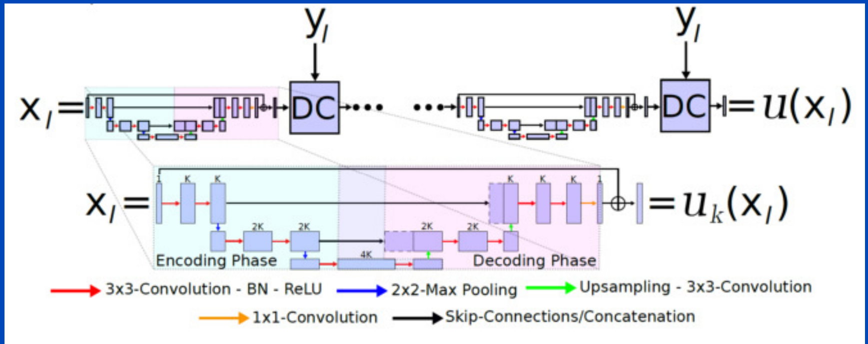

$x_l = \cdots DC \cdots DC = u(x_l)$, $x_l = \cdots = u_k(x_l)$

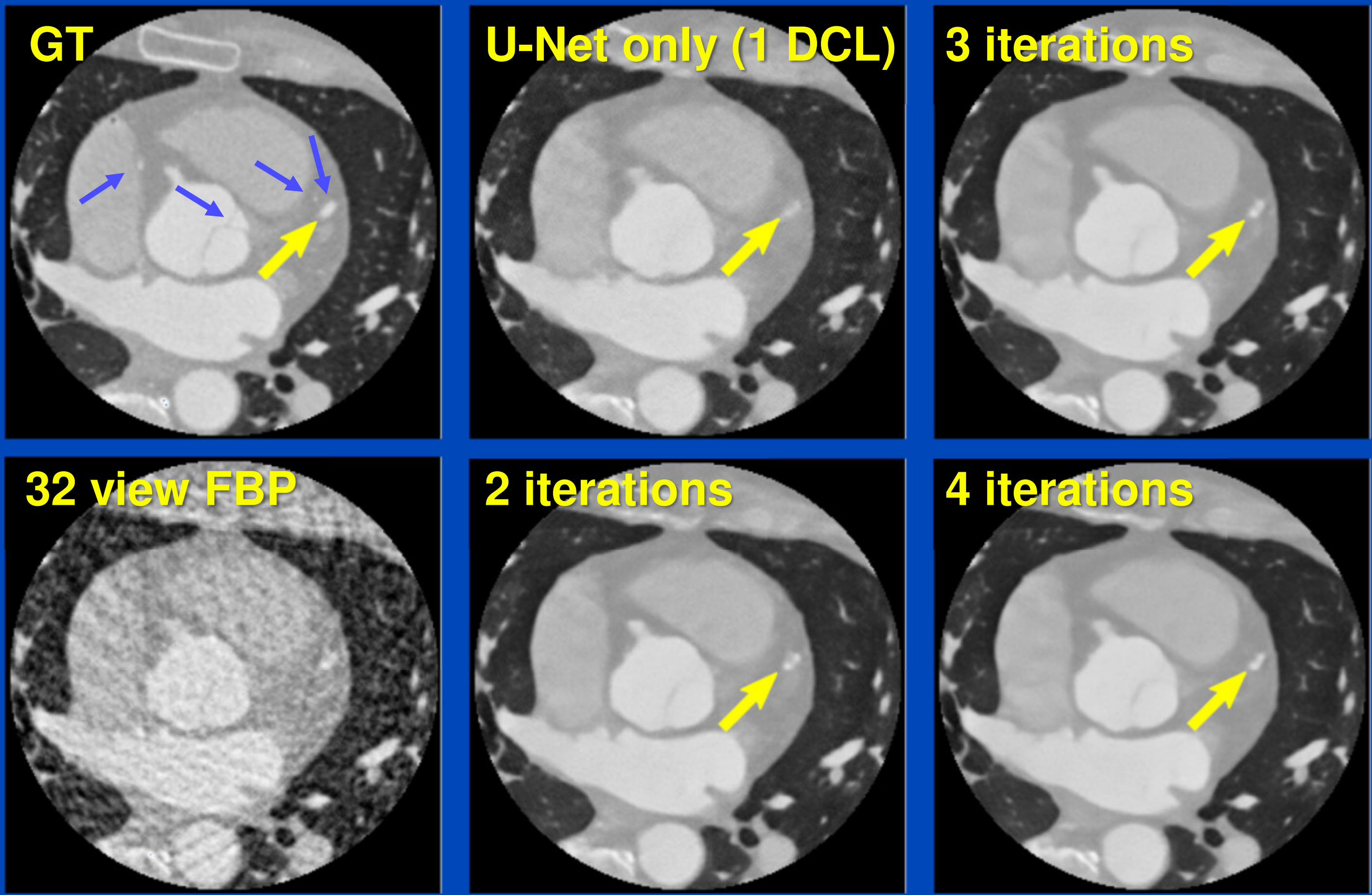

A. Kofler, M. Kachelrieß, et al. A U-Nets Cascade for Sparse View Computed Tomography, MICCAI 2018

dkfz.

Noise Removal Example

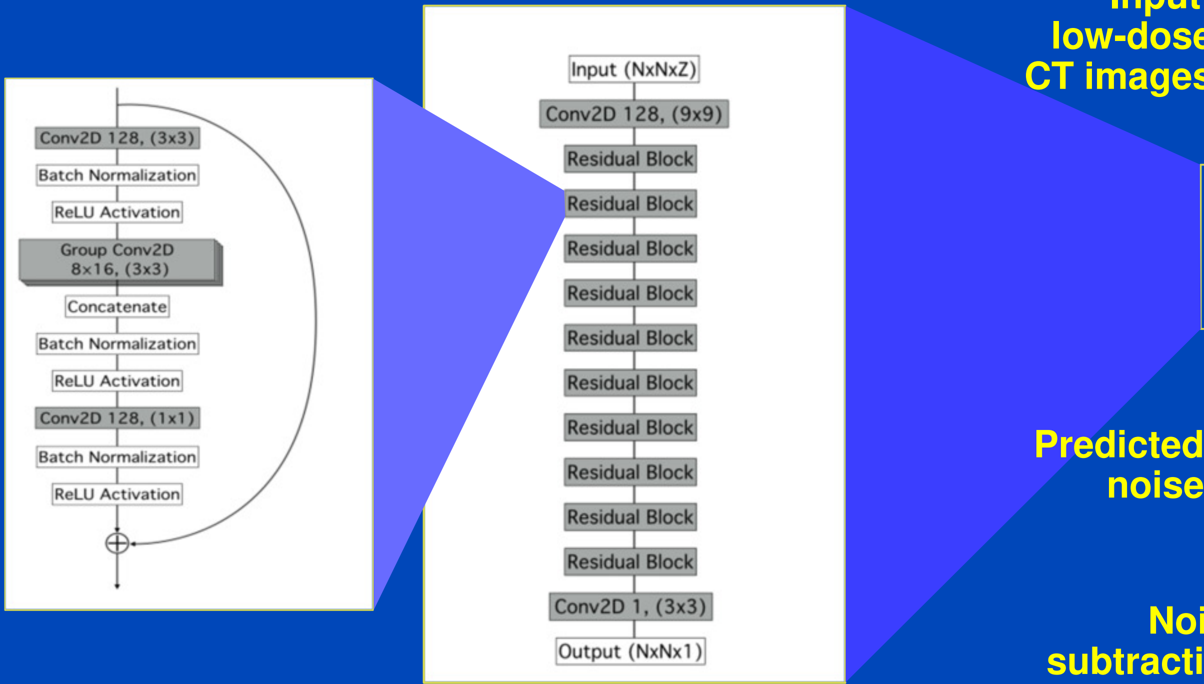

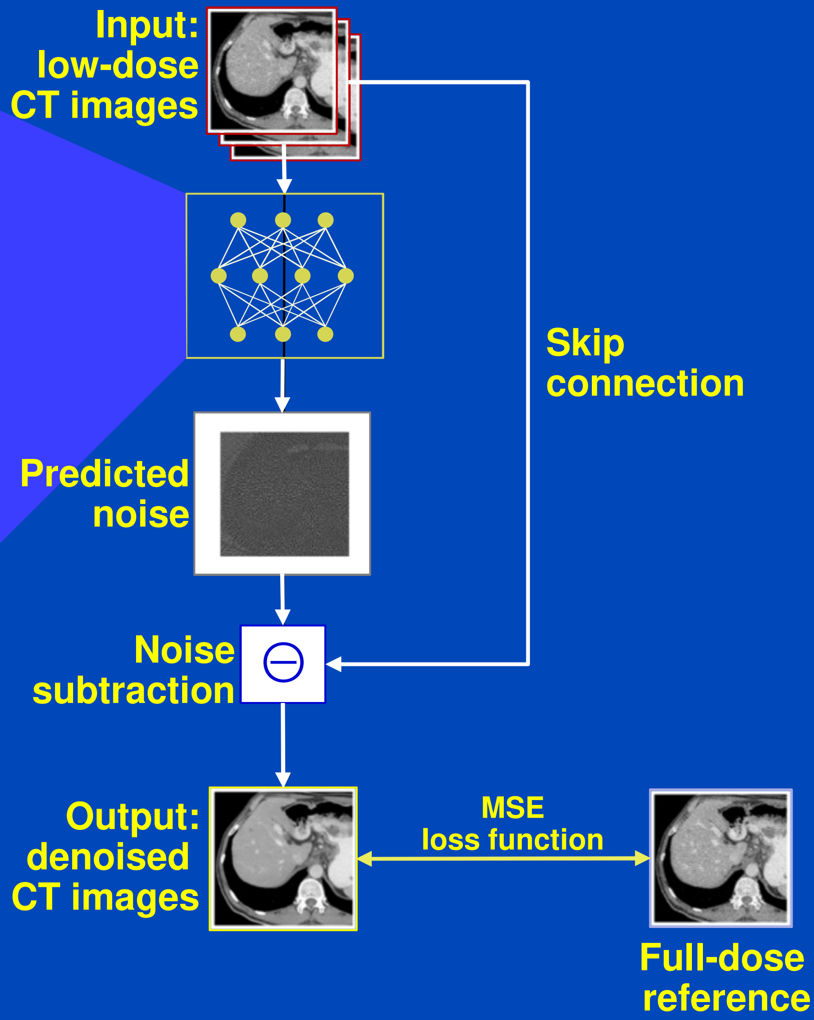

- Architecture based on state-of-the art networks for image classification (ResNet).
- 32 conv layers with skip connections
- About 2 million tunable parameters in total
- Input is arbitrarily-size stack of images, with a fixed number of adjacent slices in the channel/feature dimension.

Andrew D. Missert, Shuai Leng, Lifeng Yu, and Cynthia H. McCollough. Noise Subtraction for Low-Dose CT Images Using a Deep Convolutional Neural Network. Proceedings of the CT-Meeting 2018.

Noise Removal Example

Low dose images (1/4 of full dose)

Andrew D. Missert, Shuai Leng, Lifeng Yu, and Cynthia H. McCollough. Noise Subtraction for Low-Dose CT Images Using a Deep Convolutional Neural Network. Proceedings of the CT-Meeting 2018.

Noise Removal Example

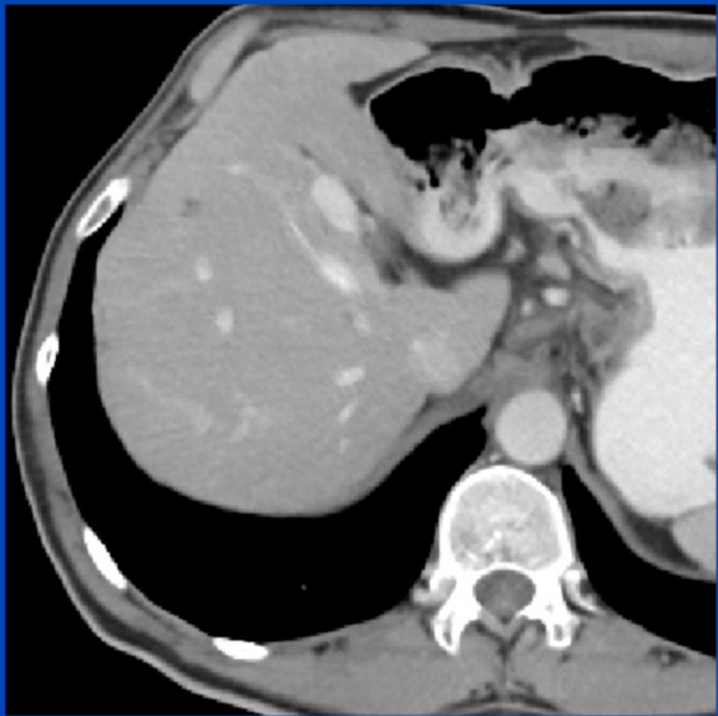

Denoised low dose

Andrew D. Missert, Shuai Leng, Lifeng Yu, and Cynthia H. McCollough. Noise Subtraction for Low-Dose CT Images Using a Deep Convolutional Neural Network. Proceedings of the CT-Meeting 2018.

Noise Removal Example

Full dose

Andrew D. Missert, Shuai Leng, Lifeng Yu, and Cynthia H. McCollough. Noise Subtraction for Low-Dose CT Images Using a Deep Convolutional Neural Network. Proceedings of the CT-Meeting 2018.

Noise Removal Example

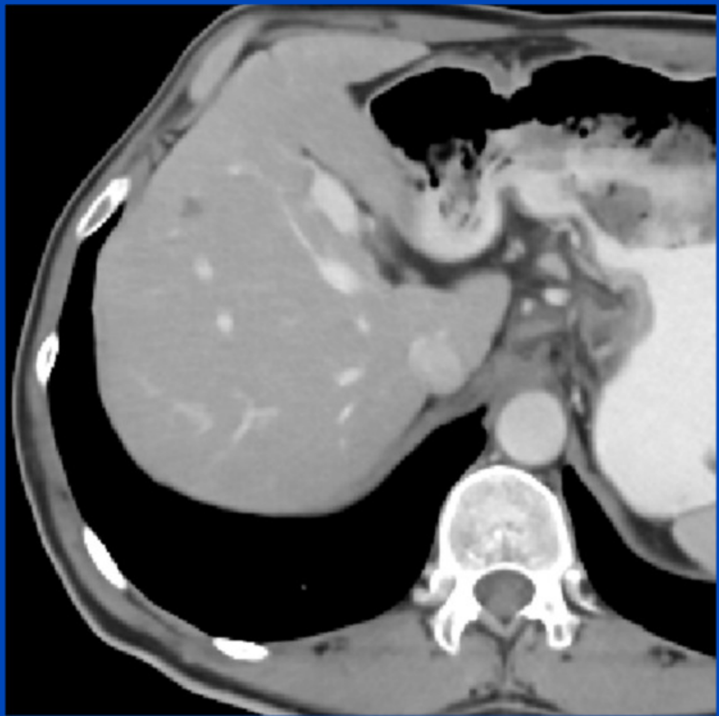

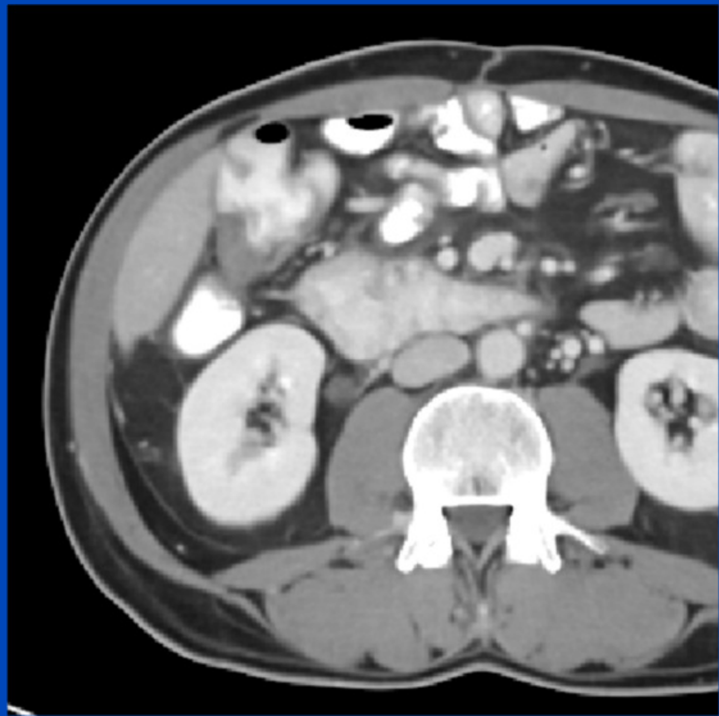

Denoised full dose

Andrew D. Missert, Shuai Leng, Lifeng Yu, and Cynthia H. McCollough. Noise Subtraction for Low-Dose CT Images Using a Deep Convolutional Neural Network. Proceedings of the CT-Meeting 2018.

Scatter

- X-ray scatter is a major cause of image quality degradation in CT and CBCT.
- Appropriate scatter correction is crucial to maintain the diagnostic value of the CT examination.

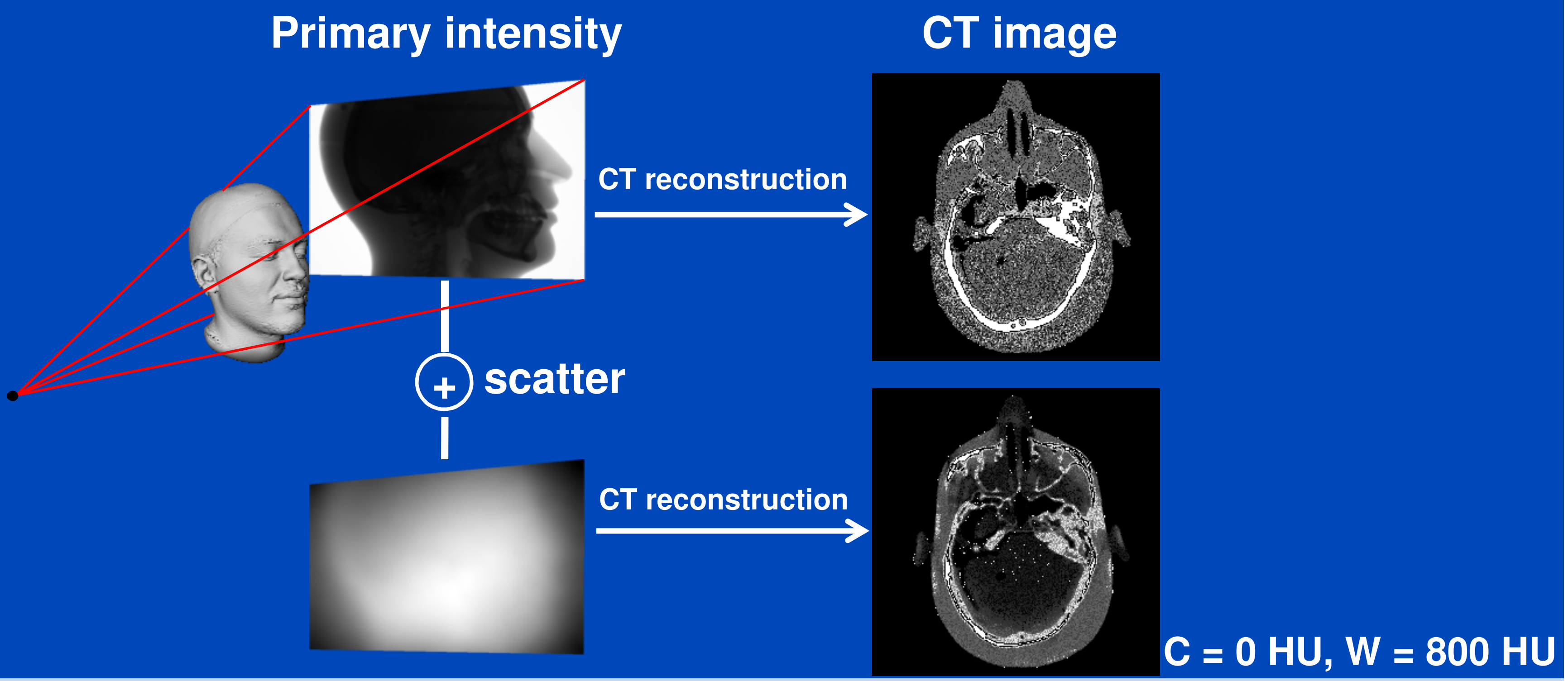

Scatter Correction

Scatter suppression

- Anti-scatter grids
- Collimators
- …

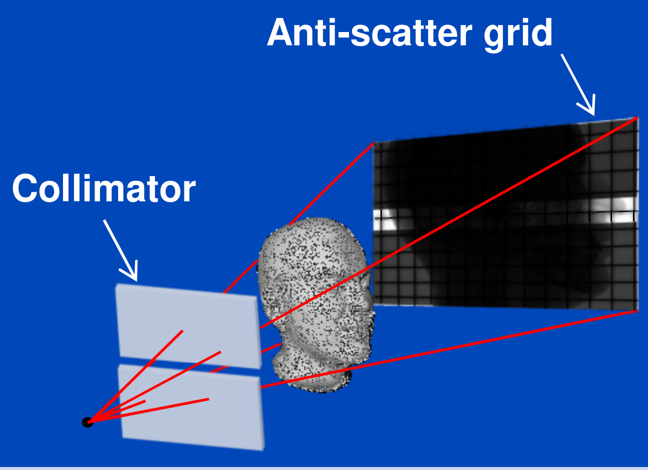

Scatter estimation

- Monte Carlo simulation
- Kernel-based approaches
- Boltzmann transport
- Primary modulation
- Beam blockers
- …

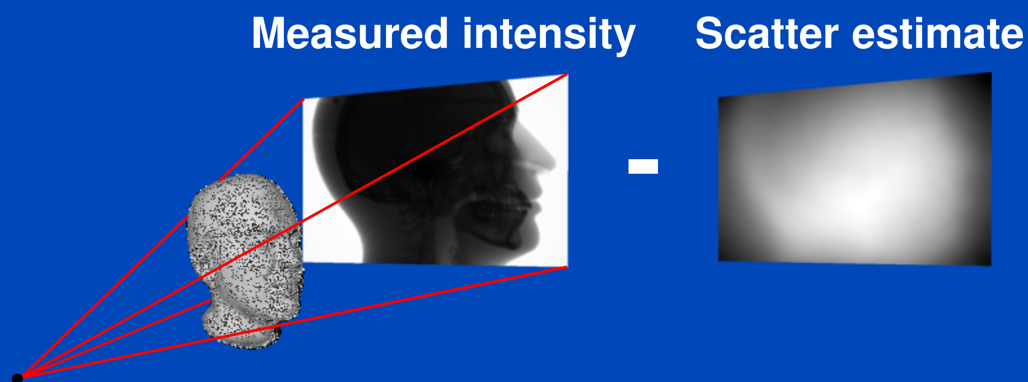

Monte Carlo Scatter Estimation

- Simulation of photon trajectories according to physical interaction probabilities.
- Simulating a large numb… …ories well approximat…

1 to 10 hours
per tomographic data set

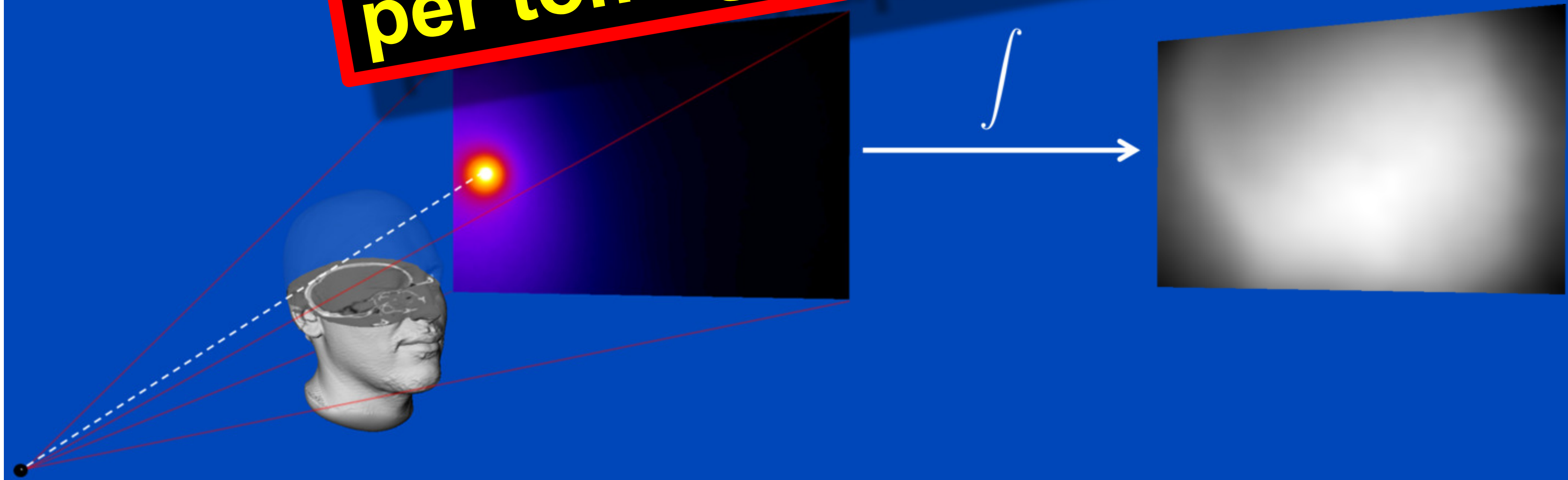

Deep Scatter Estimation (DSE)

Train a deep convolutional neural network (CNN) to estimate scatter using a functio… d projection data as in…

0.1 to 1 minute per tomographic data set

Input: $T(p)$

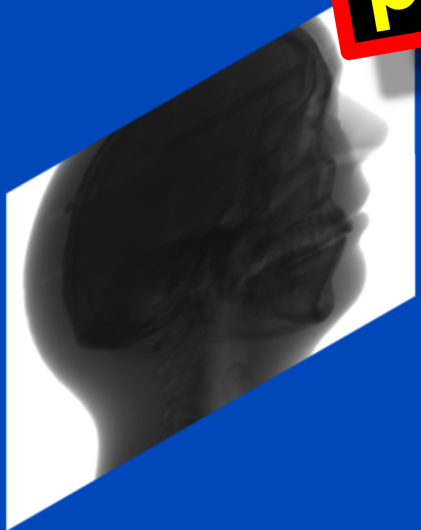

Convolutional neural network

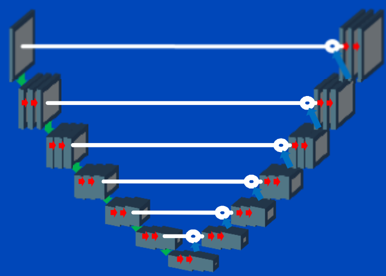

Scatter estimate

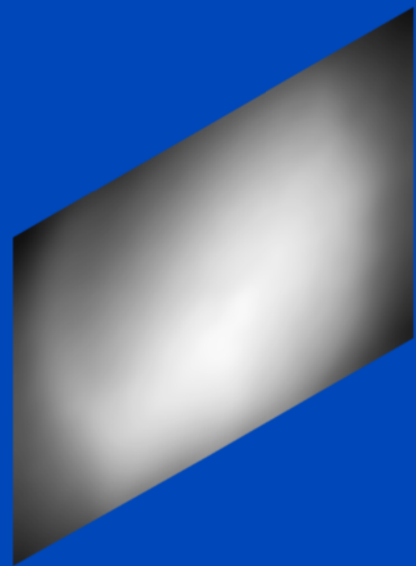

J. Maier, M. Kachelrieß et al. Deep scatter estimation (DSE). Journal of Nondestructive Evaluation 37:57, July 2018.
J. Maier, M. Kachelrieß et al. Robustness of DSE. Med. Phys. 46(1):238-249, January 2019.

dkfz.

Deep Scatter Estimation

Network architecture & scatter estimation framework

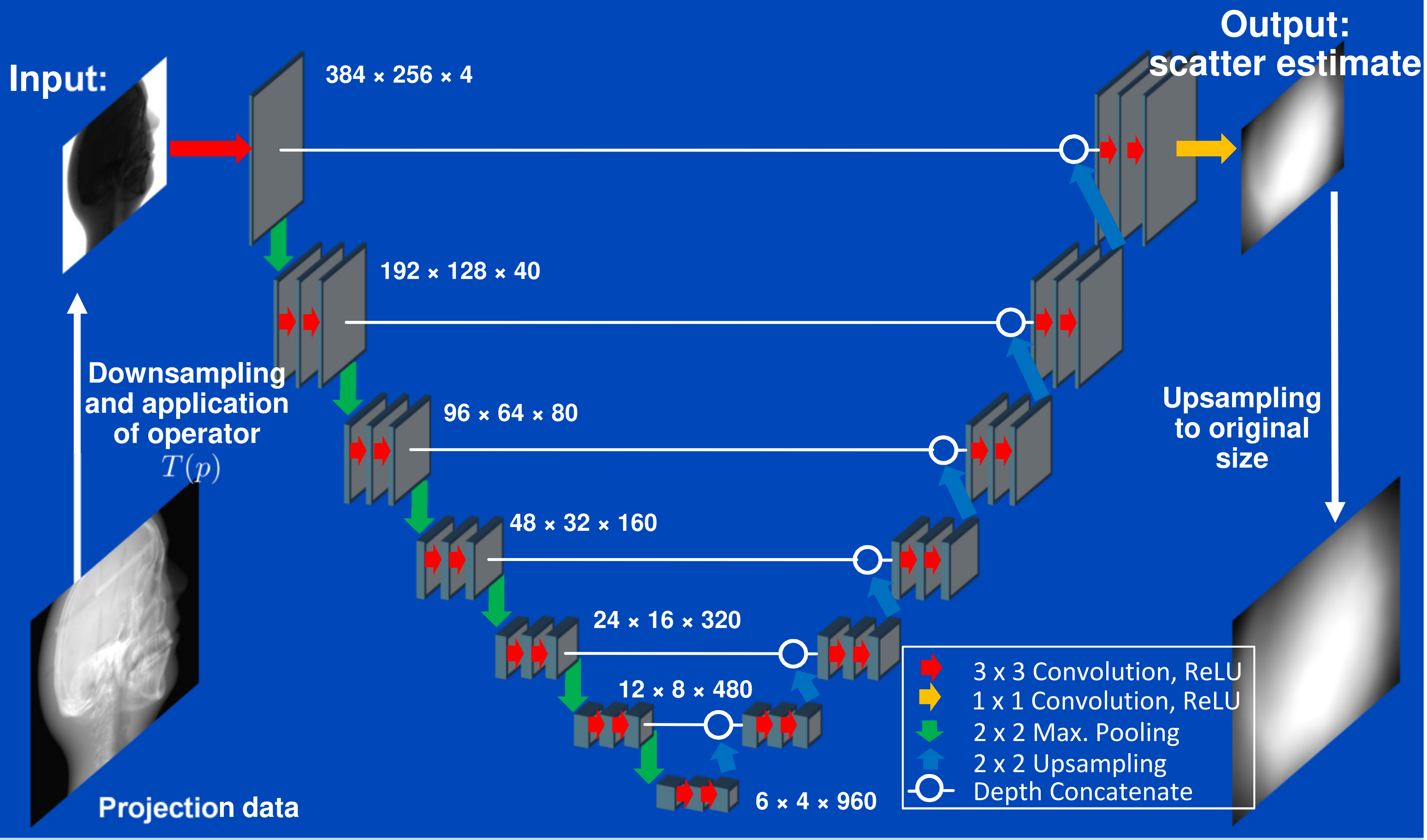

J. Maier, M. Kachelrieß et al. Deep scatter estimation (DSE). Journal of Nondestructive Evaluation 37:57, July 2018.
J. Maier, M. Kachelrieß et al. Robustness of DSE. Med. Phys. 46(1):238-249, January 2019.

Training the DSE Network

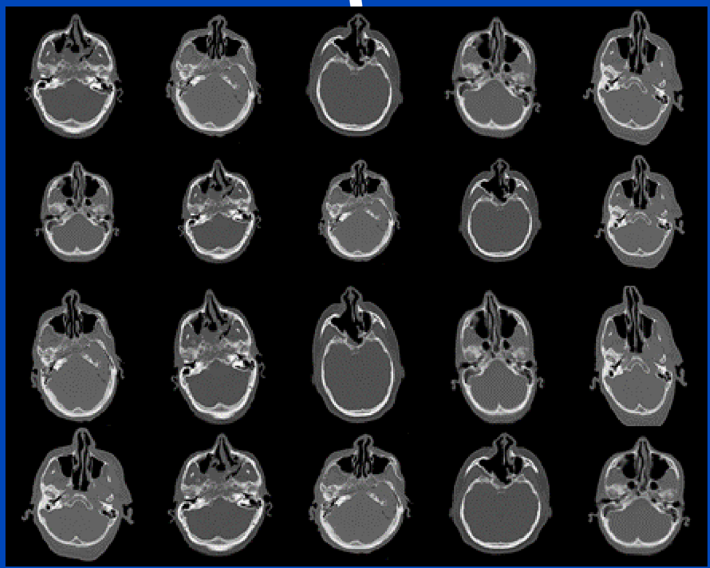

- Simulation of 12000 flat detector projection using data of different heads.
- Simulate different tube voltages.
- Splitting into 80% training and 20% validation data.
- Optimize weights of the CNN to reproduce the Monte Carlo scatter estimates:

$$(\boldsymbol{w}, \boldsymbol{b}) = \arg\min_{\boldsymbol{w},\boldsymbol{b}} \|\mathrm{DSE}_{\boldsymbol{w},\boldsymbol{b}}(T(p)) - I_{\mathrm{MC}}\|_2^2$$

- Training on a GeForce GTX 1080 for 80 epochs.

J. Maier, M. Kachelrieß et al. Deep scatter estimation (DSE). Journal of Nondestructive Evaluation 37:57, July 2018.
J. Maier, M. Kachelrieß et al. Robustness of DSE. Med. Phys. 46(1):238-249, January 2019.

dkfz.

Results on Simulated Projection Data

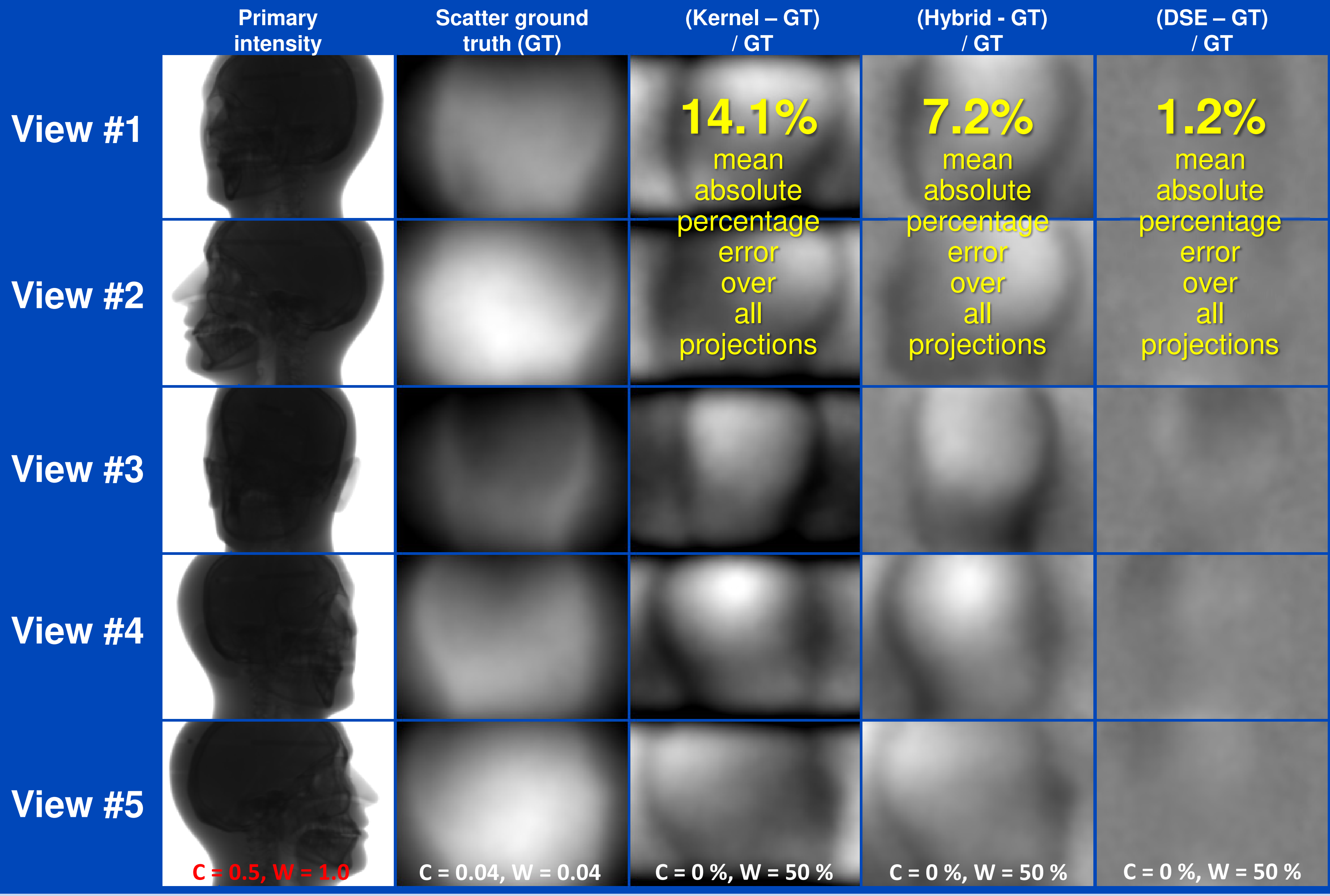

DSE trained to estimate scatter from **primary plus scatter**: High accuracy

Reconstructions of Simulated Data

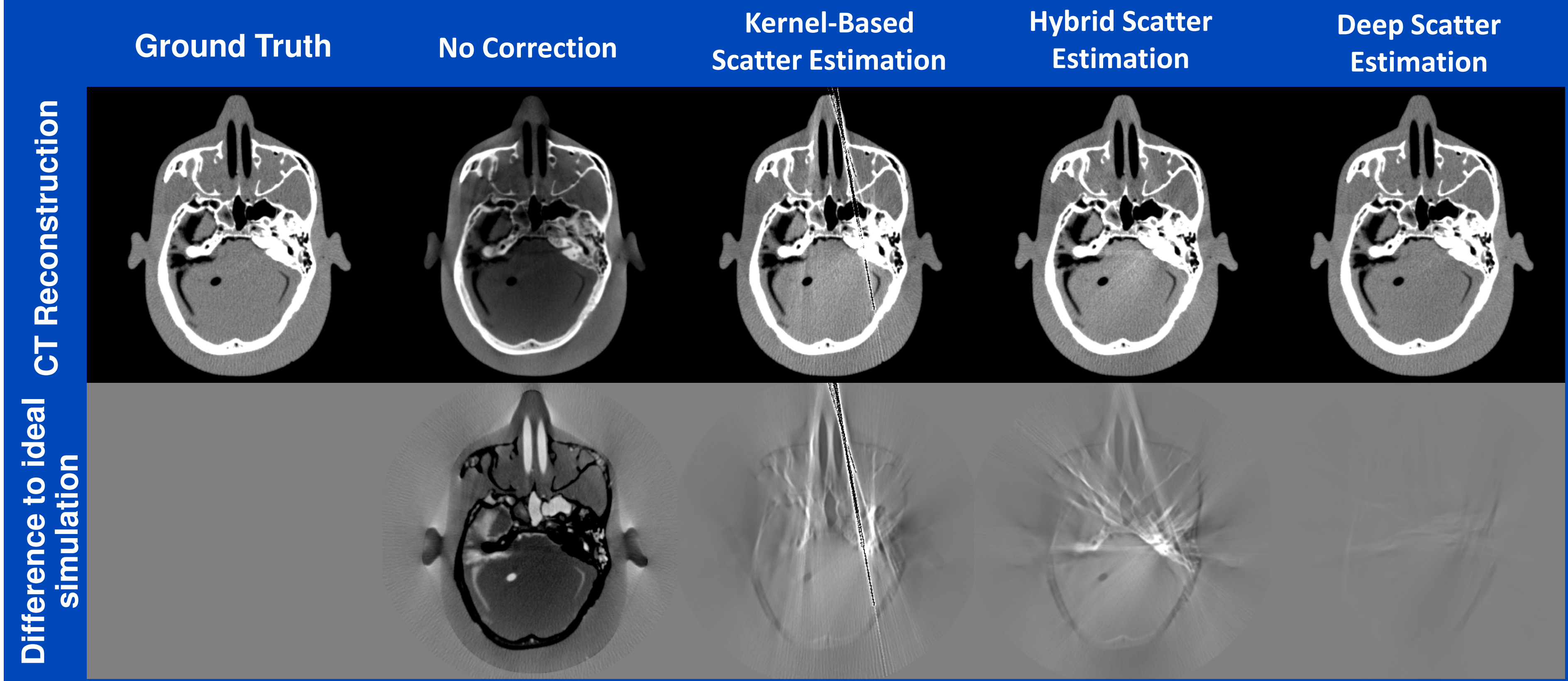

C = 0 HU, W = 1000 HU

J. Maier, M. Kachelrieß et al. Deep scatter estimation (DSE). Journal of Nondestructive Evaluation 37:57, July 2018.
J. Maier, M. Kachelrieß et al. Robustness of DSE. Med. Phys. 46(1):238-249, January 2019.

Testing of the DSE Network for Measured Data (120 kV)

DKFZ table-top CT

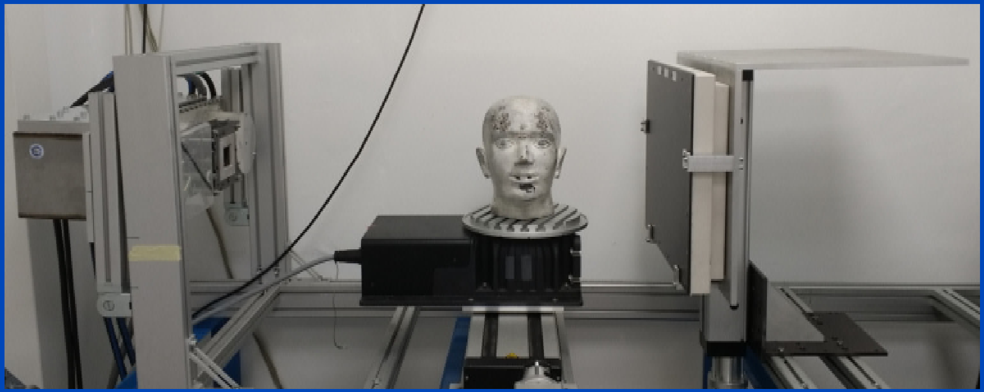

- Measurement of a head phantom at our in-house table-top CT.
- Slit scan measurement serves as ground truth.

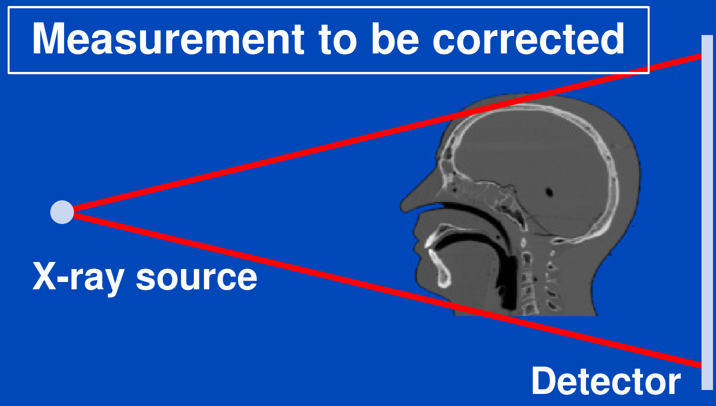

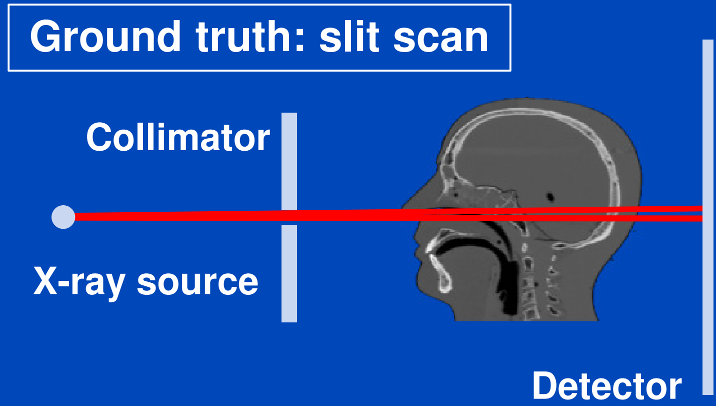

J. Maier, M. Kachelrieß et al. Deep scatter estimation (DSE). Journal of Nondestructive Evaluation 37:57, July 2018.
J. Maier, M. Kachelrieß et al. Robustness of DSE. Med. Phys. 46(1):238-249, January 2019.

Reconstructions of Measured Data

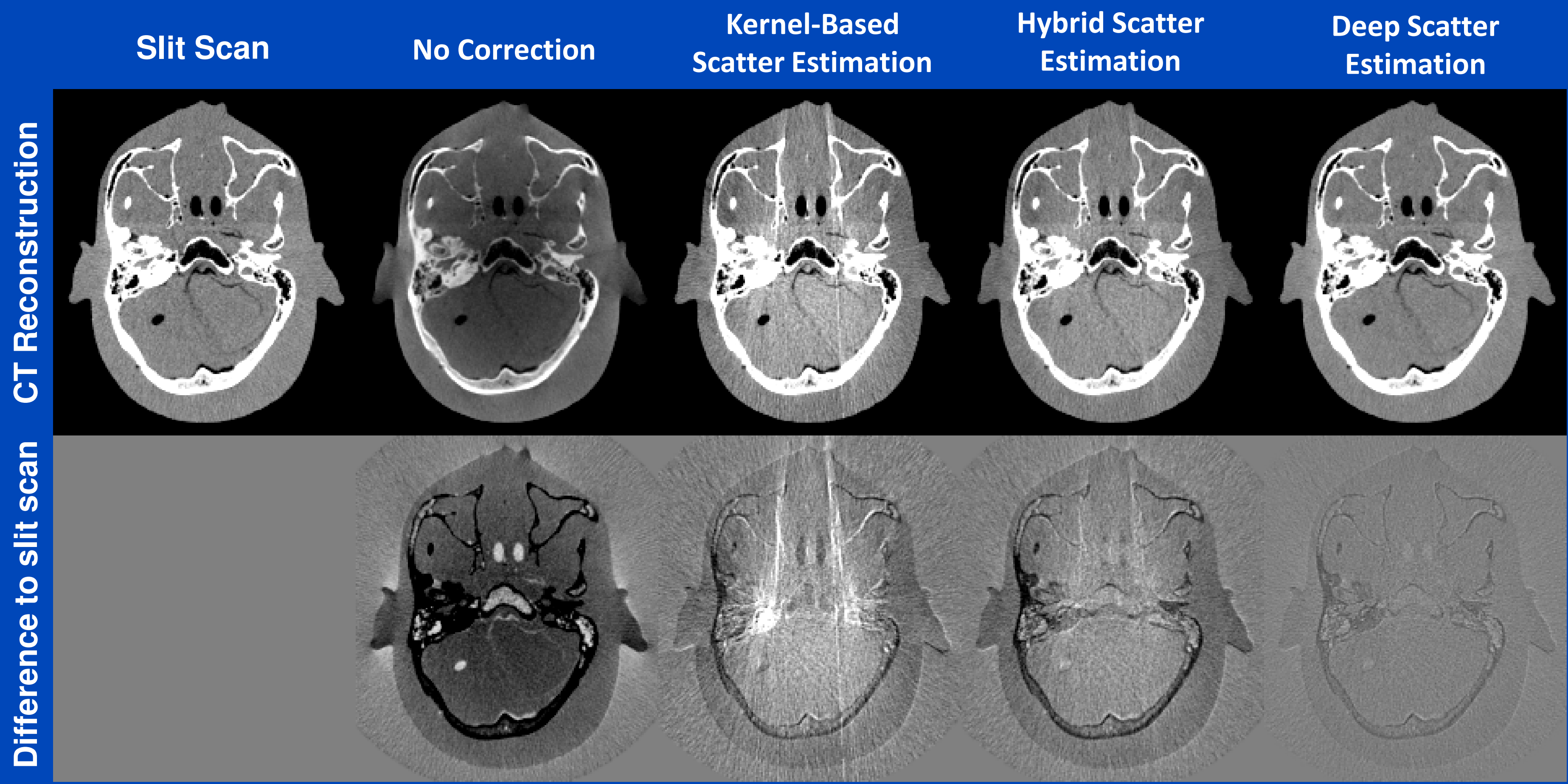

C = 0 HU, W = 1000 HU

J. Maier, M. Kachelrieß et al. Deep scatter estimation (DSE). Journal of Nondestructive Evaluation 37:57, July 2018.
J. Maier, M. Kachelrieß et al. Robustness of DSE. Med. Phys. 46(1):238-249, January 2019.

A simple detruncation was applied to the rawdata before reconstruction. Images were clipped to the FOM before display. C = -200 HU, W = 1000 HU.

Truncated DSE

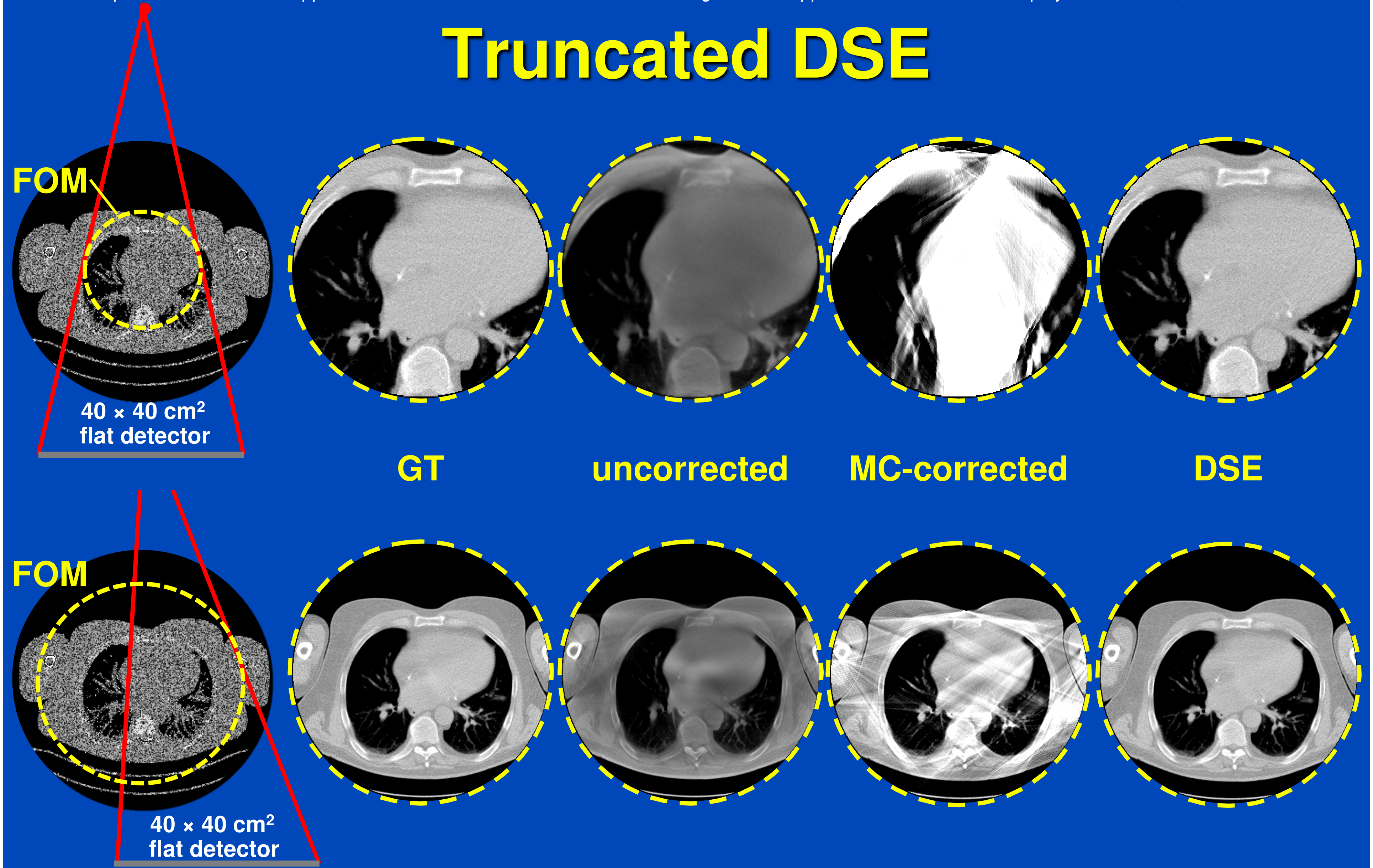

To learn why MC fails at truncated data and what significant efforts are necessary to cope with that situation see [Kachelrieß et al. Effect of detruncation on the accuracy of MC-based scatter estimation in truncated CBCT. Med. Phys. 45(8):3574-3590, August 2018].

Conclusions on DSE

- DSE needs about 20 ms per projection. It is a fast and accurate alternative to Monte Carlo (MC) simulations.
- DSE outperforms kernel-based approaches in terms of accuracy and speed.
- Interesting observations
  – DSE can estimate scatter from a single (!) x-ray image.
  – DSE can accurately estimate scatter from a primary+scatter image.
  – DSE cannot accurately estimate scatter from a primary only image.
  – DSE may thus outperform MC even though DSE is trained with MC.
- DSE is not restricted to reproducing MC scatter estimates.
- DSE can rather be trained with any other scatter estimate, including those based on measurements.

Deep Dose Estimation (DDE)

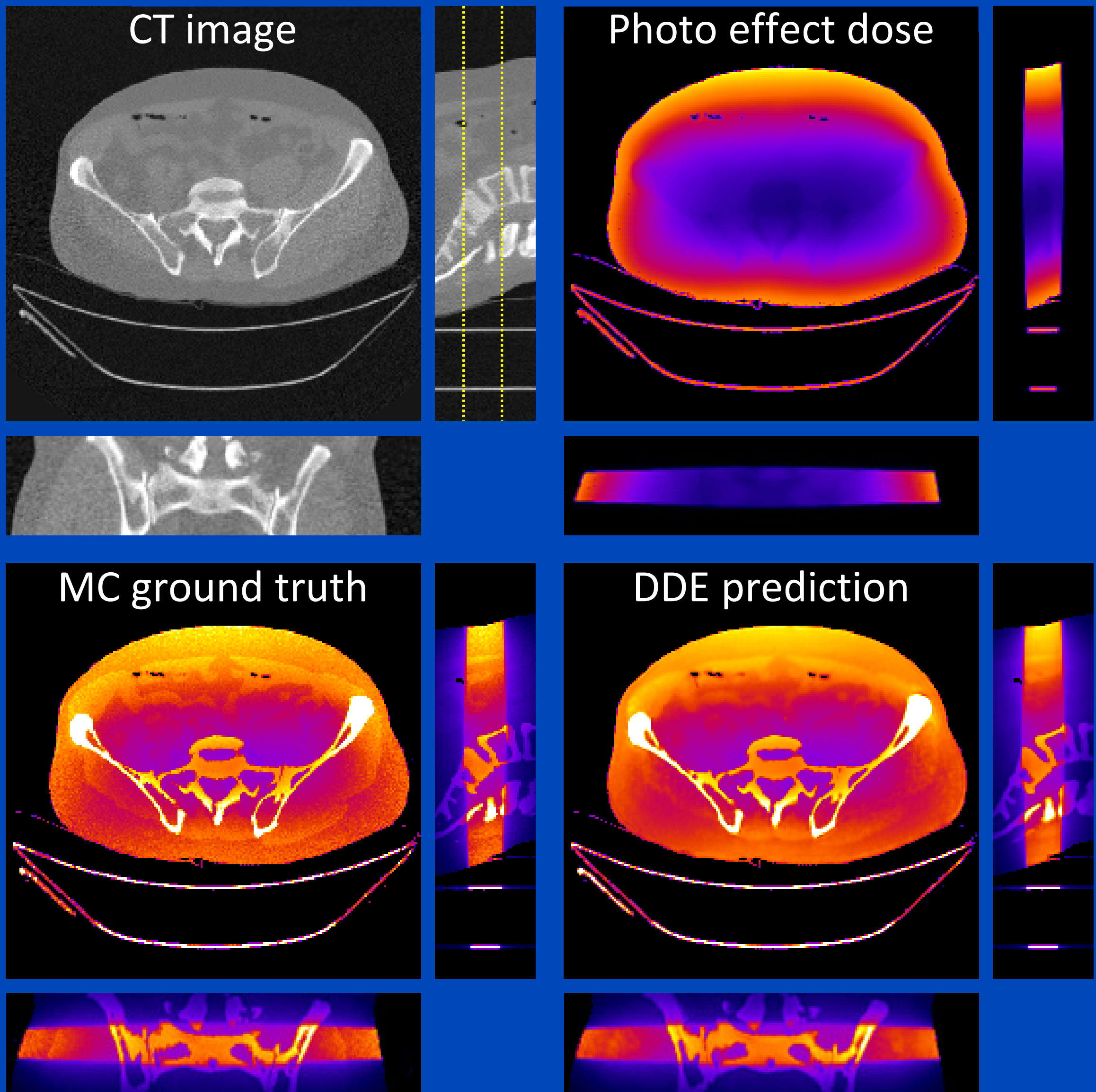

	MC	DDE
48 slices	1 h	0.25 s
whole body	20 h	5 s

MC uses 16 CPU kernels
DDE uses one Nvidia Quadro P600 GPU

DDE training took 30 h for 200 epochs, 720 samples, 48 slices per sample

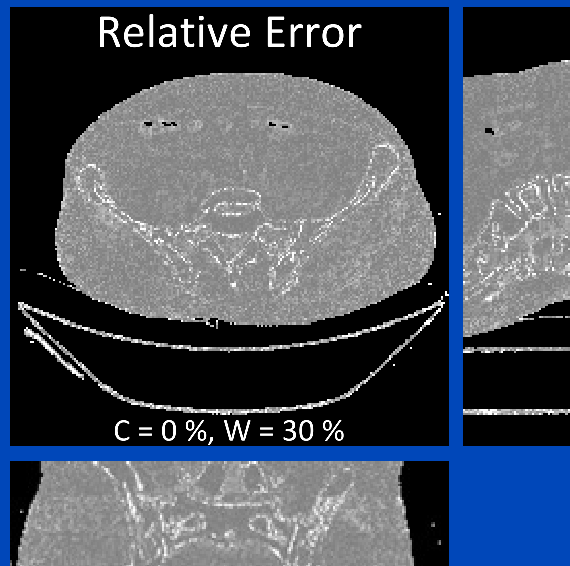

J. Maier, E. Eulig, S. Dorn, S. Sawall, and M. Kachelrieß. Real-time patient-specific CT dose estimation using a deep convolutional neural network. Proc. IEEE MIC 2018.

Conclusions on Deep CT

- Machine learning will play a significant role in CT image formation.
- High potential for
  - Artifact correction
  - Noise and dose reduction
  - Real-time dose assessment (also for RT)
  - ...
- Care has to be taken
  - Underdetermined acquisition, e.g. sparse view or limited angle CT, require the net to make up information!
  - Nice looking images do not necessarily represent the ground truth.
  - Data consistency layers may ensure that the information that is made up is consistent with the measured data.
  - ...

Thank You!

The 6th International Conference on

Image Formation in X-Ray Computed Tomography

August 3 - August 7 • 2020 • Regensburg • Germany • www.ct-meeting.org

Conference Chair: **Marc Kachelrieß**, German Cancer Research Center (DKFZ), Heidelberg, Germany

This presentation will soon be available at www.dkfz.de/ct.
Job opportunities through DKFZ's international Fellowship programs (marc.kachelriess@dkfz.de).
Parts of the reconstruction software were provided by RayConStruct® GmbH, Nürnberg, Germany.